**TOMAS BATA UNIVERSITY IN ZLIN**
**FACULTY OF TECHNOLOGY**
**Polymer Centre**

**Michal Machovský**

# COMPOSITE MATERIALS FOR MEDICAL APPLICATION

Kompozitní materiály pro medicínské aplikace

## Doctoral Thesis

| | |
|---|---|
| Programme: | P 2808 Chemistry and Materials Technology |
| Course: | 2808V006 Technology of Macromolecular Substances |
| Supervisor: | doc. Ing. et Ing. Ivo Kuřitka, Ph.D. et Ph.D. |
| Year: | 2013 |

## CONTENT

## ACKNOWLEDGEMENT

First and foremost, I would like to express my sincere gratitude to my supervisor Assoc. Prof. Ing et Ing. Ivo Kuřitka, Ph.D. et Ph.D. for his guidance, mentoring and encouragement throughout doctoral studies.

I am deeply grateful to Prof. Ing. Petr Sáha, CSc. for creation of excellent academic and social environment and for giving me the opportunity to participate on the project of Centre of Polymer Systems.

My gratitude goes to all my colleagues from the Polymer Centre, the Centre of Polymer Systems and other departments of the University Institute and Faculty of Technology of the Tomas Bata University in Zlin for their collaboration, help and enthusiasm.

Research work and studies has a social dimension as well. Thanks to my friends, roommates and other colleagues for their nice company.

Thanks to my family for all the support, patience and endless love.

The financial support granted to my work by the funding providers is partially addressed and acknowledged in the respective places in papers included to this thesis whenever the opportunity to do so is.

## ABSTRACT

The presented doctoral thesis submitted in the form of commented thematically arranged collection of original scientific articles with accompanying text is focused on preparation of polymeric composites with antibacterial properties. The development of antibacterial polymeric systems is documented from the synthesis of active fillers, investigation of their properties, compounding to polymeric matrix, testing of prepared composites and assessment of surface antibacterial activity.

At the first, antibacterial filers based on zinc oxide were proposed and the original method of their preparation by use of microwave-assisted hydrothermal precipitation from soluble zinc salts introduced. Formation mechanism of zinc oxide particles from layered basic zinc hydroxide acetate intermediate product under the mild pH condition was elucidated. The method was developed further for preparation of two-dimensional mesoporous zinc oxide particles with the aim to study effect of particles morphology on the surface antibacterial performace of the composites. Both two- and three-dimensional fillers were prepared in the size order of micrometers, however, with the nanostructured morphology on mesoscale. This approach, inspired by the shape of snow flake, was adopted to avoid adverse effects that inevitably occur during processing of nanoparticles. The micro-filler keeps all advantages of conventional powder processing and, moreover, it possesses physico-chemical attributes related to nanoparticles as well. Hybrid filler containing silver and zinc oxide was synthesized finally in order to broaden the antibacterial activity of pure zinc oxide.

Following experimental methods were used for characterization of prepared fillers; X-ray diffractometry, scanning electron microscopy, thermogravimetry, and Fourier transform infrared spectroscopy. This part of analytical work contributed to the discussion related to the structure of zinc oxide precursors, i.e. the bonding configuration of the anions in layered basic zinc acetates and sulphates was elucidated.

The medical grade of polyvinyl chloride was selected as a model matrix for preparation of composites containing 0.3-5 wt.% of various synthesized fillers. Plasticized PVC was chosen as the most widely used plastic in medical device applications because of its bio- and hemocompatibility, transparency, flexibility, durability, sterilizability and low cost. An integral part of experimental work consists in optimization of processing conditions in order to assure good dispersion and distribution of filler in matrix. Tensile tests confirmed that incorporation of filler powders at the concentration up to 5 wt.% does not influence mechanical performance of prepared antibacterial polymer composite systems in respect to intended application. The silver containing material has very good conductivity, hence, the composites containing the Ag/ZnO filler were tested on electrical conductivity as the medical device made from this material could interfere undesirably with the diagnostic and therapeutic electronic apparatuses used in medicine.

The touchstone of this work can be found in the testing of the surface antibacterial activity of the prepared composites according to the ISO 22196:2007 (E) against *Escherichia coli* and *Staphylococcus aureus* as representatives of both gram-positive and gram-negative bacteria and typical pathogens responsible for nosocomial infections. The testing method was chosen as being a standard method of quantitative assessment of antibacterial activity on plastic surfaces.

Zinc oxide has been shown to possessed strong antibacterial activity against *Escherichia coli* and mild antibacterial activity against *Staphylococcus aureus.* In order to improve antibacterial performance against *Staphylococcus aureus,* silver nanoparticles were added. However, hybrid silver zinc oxide filler prepared with three-dimensional zinc oxide particles do not bring any synergistic effect and, enhanced antibacterial activity against *Staphylococcus aureus* still remains challenge.

**Key words:** microwave synthesis, zinc oxide, polyvinyl chloride, composites, surface antibacterial activity

## ABSTRAKT

Předkládaná disertační práce ve formě komentovaného souboru čtyř původních článků se zaměřuje na přípravu polymerních kompozitů s antibakteriálními vlastnostmi. Vývoj antibakteriálního polymerního systému je dokumentován od syntézy aktivních plniv, charakterizace, míchání do polymerní matrice, testování připraveného kompozitu a hodnocení povrchové antibakteriální aktivity.

Jako první byl zvolen materiálový systém založený na oxidu zinečnatém. Pro jeho přípravu byla vyvinuta originální metoda mikrovlnné syntézy z rozpustných solí. Byl vysvětlen reakční mechanismus vzniku a růstu krystalických fází vrstevnatého bazického octanu zinečnatého a oxidu zinečnatého. Rozvinutím původní metody byla dále získána plniva s různou morfologií částic, jejíž efekt byl, s ohledem na cíl práce dosáhnout antibakteriálního účinku, také studován. Plniva byla záměrně připravována jako práškové materiály s velikostí částic v řádu jednotek mikrometrů, avšak s nanostrukturovanou morfologii v mezoškále. Tento přístup byl zvolen s ohledem na obejití neodstranitelných negativních efektů u jinak již známých a účinných nanočástic. Mikroplnivo si ponechává výhody "konvenčního" práškového materiálu, jako je jeho zpracovatelnost s polymerní matricí. Díky nanostruktuře však získává i vlastnosti, které jsou u nanočástic považovány za pozitivní. Inspirací byl tvar sněhové vločky. Pro zvětšení záběru vyvíjeného antibakteriálního systému byla připravena také hybridní plniva, obsahující kromě oxidu zinečnatého i částice kovového stříbra.

Pro charakterizaci struktury, složení a morfologie částic byly použity následující experimentální metody: rentgenová difraktometrie, skenovací elektronová mikroskopie, termogravimetrie a infračervená spektrometrie. Tato analytická část práce mimo jiné přispěla k rozřešení dosud otevřených otázek struktury prekurzorů ZnO, tj. koordinačního typu síranových a octanových aniontů ve vrstevnatých bazických octanů a síranů zinečnatých.

Jako modelová matrice pro přípravu antibakteriálních polymerních systémů bylo zvoleno medicínské PVC jako standardní systém, který jednak odpovídá nejběžněji používaným materiálům, jeho vlastnosti známy a dobře se s ním pracuje, což jej činí vhodným, aby se na něm testovaly a demonstrovaly účinky plniv, která byla přidávána v malých koncentracích v rozsahu od 0.3 až 5 hm.%. Nedílnou součástí výzkumu bylo nalezení zpracovatelských podmínek míchání, které by zajistilo co nejlepší dispergaci a distribuci plniva v matrici. Dále bylo ověřeno, že ani proces míchání, ani plniva samotná, nezpůsobují zhoršení mechanických vlastností výchozího materiálu. U kompozitů obsahujících stříbro byly zkoumány i elektrické vlastnosti připraveného materiálu, neboť by prostředek vyrobený z tohoto materiálu mohl nežádoucím způsobem interferovat s diagnostickými a terapeutickými přístroji používanými v medicíně. Ve všech případech se tyto obecnější vlastnosti materiálu ukázaly jako vhodné pro případnou medicínskou aplikaci.

Prubířským kamenem práce bylo testování povrchové antibakteriální aktivity připravených kompozitních materiálů podle normy ISO 22196:2007 (E) proti Escherichia coli jako standardnímu reprezentantu gram-negativních bakterií a proti S. aureus jako zástupci gram-pozitivních, kteří zároveň patří k nejběžnějším původcům nosokomiálních infekcí. Oxid zinečnatý se ukázal jak excelentní aditivum působící proti E. coli, a něco slabší proti S. aureus. Pro dosažení synergického účinku bylo k systému přidáno stříbro, které se ovšem doposud nepodařilo propojit s nejefektivnějším ZnO systémem majícím morfologii porézní mřížky. Zvýšení účinnosti proti S. aureus tak zůstáva otevřenou výzvou. Významným vodítkem je závěr třetího přiloženého článku, kde je formulováno obecné pravidlo o vztahu morfologie minerálního plniva a jeho účinnosti.

**Klíčová slova:** mikrovlnná syntéza, oxid zinečnatý, polyvinylchlorid, kompozity, povrchová antibakteriální aktivita

## LIST OF FIGURES AND TABLES

## LIST OF ABBREVIATIONS AND SYMBOLS

| | |
|---|---|
| PU | Polyurethane |
| PTFE | Polytetrafluoroethylene |
| PVC | Polyvinyl chloride |
| ABS | Acrylonitrile butadiene styrene |
| PE | Polyethylene |
| PP | Polypropylene |
| ISO | International Organization for Standardization |
| IMD | Indwelling medical device |
| SEM | Scanning elektron microscopy |
| TEM | Transmission elektron microscopy |
| XRD | X-ray diffraction |
| FTIR | Fourier transform infrared spectroscopy |
| EPS | Extracellular polymer matrix |
| QS | Quorum sensing |
| DNA | Deoxyribonucleic acid |
| RNA | Ribonucleic acid |
| APS | Antibacterial polymer system |
| PEEK | Polyether ether ketone |
| PC | Polycarbonate |
| PA | Polyamide |
| PMMA | Poly(methyl methacrylate) |
| EVA | Ethylene vinyl acetate |
| $E_g$ | Band gap energy |
| CVD | Chemical vapour deposition |
| ZHA | Zinc hydroxide acetate |
| MW | Microwave |

SI units are used in this work

## LIST OF ARTICLES AND AUTHOR'S CONTRIBUTION

I. MACHOVSKY, M.(50 %); KURITKA, I.; BAZANT, P.; PASTOREK, M.; SAHA, P. Formation mechanism of ZnO particles prepared by microwave assisted hydrothermal synthesis under mild pH condition. *Manuscript in preparation for Crystal Growth and Design.*

II. MACHOVSKY, M.(50 %); KURITKA I.; SEDLAK J.; PASTOREK M. Hexagonal ZnO porous plates prepared from microwave synthesized layered zinc hydroxide sulphate via thermal decomposition. *Materials Research Bulletin, 2013.*

http://dx.doi.org/10.1016/j.materresbull.2013.06.018

III. MACHOVSKY, M.(50%); KURITKA, I.; BAZANT, P.; VESELA, D.; SAHA P.; Antibacterial Performance of ZnO-based Fillers with Mesoscale Structured Morphology in Model Medical PVC Composites. *submitted to Materials Science and Engineering C: Materials for Biological Applications*

IV. BAZANT, P.; KURITKA, I.; HUDECEK, O.; MACHOVSKY, M.(30%); MRLIK, M.; SEDLACEK, T. Microwave assisted synthesis of Ag/ZnO hybrid filler, preparation and characterization of antibacterial PVC composites made from the same. *Accepted to Polymer Composites*

## INTRODUCTION

At the down of the 21st century, it is widely recognized that the rapid and continuing change in emphasis in material science away from traditional engineering materials has been largely instituted by the requirements of emerging technologies for advanced and structurally sophisticated new materials. Medical engineering, often included in the list of advanced technologies, requires the underpinning of high-tech materials. The word which is used to categorize materials for biomedical applications is “biomaterial” [1].

The use of biomaterials dates far back into ancient civilizations [2]. Over the centuries, advancements in synthetic materials, surgical techniques, and sterilization methods have permitted the use of biomaterials in many ways. Medical practice today utilizes a large number of devices and implants. Biomaterials in the form of implants (sutures, bone and joint replacements, vascular grafts, heart valves, intraocular lenses, dental implants, etc.) and medical devices (pacemakers, biosensors, artificial hearts, etc.) are widely used to replace and/or restore the function of traumatized or degenerated tissues or organs, to assist in healing, to improve function, to correct abnormalities, and thus improve the quality of life of the patients [3].

According to literature, a biomaterial is a nonviable material used in a medical device and intended to interact with biological system [4]. Another definition of biomaterial is “any substance (other than drugs) or combination of substances synthetic or natural in origin, which treats, augments, or replaces any tissue, organ, or function of the body”. This definition is somewhat restrictive, because it excludes materials used for devices such as surgical instruments [5].

Biomaterials are manufactured or processed to be suitable for use in form of implants or as medical devices that come into more or less intimate contact with biological system. An extended definition of the term “biomedical materials” is construed then as reference to materials used in biological and medical applications [6].

The contact or interaction is generally implemented in several ways: permanent implantation e.g. heart valves, total joint replacement, dental restoration, and intraocular lenses, long-term application as contact lenses, indwelling catheters, hemodialysis systems etc., and transient application, for instance needles, syringes, wound healing devices, cardiopulmonary bypass and cardiac assist systems.

All biomaterials intended for use in contact with living systems must meet certain criteria and regulatory requirements. The minimum requirements include the following [1]:

- the material must be biocompatible, such as nontoxic, blood- or tissue-compatible, noncarcinogneic, etc,
- the material must not leach or release harmful components into the living system,
- the mechanical and physical properties of the material, such as strength, elasticity, durability, stability, etc., must be appropriate for the intended application,
- the mechanical properties must last for the expected life of the medical device or implant,
- the materials must be sterilizable at least by one of standard methods,

Materials for biomedical use can be classified in a number of ways according to different criteria; categorisation into four major classes is generally adopted: polymers, metals, ceramics (including carbons, glass-ceramics, and glasses), and natural materials (including those from both plants and animals). Sometimes two different classes of materials are combined together into a composite material, giving rise to a fifth class. Among these groups of materials, polymeric materials and composites have received great attention in the past few decades. This may be attributed to their high versatility and excellent physico-chemical properties, making them favourable candidates for most biomedical applications [7].

# 1 POLYMERS

Polymers have undoubtedly been the wonder materials of the last century and represent the largest class of biomaterials [8]. Generally, polymer is a substance composed of macromolecules. The term macromolecule can be further explain as a molecule of high relative molecular mass, the structure of which essentially comprises the multiple repetition of units derived, actually or conceptually, from molecules of low relative molecular mass [9]. In particular, high molecular mass along with nature of atoms bounded in macromolecules is in most responsible for unique physico-chemical properties making polymers totally different from low molecular mass substances.

Macromolecules may be of natural or synthetic origin. Natural polymers (biopolymers) comprise such diverse groups as nucleic acids, polyprenes, polysaccharides, polypeptides, etc. and their use is as old as human being. On the other hand, the history of synthetic polymers dates only for about a century back. Within a few decades, many of the synthetic polymers have found established uses in a number of important areas involving mechanical and electrical engineering, tele-communication, aerospace, chemical, biochemical, and biomedical applications [10].

Polymers often require physical or chemical modification to achieve optimum properties, and promote non-inherent performance. Indeed, only a few of polymers can be used in pure form. The vast majority of commercial polymers are compounded with chemicals (additives) and/or other polymers to improve their usability or durability. These additives can be used to tune a polymer to a specific application, imparting high temperature oxidation resistance, improved flexibility, colour retention, anti-static performance, increased impact resistance or introduction of antibacterial properties to name a few examples. Other polymers are compounded for economics reasons, where a costly base polymer may be extended by addition of lower cost additives such as clays, reground polymer, other polymers, or a blowing agent that reduces density [11].

## 1.1 Polymers in medicine

The utilisation of a range of polymer systems in the medical industry in the new millennium spans many applications. The wide variety of natural polymers relevant to the field of biomaterials includes plant materials such as cellulose, sodium alginate, and natural rubber, animal materials such as tissue-based heart valves and sutures, collagen, heparin, and hyaluronic acid, and other natural materials such as deoxyribonucleic acid, the genetic material of all living creatures. Although these polymers are undoubtedly important and have seen widespread use in numerous applications, they are sometimes eclipsed by the seemingly endless variety of synthetic polymers available today [7].

Hundreds of polymers are now used in part or whole construction of medical devices, therefore a brief description only is provided of some of the biomaterials most frequently encountered.

**Silicone** is a general term for polysiloxanes. In 1950, silicones were first used in medical applications. Silicone has become standard against which other materials must be compared for biocompatibility. It is soft, non-irritating and clinically stable, making it ideal for long-term use. It has good surface properties, which allow easy insertion, and lower rates of encrustation and bacterial adherence [12, 13].

**Polyurethanes** (PU) are polymers containing the urethane linkage. The term polyurethane refers to a broad variety of elastomers that are usually formed by the addition of polyglycol to an isocyanate. By changing the chemical constituents, they can be readily tailored for many applications. Polyurethanes have good mechanical properties, are relatively inexpensive, and are commonly used in clinical practise [14].

**Latex** is a natural polymer dispersion and is composed of water and 30 to 35% natural rubber (poly cis-1,4-isoprene). Latex devices are inexpensive and have good elasticity, but tend to be more prone to bacterial adherence and have a greater potential for allergic sensitization than other materials. Many people

now suffer from latex allergy which can cause symptoms ranging from allergic rhinitis, urticaria and wheezing to anaphylactic shock, brain damage, or death. For example, latex urinary catheters are suitable for short-term use only and frequently are coated with additional polymers [12].

**Hydrogels** are hydrophilic polymers that swell in contact with water, retaining a significant amount of water within their polyanionic structure [15]. As the water content increases, medical devices become softer, more flexible, and more slippery, resulting in a greater ease of insertion. Hydrogels used for device coatings may include polyvinyl alcohol, hydroxy ethyl methacrylate, n-vinyl pyrollidone and a variety of other hydrophilic polymers [16].

**Poly(tetra fluoro ethylene)**, (PTFE) also known as Teflon, is used largely as a surface coating. It is usually applied by dip-coating the substrate polymer into a dispersion containing PTFE particles and dissolved binder polymer (often a polyurethane). After dip-coating, the binder polymer is cured. The resulting surface has a low coefficient of friction, but is not a continuous coating of PTFE [16].

**Poly(vinyl chloride)** (PVC) can be used for a wide range of medical device applications. It is strong, transparent, smooth and, most important, very inexpensive. In order to make it flexible, plasticizers are incorporated. PVC has been used in hundreds of medical applications for more than 50 years. In fact, 25% of all medical products containing plastic are made of PVC. Applications include blood bags and tubing, intravenous containers and components, catheters, dialysis equipment, examination gloves, inhalation masks, and many other uses. Medical device manufacturers are continually researching new and improved materials but PVC continues to be the major plastic used because it posses properties critical in medical devices as clarity and transparency, flexibility, durability, sterilizability, compatibility with most pharmaceutical products, resistance to stress cracking and kinking in tubing, ease of processing, and most importantly, reliable performance at effective cost [17].

Overview of polymers used in biomedical applications is given in Table 1.

**Table 3** Major Polymer Types and Medical Device Applications [18]

| *Polymers* | *Examples of Applications in Medical Devices* | *Special Characteristic* |
|---|---|---|
| | | |
| ABS | IV: Spikes, Luer, Y connector, Roller clamp | Irradiation stable, tough, chemical resistant, clear/opaque |
| Acetals | Stopcocks<br>Components in asthma inhalers | Strong, hard material |
| Acrylics | Tubing connectors<br>Blood set components<br>Dental polymers<br>Intraocular implants | Clear, hard surface, low cost |
| Cellulosics | Haemodialysis membranes<br>Haemo-filters<br>Structural members of medical devices<br>IV burette chambers | Insoluble in water, excellent surface gloss, clarity |
| Polyamide and copolymers | Catheters used in cardiovascular procedure<br>Sutures<br>Epidural catheters<br>Laparoscopy devices<br>Blood sets | Crystalline polymer with high strength, moderately high degree of elasticity, moderately high moisture adsorption, kink resistant, pressure sensitive, torque resistant |
| Polycarbonate | Blood oxygenators<br>Blood filters<br>Tubing connectors<br>Casing for dialysis membranes<br>Check valves<br>Luer fittings, Syringes, Containers | Excellent resistance to impact, clear, moderately strong, good resistance to moderately high temperature |
| Polyethylene terephthalate | Woven vascular prostheses<br>Sutures<br>Catheters and tubings | Good resistance to high temperature, microwaves, and UV radiation, chemical resistance, transparent |
| Polymethyl methacrylate | Ophthalmology lenses and contact lenses<br>Orthopaedics: grout for artificial joints, vertebroplasty, repair of skull defects<br>Membranes for oxygenators<br>Corneal prosthesis | Transparent, excellent surface hardness, resistant to most detergents |
| Polyolefins (e.g. PE, PP) | Films, tubing, and containers for packaging<br>IV bags, vials, containers (PP)<br>IV medicine packs (LDPE)<br>Blood oxygenators - membrane and hollow fibres (PP)<br>Syringes (PP barrel, PE plunger)<br>Dialysis membranes<br>Heart valve occluders<br>Wipes (PP)<br>Sutures<br>Catheters, Protective tubes<br>Hip joints | Low cost, flexible, low extractables, low water permeability, resistance to fats and oils, excellent electrical insulating properties, good tensile and impact strength |

| | | |
|---|---|---|
| Polystyrene | Sputum cup<br>Containers<br>Tubes | High index of refraction, excellent electrical properties |
| Polysulfones | Dialysis end Filter membrane<br>Surgical instruments<br>Hospital trays, dishes<br>Components of diagnostic devices | Transparent, good temperature resistance, good resistance to environmental stress cracking and to hydrolysis by acid and base |
| Polyurethane | IV set container<br>Enteral feeding tubes<br>Blood pumps, sets<br>Artificial heart ventricles<br>Catheters and tubing<br>Containers for IV solution feeding<br>Surgical prostheses<br>Haemostatic coatings<br>Surgical dressings | Hydrolysis to generate aromatic amines is an issue – mutagenic in some cases. Sterilizable by EtO or radiation, excellent resistance to lipids, good clarity |
| Polyvinyl chloride (PVC) | Medical tubing<br>Check valves, connectors, needle hubs, filter housings, drip chambers<br>Flexible containers for intravenous therapy: glucose solution, saline solution, drug mixture, nutrients, blood, blood components<br>Enema, urology products<br>Haemodialysis sets<br>Heart-lung bypass sets | Transparency, flexibility, biocompatibility, low cost, ease of fabrication |
| Polytetrafluoroethylene (PTFE) | Surface coatings<br>Orthopaedics: coating stem prostheses<br>Aneurysm clips<br>Neurosurgery<br>Endoscope sheaths<br>Fibre optics upjacket | Excellent resistance to high temperature and corrosives, low coefficient of friction, excellent electrical properties, abrasion resistance |
| Natural Rubber | Foley catheter for urological use<br>Needle sites<br>Gloves | Good insulation properties, excellent elasticity |
| Silicone | Tubing<br>Foley catheters (urinary drains)<br>Catheters for IV infusion, drainage, bypass<br>Membranes in blood oxygenators<br>Nasogastric tubing<br>Eustachian tube<br>Implants – digit joints, lenses, pacemaker components | Stable over wide range of temperatures, unaffected by ozone and hot oils, excellent dielectrical properties, ageing resistance |
| Thermoset polyurethane | Plastic surgery<br>Oxygenators<br>Heart valves | High performance elastomer, high tensile strength, high elongation, excellent abrasion resistance, good oil resistance |

# 2 MEDICAL DEVICES

The area of medical device technology has grown rapidly in recent years reflecting the advances made in the development of biomaterials suitable for medical device construction. The medical industry has been guided and driven by the demands of the medical profession seeking constant improvements and innovation in the devices available for an increasingly elderly and, often, affluent population [19]. According ISO 13485 Standard, a medical device is any instrument, apparatus, implement, machine, appliance, implant, in vitro reagent or calibrator, software, material or other similar or related article, intended by the manufacturer to be used, alone or in combination, for human beings for one or more of the specific purpose(s) of [20]:

- Diagnosis, prevention, monitoring, treatment or alleviation of disease,
- Diagnosis, monitoring, treatment, alleviation of or compensation for an injury,
- Investigation, replacement, modification, or support of the anatomy or of a physiological process,
- Supporting or sustaining life,
- Control of conception,
- Disinfection of medical devices, providing information for medical purposes by means of in vitro examination of specimens derived from the human body,
- And which does not achieve its primary intended action in or on the human body by pharmacological, immunological or metabolic means, but which may be assisted in its function by such means.

Among medical devices, indwelling medical devices (IMD) have become major tools in the clinical management of hospitalized patients, particularly those requiring life supporting devices. Urinary, intratracheal, central vein, peritoneal dialysis nephrostomes and other indwelling devices are become widely used in

medical practise and are applied to more than 25% of hospitalized patients [21]. IMDs providing doctors and surgeons with less invasive therapies to treat diseases, administer nutrients, obtain blood samples, deliver medicines to specific locations in the body, and so forth. Tens of millions of IMDs are used every year and, unfortunately a significant proportion of each type of device becomes subjected to bacterial infection which constitute a major limitation of the utility of medical devices [22, 23]. Magnitude of IMD-related infections may be visualized on estimated number of IMDs inserted in the United States per year with estimated infection rates and attributed mortality (Table 2).

**Table 4** Estimated Number of IMDs Inserted in the U.S. Per Year with Estimated Infection Rates and Attributed Mortality [24]

| *Device* | *Estimated No. of Devices Placed/Year* | *Infection Rate (%)* | *Attributable Mortality* |
|---|---|---|---|
| Urinary catheters | >30,000,000 | 10-30 | Low |
| Central venous catheters | 5,000,000 | 3-8 | Moderate |
| Fracture fixation devices | 2,000,000 | 5-10 | Low |
| Dental implants | 1,000,000 | 5-10 | Low |
| Joint prostheses | 600,000 | 1-3 | Low |
| Vascular grafts | 450,000 | 1-5 | Moderate |
| Cardiac pacemakers | 300,000 | 1-7 | Moderate |
| Breast implants (pairs) | 130,000 | 1-2 | Low |
| Mechanical heart valves | 85,000 | 1-3 | High |
| Penile implants | 15,000 | 1-3 | Low |
| Heart assist devices | 700 | 25-50 | High |

Scale for attributable mortality: low,<5%; moderate, 5-25%, high,>25%..

## 2.1 Indwelling medical device-related infection

Since time immemorial, human societies have been beset by acute infectious diseases, in which planktonic cells of specialized pathogens mounted life-threating attacks on our bodies [25]. Therefore, it is not surprising that nature of bacteria and the role they play in infectious disease has been one of the most extensively researched areas in biomedical science. It has led to tremendous scientific breakthroughs aimed at eradicating a myriad of diseases and improving the overall quality of life [26, 27]. Indeed, due to the epochal discovery and development of antibiotics in the early 1940s, these acute infection are now largely under some measure of control [28-31]. However, there are two exceptions to this rule. First are bacteria that are innately antibiotic resistant, and the second pertains to bacteria that reside within a consortium associated with surface, so called biofilm.

As IMDs comes into more regular use, the surgeons who placed them noted that antibiotic therapy frequently failed in threatening of infection associated with IMDs and gradually persuaded medical microbiologist and infectious disease specialists that device-related infections differed significantly from acute bacterial infections [32].

Rapid development in microscopic techniques contributed to a great degree to better understanding of IMD-related infections. In 1980s, pioneering microscopic studies of the surface of failed IMDs, such as intravenous catheters and cardiac pacemakers, by both scanning (SEM) and transmission (TEM) electron microscopy has revealed that almost all of these devices are colonized by bacteria despite of many advances in biomaterials, non-septic conditions during the surgical process, and systemic administration of antibiotics. Because both, SEM, and TEM involve dozens of washing steps that remove floating or loosely adherent bacteria, it has became evident that observed bacteria remained on the surface were biofilm bacteria which are responsible for IMD-related infections [33-37].

These infections were often very slow to develop, with overt symptoms sometimes being seen almost immediately and sometimes being seen long after the device was inserted. Inflammation and pus formation were often local, but a certain proportion of patient with device-related infection suddenly develop acute disseminated infection by the same species that had colonized the device. These acute exacerbations of device-related infections responded well to antibiotic therapy. However, this treatment almost never reversed the local symptoms, and colonized devices often gave rise to a predictable series of acute exacerbations. Often, the only reliable treatment is the removal of the infected device, which in turn leads to prolonged hospitalization, increased morbidity, mortality, and healthcare cost. It has been estimated that the cost for treating IMD-related infection can range from 5-7 times the cost of the original implantation [24, 38]. Bacteria isolated from these devices were common skin biota and environmental organisms, including the gram-positive *Enterococcus faecalis*, *Staphylococcus aureus*, *Staphylococcus epidermis*, and *Streptococcus viridans*; and the gram-negative *Escherichia coli*, *Klebsiella pneumoniae*, *Proteus mirabilis*, and *Pseudomonas aeruginosa* [39, 40]. Sources for infectious bacteria include the ambient atmosphere of the operating room, surgical equipment, clothing worn by medical professionals, resident bacteria on the patient's skin and bacteria already in the body [41]. Although the infecting bacteria and occasionally fungi were so ubiquitous in the modern human environment, and device recipients always had good immunity against these low-level pathogens, the patient's antibodies failed to prevent infection with the source in biofilm.

Most, if not all, of the characteristics of device-related infections can be explain in terms of the characteristics of biofilms, so it may be useful to examine the burgeoning field of biofilm microbiology, as an early step in the search for new biomaterial that will control these infections.

# 3 BIOFILMS

Our perception of bacteria as unicellular forms is deeply rooted in the pure-culture paradigm. Since bacteria can, in a strict sense, be diluted to a single cell and studied in liquid culture, this mode of operation has been exploited and used to study many bacterial activities. Although this traditional way of culturing bacteria in liquid medium has been instrumental in the study of microbial pathogenesis and enlightening as to some of the amazing facets of microbial physiology, planktonic (free-floating) growth is rarely how bacteria exist in nature. Direct observation of a wide variety of natural habitats has established that the majority of bacteria persist attached to surfaces within a sessile communities known as biofilm rather than in form of planktonic organisms [27].

Historically, Van Leeuwenhoek has been probably the first who observed microbial biofilm when examined plaque on teeth surface using his primitive microscope as early as in the seventeenth century, but the general theory of biofilm predominance was not promulgated until the 1970s [42-45]. The data on which this theory is predicated came mostly from both natural and industrial water systems. By the mid-twentieth century, Heukelekian [46] and Zobell [47] found out that for marine microbes, growth and activity were enhanced by the presence of a surface onto which they could adhere. In 1973, Characklis founded biofilms in industrial water systems to be highly resistant to disinfectants such as chlorine [48]. The term “biofilm” was coined and described in 1978 when Costerton noted that in alpine streams, sessile bacterial biofilm populations outnumber the planktonic populations by a factor between 1,000 and 10,000 [49].

This consensus that bacteria grow preferentially in biofilms in natural systems was not immediately accepted in the medical and dental areas in spite of the universal acceptance of dental plaque as a type of biofilm. However, the prevalence of the IMD-related infections and their impact on medical and financial aspects of modern hospital medicine has triggered an intensive research on biofilms.

Our understanding of biofilm has evolved during the years as the methods for its examination and characterization have developed. Much of the early investigation on biofilms has relied on tools such as SEM and TEM or standard microbiological culture techniques for characterization [50, 51]. Two major groups of experimental techniques have dramatically impacted our understanding of biofilms in the last two decades: the utilization of confocal laser scanning microscope for characterization of biofilm ultra-structure, and an investigation of the genes involved in cell adhesion and biofilm formation [42]. Current definition of biofilm, taking into account not only readily observable characteristics but also physiological attributes is as follows; Biofilm is a microbially derived sessile community characterized by cells that are irreversibly attached to a substratum or interface or to each other, are embedded in a matrix of extracellular polymeric substances (EPS) that they have produced, and exhibit an altered phenotype with respect to growth rate and gene transcription [25].

## 3.1 Biofilm formation

Numerous studies have revealed, that biofilm formation is a continual dynamic sequence of events, largely dictated by a number of variables, including the species of bacteria, cell surface composition, nature of substrates, nutrient availability, hydrodynamics, and cell-to-cell communication. Generally, biofilm formation involved four stages; reversible attachment, irreversible attachment, maturation, and dispersal of biofilm [19, 52-55].

### 3.1.1 Reversible attachment

The solid-liquid interface between a surface and an aqueous medium (e.g., blood, water) provides an ideal environment for the attachment and growth of

bacteria [42]. Bacteria attach at a surface more or less at randomly as a result of diffusion by Brownian motion, convection arising from currents in the surrounding medium, or by the chemotactic ability [56]. Study using time-lapse phase-contrast microscopy have visualised so called surface-associated motility of bacteria. The bacteria initially attach to a surface in a reversible manner, so that they can easily detach and move along the surface [57].

The solid surface has several characteristic that are important in the attachment process. These include surface roughness, charge, and hydrophobicity. The in vitro studies of bacterial adherence have revealed that the extent of bacterial colonization increase as the surface roughness rises. This is most likely due to diminishing of shear forces in proximity of rougher surface, and its larger surface area giving more opportunity for bacterial attachment [58, 59]. As most bacteria exhibit a negative surface charge in aqueous medium, negatively charged substratum amplified the repulsion effect between both bacteria and substratum surface, decreasing the adherence [60, 61]. In next, bacterial cells, which tend to have hydrophobic surface attach more rapidly to hydrophobic, non-polar surfaces, rather than to hydrophilic ones [62, 63].

However, a material surface exposed to a body liquid will inevitably and almost immediately become conditioned with lipids, albumin, extracellular polymer matrix, or other nutrients. The conditioning layer will influence which bacterial strain will act as primary colonizers and adhere to the surface first [64]. For example, fibronectin, fibrinogen, and fibrin have been shown to enhance the adherence of Gram positive cocci, Gram negative rods, and *Candida albicans* [65, 66].

### 3.1.2 Irreversible attachment

It is widely accepted that the bacteria become irreversibly attached to a surface through non-specific interactions such as electrostatic, hydrophobic, van der Waals forces and hydrogen bonds [67]. However, there is a growing evidence

that up- and down-regulation of a number of genes occurs in the attaching cells upon initial interaction with surface. Profound physiological changes may occur during transition from reversible to irreversible form of the attachment. As an example, *Pseudomonas putida* irreversible attachment has been shown to occur by switching from flagella-based motility to type IV pili-based twitching motility [68]. Another study has shown that adherent cells of *Staphylococcus epidermis* produce intercellular polysaccharide that bonds the cells to surface and each together and facilitates the formation of microcolonies [69].

### 3.1.3 Maturation of biofilm

The generation of the complex architecture characterizing mature biofilm has been shown to be under genetic control as well. Davies and Geesey demonstrated specific genes up-regulation in individual bacterial cells of *Pseudomonas aeruginosa* within minutes after attachment [70]. It was found that 22% of these genes were up-regulated in the biofilm state and 16% were down regulated [71]. DNA microarray result revealed that over 70 genes unexpressed in mature biofilms were genes encoding proteins involved in translation, metabolism, membrane transport, and gene regulation [72].

The regulation of gene transcription during biofilm growth is possible by the accumulation of signal molecules that orchestrate wide phenotypic responses through a process termed qourum sensing (QS). In this regard, QS is defined as a cell-density dependent bacterial signalling mechanism that enables bacteria to coordinate the expression of certain genes able to coordinate the collective group behaviour [73-75]. QS signals regulate a number of physiological processes, including swarming, bioluminescence, conjugated plasmid transfer, expressions of virulence factors and secretion of EPS [76, 77].

At first sight, EPS matrix (also known as glycocalyx or “slime”) is one of the most distinctive features of bioflms bacteria when compared to planktonic cells. The composition of the matrix may vary in chemical and physical properties,

depending upon the organisms present and environmental conditions, but it is primarily composed of water, which is believed to constitute approximately 95-99% of the biofilm. The bacterial content is only 2-5%, surrounded by exopolysaccharides that may reach up to 2% of the total matrix. In Gram-negative bacteria, some of these polysaccharides are neutral or polyanionic, whereas EPS in gram-positive bacteria may be cationic in nature. Other substances often found in the biofilm matrix include DNA, RNA, proteins and enzymes reaching levels of approximately 2% in total [45, 78].

### 3.1.4 Dispersal of biofilm

Biofilm cells may disperse either by shedding of daughter cells from actively growing cells, by detachment as a result of low nutrient levels or QS, or by shearing of biofilms aggregates (removal of small portions of the biofilm) because of flow effect. Therefore, biofilm formation may be cyclic in nature. Whereas the mechanism underlying the process of shedding by actively growing cells is not well understood, detachment of planktonic cells has been shown to be induced by alginate lyase expression in case of *Pseudomonas aeruginosa* [79, 80]. Studies on shearing of biofilm aggregates have emphasized the importance of physical forces in erosion-like detachment process [81, 82].

The mode of dispersal apparently affects the phenotypic characteristics of the bacteria. Eroded or sloughed aggregates from the biofilm are likely to retain certain biofilm characteristics, such as antibacterial resistance properties, whereas cells that have been shed as a result of growth may revert quickly to the planktonic phenotype [42].

## 3.2 Biofilm resistance to antibiotics

In former standard medicine paradigm, we used to look for bacterial infections by taking a few bacteria and putting them into a growth medium to see how they will grow. Antibiotics were then added to the growth medium to see

which ones are effective against the bacteria and what dose is needed. For early acute infection, this approach can be effective, however, what medicine has ignored is that bacteria that cause many IMD-related infections grown in biofilms.

The nature of biofilm structure and the physiological attributes of biofilm organisms confer an inherent resistance to antibiotics. It has been reported, that biofilm bacteria may exhibit antibiotic resistance three or more order in magnitude greater than those displayed by planktonic bacteria of the same strain depending on the species-drug combination [83-86]. The general consensus is that no single property of a biofilm can universally explain this heightened resistance, yet it is probably the manifestation of a number of factors [83, 85, 87-90]:

- delayed penetration of the antibiotics through biofilm matrix,
- nutrient limitation resulting in slowed growth rate of biofilm cells,
- phenotypic changes in bacteria resulting in resistance occur within the biofilm environment,

First two factors are related to mass transport phenomena. Antibiotics molecules must diffuse through the biofilm matrix in order to inactivate the encased cells. The extracellular polymeric substances have a potential to reduce the penetration of antibiotics either by physically slowing transport of the molecules to the biofilm interior or by chemical reaction. However, these subtle mechanisms are still the matter of controversy in the literature. E.g. delayed penetration of tobramycin and gentamicin (aminoglycosides) *into Pseudomonas aeruginosa* biofilm has been documented [91]. Contradictory to these findings, ofloxacin and ciprofloxacin (flouroquinolones) have been shown to readily diffuse through the biofilm of the same strain. Comparative study of of antibiotic penetration, oxygen limitation and metabolic activity suggested that both, oxygen limitation and metabolic activity are responsible for the increased antibiotics resistance rather than poor antibiotic penetration [92]. Due to nutrient limita-

tion, biofilm cells have slow growth rates in comparison to planktonic cells. As a result, biofilm cells take up antibiotics more slowly. Also, bacterial cells in biofilms constitute a heterogeneous population with varied growth rates in different compartments of the biofilm, and varied sensitivity to antibiotics. These hypothesis have been supported by several studies which demonstrated that the slowest growing biofilm bacteria cells were the most resistant to antibiotics such as cetrimide and ciprofloxacin [93, 94]. Additionally to these findings, older biofilms have been found to be significantly more resistant than younger [95, 96].

The third factor that contributes to the anibiotic resistance originates from the adaptability of biofilm bacteria. They may acquire new traits by either attaining a different phenotype within the biofilm due to heterogeneous growth conditions or at the genetic level by gene exchange or mutation. Contemporary studies emphasize phenotypic plasticity or the ability of bacteria to alter their phenotype in response to their immediate surroundings. As an example, plasmid conjugation rates in biofilm bacteria were three orders in magnitude higher than those in planktonic bacteria of the same species [97].

A simultaneous effect of all of these three factors results into a general protective function that favours survival of biofilm bacteria over planktonic under antibiotic exposure. This synergy is the main source of difficulty in treatment of biofilm related infections, thus, recent approaches to control biofilm growth have to be revised.

# 4 CONTROL OF IMD-RELATED INFECTION

With the better understanding of biofilm formation, the number of possible strategies leading to its eradication available in contemporary literature increases exponentially. According to the considerations presented in foregoing chapters, the field should be somewhat restricted and a most promising approach has to be selected with regard to the pathogenesis of IMD-related infections.

Although other strategies targeted to later biofilm formation stages have been proposed such as interference with the QS signal molecules modulating biofilm development [98, 99] or even enhanced penetration of antibiotics through biofilm matrix by using ultrasound waves or electric current has been considered [100, 101], it seems that the most effective would be avoiding of the initial bacteria attachment at the first, reversible, stage of biofilm formation [64]. This includes inhibition of bacterial adhesion to the surface and hindering of subsequent colonization. As bacterial adhesion to material being an essential step for the onset of biofilm formation and possible infection, a lot of works have been devoted to develop material that can inhibit initial bacterial attachment [102, 103]

Current efforts in this area have focused on imparting infection-resistant properties to materials via:

- minimization of bacterial adhesion by surface free energy modification [104, 105], control of surface hydrophobicity/hydrophilicity [106, 107], and surface charge modification [60, 61],
- creation of bactericidal surfaces by incorporation of anti-infective agents [108-111],

There are a lot of reports in the literature involving modification of surface energy and other surface related properties of biomaterials to minimize bacterial adhesion [26, 112-114]. Such surfaces are, however susceptible to fouling,

especially upon contacting physiological fluids that subsequently results in bacterial colonization and biofilm formation [115].

Despite the surface properties may improve the device performance, an active agent that inhibits bacterial growth is needed. Thus, such species as antibiotics and antibacterial and anti-viral compounds are used in the second approach. Surface treatment of IMDs such as catheters with antibiotics, for example, has been shown to lower incidence of infection [116, 117]. Nevertheless, its inability to eliminate resistant strains, coupled with the treat of spawning new ones, has limited their utilization. As the most effective approach has been preferred incorporation of anti-infective agents into the materials used in the medical device [118-120].

# 5 ANTIBACTERIAL POLYMER SYSTEMS

Antibacterial polymer system (APS) is a polymer based material system (blend or composite) that shows effective antibacterial properties with respect to specific applications. APS consist of a polymer matrix and active antibacterial additive that possess antibacterial properties at low concentration.

The basic requirements for antibacterial additives are the following:

- low toxicity to humans, animals, and the environment (i.e., safe for both, manufacturing process and under the conditions of use),
- easy application,
- compatibility with processing aids and other additives,
- no negative impact on the properties and appearance of the plastic article,
- storage stability and long-lasting efficacy,

## 5.1 Inorganic systems

In recent years, the use of inorganic antibacterial agents has attracted large interest for the control of micro-organisms. The key advantages of inorganic antibacterial agents over organic are improved safety and stability, which are lacking in organic antibacterial agents [122, 123].

Inorganic antibacterials utilise metal ions as their active biocidal agent, and once incorporated into the polymer matrix, these remain in-situ. The most commonly used metal ion is silver; other include copper and zinc. The metal ions are usually bound within a delivery system that stabilise them, allowing their incorporation into the polymer, and then releases them through a process of ion exchange at the plastics surface. Delivery systems on the market today include those relying on ceramic glasses, doped titanium dioxides, and even zeo-

lites as their carrier and release mechanisms. Inorganic systems tend to be much more thermally stable than their organic counterparts, although some are plagued by discolouration. However, this thermal stability enable a broad range of plastics (e.g. PO, ABS, PEEK, PET, PC, PU, PA, PMMA, EVA, and PVC) to benefit from these additives.

One of the most recently popular variations on the inorganic carriers are metal ion systems based around nanosized particles. These have primarily been developed to explore the possibilities that rapid ion release can offer (as a result of their high particulate aspect ratio). Obviously the active ingredient, the metal ion, remains the same, but coupled with this are adverse issues such as unquantified toxicity, excessive discolouration resulting from rapid oxidization and the increased complexities of producing nano-scale active grades [121].

### 5.1.1 Silver as antibacterial additive

The use of silver to control putrefaction of liquids and to mitigate the incursion and spread of disease can be traced to ancient times. Over these millennia, silver salts, complexes and the metal itself have been exploited for their medicinal properties, mostly empirically before the realization that bacteria were the agents of infection [124-127]. It is well known that Ag ions and Ag-based compounds are highly toxic to microorganisms [128, 129], having a broad-spectrum of antibacterial activity against Gram-positive and Gram-negative bacteria, fungi, protozoa and certain viruses [130], including antibiotic-resistant strains [131-134]. In fact, silver compounds such as silver nitrate, and silver sulfadiazine became the mainstay of antibacterial therapy until the introduction of antibiotics in the early 1940s [135-137]. However, the large increase in the number and occurrence of antibiotic-resistant bacterial strains has prompted a renewed interest in the use of silver as an antibacterial agent during last two decades [133].

The rapid development of nanotechnology accompanied with emerging of new synthesis routes for nanoparticles production has extended biomedical applications of silver and is currently used to reduce infections in the treatment of burned areas [138-141], to prevent bacterial colonization on medical devices [142-145] as well as in textile fabrics [146-149] and for water treatment [150, 151]. The most common method for producing silver nanoparticles is chemical reduction of a silver salt dissolved in water with reducing compound such as citrate, glucose, hydrazine, and ascorbate. Since reducing agents for silver nanoparticles synthesis are often conersidered to be toxic or hazardous, green synthesis methods which utilized polysaccharides, polyphenols, Tollens agent, polyoxometalate, irradiation, and biological reduction are gaining increasing importance [152-158].

Silver is thought to disable bacterial cells at the first stage of biofilm formation by acting on them by any or all three of the following mechanisms, and this multiplicity of action results in a strong biocidal effect [142, 151]:

- destruction of microorganisms by oxidation catalyzed by silver,
- disruption of electron transfer in bacteria by monovalent silver, and/or preventing the unwinding of DNA in viruses with the substitution of hydrogen ions by monovalent silver,
- destruction of bacteria and viruses by bivalent and trivalent silver,

However, any form of silver additive appears to be ineffective once a mature biofilm covers the surface of device [159].

### 5.1.2 Zinc oxide as prospective antibacterial additive

Zinc oxide is a versatile, multifunctional material with unique properties. It has been extensively used in several industrial products, such as ceramics, rubber additives, pigments, personal cares, medicines. [160-162]. Furthermore, ZnO as a wide-band gap ($E$g = 3.37 eV at 300 K) semiconductor with a large excitation binding energy (60 meV) has gained wide attention for its potential appli-

cations in light emitting diodes, data storages, gas sensors, or catalyst supports [163-165].

Generally, keep apart unique inherent properties, the interest in metal oxides stems from ease of preparation particles with extremely high surface areas and with unusual crystal morphologies that possess numerous edge/corner and other reactive surface sites, because the size and the morphology have great effects on its properties [166]. Indeed, many different-shaped ZnO structures in nano- or microscale have been reported so far, wire-like [167-169], rod-like [170, 171], belt-like [168, 169, 172], flower-like [173, 174], tubular [173, 175], prismatic [176], comb-like [177, 178], etc. Various different approaches have also been applied to synthesize these ZnO structures, such as thermal evaporation method [179], hydrothermal process [180], non-aqueous approach [181], chemical vapor deposition (CVD) [182], sol-gel process [183], gas condensation [184], laser ablation [185], template-assisted growth [186], refluxing method [187], or microwave heating [188].

The research on ZnO as an antibacterial material had already started as early as 1950s [189]. Since then, more and more researchers have paid attention to the fundamental studies on the antibacterial activities of the metal oxides. The real move toward the use of ZnO as an antibacterial agent was in 1995, when Sawai and his colleagues found that MgO, CaO and ZnO powders have antibacterial activities against some bacteria strains. Among these ceramics, ZnO exhibits strong antibacterial activity against Gram-positive bacteria (Staphylococcus, Streptococcus, Enterococcus) [190]. ZnO has several advantages; showing a strong antibacterial activity in neutral region (pH 7) and being a mineral element essential to human being. Therefore, many reports have been devoted to antibacterial activity of ZnO [191-205] . Factors related to the antibacterial activities have been investigated, such as the concentrations of the metal oxides particles [190, 192, 204], the particle size of the metal oxide powder [204, 205], and the specific surface area of the powder [196].

In general, the following four factors may affect the antibacterial activity of ceramic powders [193]:

- the cations eluted from powder,
- active oxygen generated from powder,
- the pH value,
- the mechanical destruction of cell membrane,

Nevertheless, the mechanisms of the antibacterial activity of ZnO particles are not fully understood although Sawai et al. [199, 202, 203] proposed that the generation of hydrogen peroxide may be a main factor of the antibacterial activity, while Stoimenov et al. indicated that the binding of the particles on the bacteria surface due to the electrostatic forces could be a mechanism [206]. According to my best knowledge there are no studies on ZnO effects on biofilms in recent literature. The complex behavior of this compound gives opportunity to find new effects on biofilm forming bacteria.

# 6 AIMS OF WORK

The aim of the present work is to contribute to the field of biomedical applications of composite materials possessing antibacterial activity. According to the literature review and the experience that has been gained during the doctoral studies, development of a new antibacterial inorganic/polymer system for biomedical application has been set as the main aim for this thesis.

The main goal of this dissertation has been subdivided into following goals that may yield original scientific results:

- Adoption of microwave-assisted hydrothermal synthesis of ZnO and other zinc based compounds possessing antibacterial activity and understanding the basic mechanisms of crystal growth
- Tailored preparation of ZnO and zinc based particulate compounds of different morphologies, synthesis of Ag/ZnO hybrid fillers for prospective antibacterial polymer systems
- Optimization of compounding process, manufacturing of composites by incorporation of prepared powders into model medical PVC
- Evaluation of assays available for the testing of antibacterial activity and selection of proper method, quantitative assessment of surface antibacterial activity of prepared composite materials, characterization of the influence of used filler parameters on the final performance of the composite

# 7 METHODOLOGY

## 7.1 Materials

Zinc acetate dihydrate $Zn(CH_3COO)_2.2H_2O$, zinc sulphate monohydrate $ZnSO_4.H_2O$, hexamethylenetetramine $(CH_2)_6N_4$ were all supplied by PENTA (Czech Republic). Medical grade PVC RB3 was delivered by Modenplast (Italy). Distilled water was used throughout all experiments.

Nutrient Broth w/1% Peptone, Nutrient Agar No. 2, Soyabean Casein Digest Medium and TWEEN 80 was purchased by HIMEDIA (India). Lecithin natural was received from Mogador (Czech Republic). All chemicals and ingredients mentioned were used without further purification

## 7.2 Fillers synthesis

Zinc oxide (ZnO) of different morphology, zinc hydroxide acetate (ZHA), and Ag/ZnO particulate fillers were prepared via microwave-assisted hydrothermal synthesis in modified microwave open vessel system MWG1K-10 (RADAN, Czech Republic; 1.5 kW, 2.45 GHz) operated in continuous mode (zero idle time, maximum power) with the temperature monitored by an industrial contactless thermometer (Raytek CM, Germany).

Specific details on synthesis and post-treatment procedures can be found in the experimental sections of included papers.

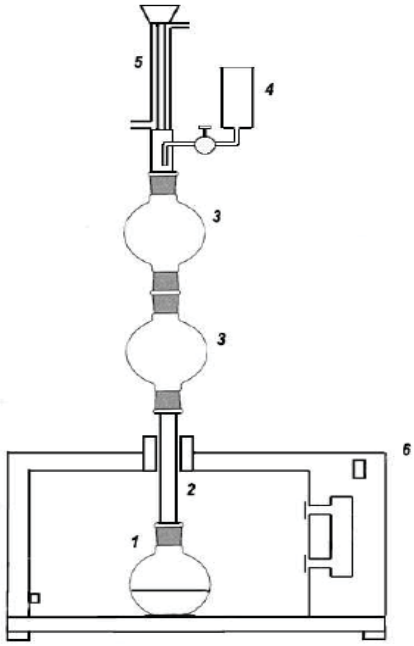


**Figure 1.** Modified MW-reactor: 1-reaction bottle, 2-extension tube, 3 defoamig flask, 4-dropping funnel, 5-external cooler, 6-MW-oven [own resource]

## 7.3 Composites preparation

For composites preparation, melt mixing was chosen as appropriate method. Composites were prepared by incorporation of fillers in concentration ranging from 0.5-5 wt % into plasticized PVC matrix in the Brabender measuring mixer W50 EHT PL. Sheets 1 mm in thickness were produced by hot press procedure. Obtained sheets were characterized by common instrumental methods and used for testing of antibacterial activity, mechanical and/or dielectric properties.

## 7.4 Characterisation

A lot of instrumental methods are available nowadays for characterization of inorganic particulates. The characterization methods employed was chosen carefully with respect to aims of work and are listed below, including methods applied for testing of composites materials made thereof.

*X-ray diffraction (XRD)* analysis for the phase identification of prepared fillers and PVC composites was conducted on the multi-purpose X-ray diffractometer X´Pert PRO MPD (PANalytical, The Netherlands) with a Cu-Kα X-ray source ($\lambda$ = 1.5418 Å).

*Scanning electron microscopy (SEM)* was used to investigate the morphologies of fillers (Vega II/LMU, Tescan, Czech Republic). SEM examination was also performed onto composites fractured surfaces in order to evaluate the degree of homogeneity and to gain insight into composites internal structure.

*Thermogravimetric analysis (TGA)* was carried out on the thermogravimeter Q500 (TA instruments, United States) to obtain information about purity of prepared fillers and thermal decomposition profile.

*Mechanical properties* (Young's modulus, tensile strength) of composites were evaluated using the Testometric universal-testing machine M 350-5CT (LABOR machine, Czech Republic) according to the ISO 527-2:1996.

*Electrical properties* were measured by the use of the four-point van der Pauw at the room temperature on the Electrometer/High resistance Meter KEITHLEY 6517B.

## 7.5 Testing of antibacterial activity

The antibacterial activity of prepared composites was assessed against *Escherichia coli* ATCC 8739 and *Staphylococcus aureus* ATCC 6538P ( Czech Collection of Microorganisms, Czech Republic) according ISO 22196: 2007 (E) with slight modification. The results expressed in terms of antibacterial activity value *R* enable quantitative assessment of antibacterial activity on plastics surfaces.

As the testing of antibacterial activity present probably the most important part of work, description of this standard assay for evaluation of antibacterial activity on plastic surfaces is given in brief. First, a test inoculum was prepared by transferring one loop of the pre-incubated bacteria into a small amount 1/500 diluted nutrient broth so that the bacteria concentration was in between $2.5 \times 10^5$ and $10 \times 10^5$ cells /mL. The test specimens (three specimens treated and three untreated) with dimensions 50 mm x 50 mm x 1 mm were placed in Petri dishes and inoculated by 0.4 mL of the test inoculum. Inoculated specimens surface was covered with thin piece of polypropylene film (40 mm x 40 mm) and pressed down gently so that test inoculum spread to the edges. After incubation for 24 h at 35 °C under humid condition (95 %), test inoculum remaining on covers film and test specimen was completely recovered by 10 mL of SCDLP broth (prepared by adding 1 g of lecitin and 7 g of polysorbate per liter of Tryptone Soya Broth). Recovered SCDLP broth was 10-fold serial diluted in phosphate-buffered physiological saline and 1 mL of each dilution was placed together with 1 mL of undiluted recovered SCDLP into separate Petri dishes. Than, 15 mL of plate count agar was poured into each Petri dish, swing gently to disperse bacteria and incubated for 48 h at 35 °C under humid condition (95 %). After incubation, the number of colonies was counted in the Petri dishes containing from 30 – 300 colonies and the number of viable bacteria recovered was determined according Eq. 1.

$$N = (100 \times C \times D \times V)/A, \quad (1)$$

where,

N is the number of viable bacteria recovered per $cm^2$ per test specimen;

C is the average plate count for the duplicate plates;

D is the dilution factor for the plates counted;

V is the volume, in, mL, of SCDLP added to the specimen

The results are expressed in terms of the antibacterial activity R, which is defined as the difference in the logarithm of the viable cell count found on an antibacterial-treated sample and an untreated sample after inoculation with an incubation of bacteria

$$R=(U_t-U_0)-(A_t-U_0)=U_t-A_t, \quad (2)$$

where,

R is antibacterial activity;

$U_0$ is the average of the common logarithm of the number of viable bacteria, in cells/$cm^2$, recovered from the untreated test specimens immediately after inoculation;

$U_t$ is the average of the common logarithm of the number of viable bacteria, in cells/$cm^2$, recovered from the untreated specimens after 24 h;

$A_t$ is the average of the common logarithm of the number of viable bacteria, in cells/$cm^2$, recovered from the treated test specimens after 24 h.

At this point, we have omitted evaluation of the number of viable bacteria recovered from the untreated test specimens immediately after inoculation because of extensiveness of the experiments and the value of the antibacterial activity R was determined simply according

$$R=U_t-A_t, \quad (3)$$

# 8 SUMMARY OF RESULTS

The doctoral thesis is focused on preparation of composite materials possessing antibacterial properties. First part of the experimental work is devoted to the development of microwave-assisted hydrothermal synthesis technique for preparation of zinc oxide and zinc oxide based fillers of different morphologies. Microwave heating offers several advantages in comparison to conventional heating such as rapid and selective heating, higher reaction rates, and energy savings. During these studies, basic understanding of ZnO chemistry and the process of ZnO crystal growth was obtained and the results are summarized in **Paper I** and **II**. In the second part of the work, prepared fillers were compounded with medical grade plasticized PVC matrix and tested against representatives of both Gramm-positive and Gramm-negative bacteria by use of the standard ISO 22196. This standard assay for measurements of antibacterial activity on plastic surfaces enables not only qualitative, but also quantitative assessment of antibacterial performance of ZnO based fillers in model PVC composites as presented in P**aper III** and **IV**.

*****

In the first article (**Paper I)**, microwave assisted synthesis, a powerful tool in modern inorganic chemistry, was adopted to drive precipitation reaction of zinc acetate dihydrate and hexamethylenetetramine from relatively concentrated solutions at mild pH. Zinc oxide particles with specific morphology of twinned frustums shown in Figure 2.b can be obtained with the use of MW assisted synthesis with all its advantages. The reaction time is shortened from tens of hours up to tens of minutes in comparison with conventional hydrothermal methods. Moreover, if needed, the developed method allows synthesizing of well crystallized layered basic zinc acetate (LBZA) material shown in Figure 2.a in even shorter synthesis time too just by stopping the procedure in its early stage after 2 minutes.

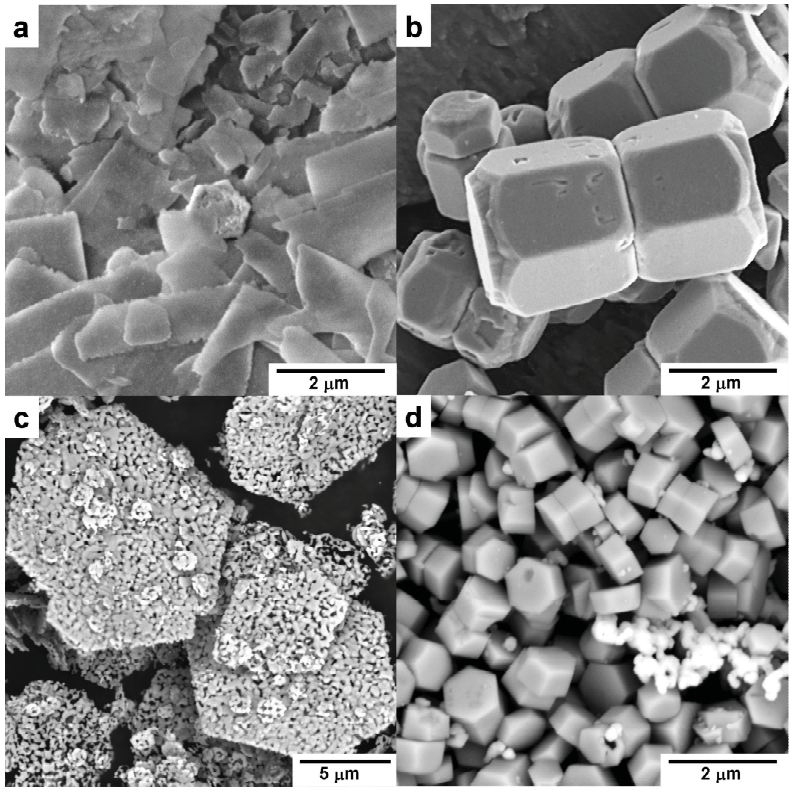


**Figure 2.** SEM image sof prepared fillers. a) layered LBZA materials [Paper I], b) ZnO particles [Paper I], c) ZnO mesh-like porous particles [Paper II], d) hybride Ag-ZnO material [Paper IV].

Time-lapse series of samples was synthesised by repeating the experiment under the same condition but with prolonging time, so that an interval from 2 to 60 minutes of the synthesis time was covered sufficiently by samples of product prepared in reasonable amounts. In order to understand the formation process of ZnO crystals, characterization of obtained samples was performed by powder X-ray diffraction (XRD), scanning electron microscopy (SEM), thermogravimetric analysis (TGA) and attenuated total reflection Fourier transform infrared spectroscopy (ATR-FTIR).

**Figure 3.** Time evolution of normalised intensity of selected peaks in the diffractograms of obtained samples. Full squares represent the most intensive reflection 101 for ZnO phase at 2θ = 36.2°; hollow circles correspond to the most intensive (first order) reflection 001 for LBZA phase at 2θ = 6.6°. [Paper I]

Analysis of results obtained with the help of these complementary instrumental techniques revealed the mechanism of crystal growth mechanisms under given condition of the mild pH and MW exposure. The use of zinc acetate salt contributes to a buffer system formation during the synthesis. Although HMTA serves as the source of hydroxyl anions and ammonium cations, the hydroxyl groups are built in the structure of the precursor (LBZA) during its formation while ammonium cations and acetate anions are involved in the complex equilibrium of hydrolysis reactions responsible for the buffering effect of a weak acid – weak base salt solution in the reaction system. It was confirmed, that the mechanism of ZnO formation does involve neither $Zn(OH)_2$ phase nor direct ZnO phase formation as observed elsewhere for single source methods or for precursors with non-hydrolysing anions like ZnCl or $ZnNO_3$. It is the intermediate prod-

uct LBZA, which precipitates first in the system during the first stage of the process, and is subsequently transformed into ZnO. The phase transformation of LBZA to ZnO proceeds rapidly within the fifth and sixth minute of the synthesis which represents the second stage of the process. The last, third, stage of the process is characterised by the maturation of ZnO particles involving their re-crystalisation and densification after seventh minute. The three stages are clearly observable in the Figure 3.

Moreover, the joint XRD, FTIR and TGA study contributed to the elucidation of the LBZA structure. It was established that acetate anion is not directly bonded to the zinc atom in the layered structure, but that it is in coordination state of a free anion in the interlayer galleries of the LBZA compound compensating the positive charge of the brucite-like layers. In other words, the material synthesised within two minutes (the S2 sample) is actually a dihydrate and the chemical formula should be better written as $[Zn_3(OH)_8Zn_2(H_2O)_2](CH_3CO_2)_2.2H_2O$ rather than $Zn_5(OH)_8(CH_3CO_2)_2.4H_2O$ forcing an improper notion of the compound being a tetrahydrate. Consistently, the formula $[Zn_3(OH)_8Zn_2(H_2O)_2](CH_3CO_2)_2$ has to be used instead of wrong $Zn_5(OH)_8(CH_3COO)_2.2H_2O$ as this compound is not a hydrate in the strict sense of that term at all.

*****

In the second article (**Paper II**), the main attention has been paid to preparation of ZnO powder with a two dimensional morphology of mesh-like hexagonal microplates. The research was motivated by searching of microparticles with hierarchical nanostructure developed on mesoscale which should assure the good properties of microparticulate powder as well as to impart the features of the nanosize to the material. With better understanding of zinc oxide chemistry and ZnO crystal process growth, two step synthesis via precursor was employed, as it is rather difficult to prepare ZnO with two dimensional morphology without any capping or directing agents that can adversely affect the surface chemistry of resulted ZnO crystals. In the first step, layered precursor material identified

as combination of zinc hydroxide sulphate tetra- and pentahydrate with very well developed crystalline structure was obtained via MW-assisted hydrothermal precipitation of zinc sulphate monohydrate by hexamethylenetetramine within the very short time of three minutes. The bonding configuration of the sulphate anion ($SO_4^-$) was identified as a bridging coordination type from the obtained well-resolved IR absorption spectra. Based on the interpretation of temperature decomposition profile obtained by an otherwise routine TGA investigation, porous mesh-like ZnO hexagonal porous plates shown in the Figure 2.c was prepared by calcination of the precursor material at 900°C for 2 hours. Porous ZnO phase was found to be developed from the zinc hydroxide sulphate precursor at the expense of mass removal due to the release of water and sulphate during the calcination. Moreover, it was found that the mechanism of conversion is topotactic as prepared ZnO kept the original shape of the precursor's crystals.

*****

The study presented in the **Paper III** showed that the antibacterial effect of ZnO based materials is strongly depended on their particle morphology. Material LBZA and ZnO from the study in **Paper I** and the mesh-like ZnO material described in **Paper II** were investigated as prospective inorganic fillers for design of new antibacterial polymer systems with enhanced properties.

In order to asses the efficacy of synthesized fillers, a model composite material was required, as it is the surface antibacterial activity which is the key performance factor for the medical materials as emphasized in the previous parts of the thesis. Plasticized PVC is the most widely used plastic in medical device applications because of its bio- and hemocompatibility, transparency, flexibility, durability, sterilizability and low cost. Typical medical products made thereof including blood bags and tubing, gloves, dialysis equipment, catheters, or device packaging. Therefore, medical grade PVC was used as polymer matrix for incorporation of zinc based antibacterial fillers and antibacterial activity on plastic surface of prepared composites was evaluated.

Although ZnO is strain specific and performs more against representative gram negative bacteria than against gram positive bacteria, the two best composite materials based on the medical grade flexible PVC compounded with the prepared filler with the two dimensional mesh-like porous hexagonal plate morphology (denoted as ZnO **2** in the **Paper III** and identical with the material obtained in **Paper II**) were shown as excellent antibacterial polymer system with considerable surface antibacterial activity value higher than 6 against *Escherichia coli* and higher than 5 against *Staphylococcus aureus* which represents in other words $10^6$x and $10^5$x respectively reduction of viable cells in comparison to untreated PVC.

**Table 3**. Summary of surface antibacterial activity against *E. coli* and *S. aureus* evaluation for prepared composite materials. [Paper III]

| Filler content | R – value for *E. coli* | | | R – value for *S. aureus* | | |
|---|---|---|---|---|---|---|
| [wt%] | [-] | | | [-] | | |
| | Filler code | | | Filler code | | |
| | ZHA | ZnO **1** | ZnO **2** | ZHA | ZnO **1** | ZnO **2** |
| 0.5 | 4.0 | 1.2 | > 6.6 | 1.8 | 0.9 | 0.2 |
| 1 | 4.5 | 3.6 | > 6.6 | 1.8 | 2.4 | 2.3 |
| 2 | 4.6 | 3.5 | > 6.6 | 1.9 | 2.4 | > 5.1 |
| 5 | 5.4 | 5.2 | > 6.6 | 2.5 | 3.3 | > 5.1 |

In next, almost all prepared composite materials were found as efficient for less demanding applications in plastic products for hygiene, household and public interiors etc. according to the weaker criterion of minimal antibacterial activity being at least 2 which was required by previous standard JIS Z 2801:2000 (E). All results of surface antibacterial activity tests are summarised in Table 3.

It is noteworthy, that prepared fillers consist of nanostructured particles with the overall particle size greater than one micrometer and behaves like common powders which make them unproblematic for mixing with plastics avoiding all technical difficulties usually related to the nanoparticles. Besides, the filler and the mixing procedure demonstrated no adverse effect on good mechanical properties of the used medical grade PVC. These facts suggest that studied ZnO based nanostructured microfillers, namely ZnO **2**, have potential in medical plastics industries as additive materials for PVC medical devices.

As the final conclusion derived from investigation presented in the **Paper III**, a general rule for proneness of the inorganic nanostructured microparticles to be efficient as antibacterial additives can be formulated. The ideal inorganic nanostructured microparticle intended for being used as antibacterial filler has to have the lowest ratio between envelope and true material density as possible to maximize the particle-matrix interface area and to assure the shortest average distance between particles at given filler concentration.

*****

Another approach to the efficacy of antibacterial systems based on inorganic ZnO filler was applied in **Paper IV**. The well known antibacterial activity of metallic silver nanoparticles offers possibility to improve the filler material performance by simply being co-precipitated within one synthesis step with the ZnO- Moreover, synergic effects are expected to be manifested in such hybrid metal/semiconductor material.

Hybrid Ag/ZnO (silver/zinc oxide) nano-structured microparticles were obtained via the fast and simple microwave assisted synthesis developed and presented in previously discussed works. Similarly as in Paper I, the soluble zinc acetate and HMTA was employed with addition of silver nitrate. HMTA has two roles in this system. It is not only a precipitating agent but also a reducing agent as it releases formaldehyde besides hydroxide anions during its thermal decomposition. The phase structure of filler particles was revealed by X-ray diffracto-

metry and identified as pure face-centered-cubic Ag metal and wurtzite ZnO phase without other impurities. The scanning electron microscopy was used for morphology characterization and elemental analysis of the prepared filler. A representative image is shown in Figure 2.d. The grey twinned hexagonal frustums are ZnO and the white spherical particles are metallic silver particles.

Medical grade Poly (vinyl chloride) (PVC) was selected as the representative polymer for the antibacterial polymer system's matrix similarly as in **Paper III**. Although a lot of effort has been made to replace PVC in biomedical applications, it still remains the most used polymer in medical device fabrication. Applications of PVC include blood bags and tubing, intravenous containers and components, catheters, dialysis equipment, examination gloves inhalation masks and other generally known uses.

Composites with medical-grade PVC were prepared with filler concentration from 1 to 5 wt. %. The mechanical properties of composites were tested and it was found that the compounding process as well as the used fillers does not deteriorate the properties of the original already optimised PVC matrix. The hybrid Ag/ZnO powder has very good electrical conductivity, therefore the electrical resistivity of prepared composited had to be verified and it was found to be about $10^7$ Ω cm, which is a suitable range for medical device application.

For APS, not only the antibacterial properties of the selected combination of fillers are important but the whole system including the polymer matrix must assure a reasonable release rate of the active species to the surface of the plastic article. The surface antibacterial performance of the prepared composite was tested according to ISO 22196: (2007) against *E. coli* and *S. Aureus*. A quantitative assessment of the antibacterial activity of the tested samples was performed, and the R-values are shown in Table 4. The value of the antibacterial activity R of the composite against E. coli is very high, of about 6.6 for all (1, 3, 5 wt. %) concentrations of filler in the PVC matrix. The antibacterial activity of the composite against S. aureus is lower, but it is still high enough for 3 and 5

wt. % of the filler in PVC, as the critical R-value should not be less than 2.0 for materials that can be categorized as having an effective antibacterial surface.

**Table 4** Antibacterial activity of Ag/ZnO/PVC composites tested according to the modified ISO 22196:2007 (E) [Paper IV]

| Concentration of the Ag/ZnO filler in polymer | Antibacterial activity (Log CFU) *E. coli* | Antibacterial activity (Log CFU) *S. aureus* |
|---|---|---|
| (wt %) | $R = U_t - A_t$ | $R = U_t - A_t$ |
| 0[a] | $U_t = 6.6$ | $U_t = 5.3$ |
| 1 | 6.6 | 1.8 |
| 3 | > 6.6 | 4.0 |
| 5 | 6.6 | 3.5 |

[a] zero concentration represents the reference neat PVC sample

It can be summarised, that the composite material based on the medical grade flexible PVC compounded with the prepared Ag/ZnO filler was shown as an effective Antibacterial Polymer System with a surface activity excellent against Escherichia coli and sufficient against Staphylococcus aureus. Besides, the composite demonstrated suitable electrical and mechanical properties with respect to its utilization in medicine in contact with a patient's body. These facts suggest that the prepared PVC composite has potential in medical plastics industries as a material for medical devices.

# 9 CLOSING REMARKS

## 9.1 Conclusions and contribution to science and technology

The work contributes to the general knowledge as well as to technology according to the goals as follows:

- Novel microfillers nanostructured on mesoscale introduce a new concept into the field of composite and science and technology.
- Three ZnO based fillers and one hybrid Ag/ZnO filler were originally developed for novel efficient antibacterial polymer systems using medical grade PVC matrix. These materials perform very well against *E. coli* and *S. aureus*.
- The formation mechanism of ZnO based fillers during microwave assisted synthesis was described and explained.
- The bonding coordination types of sulphate and acetate anions in layered basic zinc hydroxide salts were revealed.

Imparting the understanding of the reaction and crystal growth mechanisms and further development of the MW assisted solvothermal methods of ZnO and hybrid Ag/ZnO materials synthesis will contribute to the environmental sustainability due to the enormous decrease of the synthesis time, energy and possibly material savings as well as it will conduce to the development of high performance functional materials as demonstrated on the development of novel antibacterial polymer systems.

## 9.2 Future prospective

The results of the work can be used in material design for medical plastics. Conceptual directions are laid out in the synthesis of mesoscale nanostructured microfillers as well as a rule for morphology design of such particles was formulated pointing toward maximum antibacterial performance of the composites made thereof.

The improvement of antibacterial activity against *Staphyloccocus aureus* still remains as a challenge rather than closed chapter in current research.

## REFERENCES


1. SHI, D. *Biomaterials and tissue engineering*. Biological and medical physics, biomedical engineering, 1618-7210. Berlin ; New York: Springer, 2004. xi, 246 p. ISBN 3540222030.
2. WILLIAMS, D.F.; CUNNINGHAM, J. *Materials in clinical dentistry*. Oxford: OUP, 1979. 376p. ISBN 0192670077.
3. PARK, J.B. *Biomaterials science and engineering*. New York ; London: Plenum, 1984. xv,459p. ISBN 0306416891 : No price.
4. WILLIAMS, D.F. *Definitions in biomaterials : proceedings of a Consensus Conference of the European Society for Biomaterials, Chester ... 1986*. Progress in biomedical engineering ; 4. Amsterdam: Elsevier, 1987. 72p. ISBN 0444428585.
5. WISE, D.L. *Encyclopedic handbook of biomaterials and bioengineering*. New York: Marcel Dekker, 1995. xv,974p. ISBN 0824795938.
6. BHAT, S.V. *Biomaterials*. Boston, Mass. ; London: Kluwer Academic, 2002. xii, 265 p. ISBN 0792370589.
7. RATNER, B.D. *Biomaterials science : an introduction to materials in medicine*. 2nd ed. Amsterdam ; London: Elsevier Academic Press, 2004. xii, 851 p. ISBN 0125824637.
8. LOBO, H.; BONILLA, J.V. *Handbook of plastics analysis*. New York, N.Y.: Marcel Dekker, 2003. viii, 650 p. ISBN 0824707087.
9. MCNAUGHT, A.D.W., A. *IUPAC. Compendium of Chemical Terminology*. 2nd ed.: Blackwell Scientific Publications, Oxford, 1997. ISBN 0-9678550-9-8.
10. OSSWALD, T.A.; MENGES, G. *Materials science of polymers for engineers*. 2nd ed. Munich: Hanser Publishers ; Cincinnati : Hanser Gardner Publications, 2003. ISBN 1569903484.
11. BOLGAR, M. *Handbook for the chemical analysis of plastic and polymer additives*. Boca Raton, Fla.: CRC ; London : Taylor & Francis [distributor], 2008. xvi, 481 p. ;. ISBN 9781420044874.
12. DENSTEDT, J.D.; WOLLIN, T.A.; REID, G. Biomaterials used in urology: Current issues of biocompatibility, infection, and encrustation. *Journal of Endourology*, 1998. Vol. 12, No. 6, p. 493-500. ISSN 0892-7790.
13. WOOLFSON, A.D.; MALCOLM, R.K.; GORMAN, S.P.; JONES, D.S.; BROWN, A.F.; MCCULLAGH, S.D. Self-lubricating silicone elastomer biomaterials. *Journal of Materials Chemistry*, 2003. Vol. 13, No. 10, p. 2465-2470. ISSN 0959-9428.
14. LAMBA, N.M.K.; WOODHOUSE, K.A.; COOPER, S.L.; LELAH, M.D.P.I.M. *Polyurethanes in biomedical applications*. Boca Raton ; London: CRC, 1998. 277p. ISBN 0849345170.
15. DENSTEDT, J.D.; REID, G.; SOFER, M. Advances in ureteral stent technology. *World Journal of Urology*, 2000. Vol. 18, No. 4, p. 237-242. ISSN 0724-4983.
16. WIRONEN, J.; MAROTTA, J.; COHEN, M.; BATICH, C. Materials used in urological devices. *Journal of Long-Term Effects of Medical Implants*, 1997. Vol. 7, No. 1, p. 1-28. ISSN 1050-6934.
17. WILKES, C.E.; SUMMERS, J.W.; DANIELS, C.A.; BERARD, M.T. *PVC handbook*. Munich ; Cincinnati: Hanser, 2005. xxvi, 723 p. ISBN 3446227148.

18. LAMBERT, B.J.; ROGERS, W.J.; TANG, F.W. *Polymers in medical applications*. Rapra review reports, 11,7. Shawbury, Shrewsbury: Rapra Technology Ltd., 2000. ISBN 1859572596 9781859572597.

19. PACE, J.L.; RUPP, M.; FINCH, R.G. *Biofilms, infection, and antimicrobial therapy*. Boca Raton ; London: Taylor & Francis, 2006. 494 p. ISBN 9780824726430.

20. HTTP://WWW.13485QUALITY.COM/ISO-13485-STANDARD-SCOPE-AND-APPLICATION/58-ISO-13485-STANDARD-SCOPE-AND-APPLICATION-/102-ISO-13485-STANDARD-TERMS-AND-DEFINITIONS-REQUIRE.HTML. [cit. >.

21. NAAMA, D.; MATHILDA, M.; ZADIK, H.; GAD, L., *Advances in Microbial Biofilm Prevention on Indwelling Medical Devices with Emphasis on Usage of Acoustic Energy*. 2009, Molecular Diversity Preservation International.

22. PEARSON, M.L. Guideline for prevention of intravascular-device-related infections. *Infection Control and Hospital Epidemiology*, 1996. Vol. 17, No. 7, p. 438-473. ISSN 0899-823X.

23. SUGARMAN, B. Infections and Prosthetic Devices. *American Journal of Medicine*, 1986. Vol. 81, No. 1A, p. 78-84. ISSN 0002-9343.

24. DONLAN, R.M. Biofilm Formation: A Clinically Relevant Microbiological Process. *Clinical Infectious Diseases*, 2001. Vol. 33, No. 8, p. 1387-1392.

25. DONLAN, R.M.; COSTERTON, J.W. Biofilms: Survival mechanisms of clinically relevant microorganisms. *Clinical Microbiology Reviews*, 2002. Vol. 15, No. 2, p. 167-+. ISSN 0893-8512.

26. RICHARDS, J.J.; MELANDER, C. Controlling Bacterial Biofilms. *ChemBioChem*, 2009. Vol. 10, No. 14, p. 2287-2294.

27. DAVEY, M.E.; O'TOOLE, G.A. Microbial Biofilms: from Ecology to Molecular Genetics. *Microbiol. Mol. Biol. Rev.*, 2000. Vol. 64, No. 4, p. 847-867.

28. WALSH, C. Where will new antibiotics come from? *Nat Rev Micro*, 2003. Vol. 1, No. 1, p. 65-70.

29. FINCH, R. Bacterial resistance—the clinical challenge. *Clinical Microbiology and Infection*, 2002. Vol. 8, p. 21-32.

30. CHOPRA, I.; HESSE, L.; O'NEILL, A.J. Exploiting current understanding of antibiotic action for discovery of new drugs. *Journal of Applied Microbiology*, 2002. Vol. 92, p. 4S-15S.

31. OVERBYE, K.M.; BARRETT, J.F. Antibiotics: Where did we go wrong? *Drug Discovery Today*, 2005. Vol. 10, No. 1, p. 45-52.

32. COSTERTON, B.; COOK, G.; SHIRTLIFF, M.; P.STOODLEY; M.PASMORE, *Biofilms, Biomaterials, and Device-Related Infections*, in *Biomaterial science: an introduction to materials in medicine*. 2004, Elsevier Academic Press. p. 345-354. ISBN 978-0-12-582463-7.

33. MARRIE, T.J.; NELLIGAN, J.; COSTERTON, J.W. A scanning and transmission electron microscopic study of an infected endocardial pacemaker lead. *Circulation*, 1982. Vol. 66, No. 6, p. 1339-1341.

34. MARRIE, T.J.; COSTERTON, J.W. Scanning and transmission electron microscopy of in situ bacterial colonization of intravenous and intraarterial catheters. *J. Clin. Microbiol.*, 1984. Vol. 19, No. 5, p. 687-693.

35. KHOURY, A.E.; LAM, K.A.N.; ELLIS, B.; COSTERTON, J.W. Prevention and Control of Bacterial Infections Associated with Medical Devices. *ASAIO Journal*, 1992. Vol. 38, No. 3, p. M174-M178. ISSN 1058-2916.

36. RADD, I.; COSTERTON, W.; SABHARWAL, U.; SACILOWSKI, M.; ANAISSIE, E.; BODEY, G.P. Ultrastructural Analysis of Indwelling Vascular Catheters - a Quantitative Relationship between Luminal Colonization and Duration of Placement. *Journal of Infectious Diseases*, 1993. Vol. 168, No. 2, p. 400-407. ISSN 0022-1899.

37. STICKLER, D.; MORRIS, N.; MORENO, M.C.; SABBUBA, N. Studies on the formation of crystalline bacterial biofilms on urethral catheters. *European Journal of Clinical Microbiology & Infectious Diseases*, 1998. Vol. 17, No. 9, p. 649-652. ISSN 0934-9723.

38. BANDYK, D.F.; ESSES, G.E. Prosthetic Graft Infection. *Surgical Clinics of North America*, 1994. Vol. 74, No. 3, p. 571-590. ISSN 0039-6109.

39. STICKLER, D.J. Bacterial biofilms and the encrustation of urethral catheters. *Biofouling*, 1996. Vol. 9, No. 4, p. 293-305. ISSN 0892-7014.

40. DONLAN, R.M. Biofilms and device-associated infections. *Emerging Infectious Diseases*, 2001. Vol. 7, No. 2, p. 277-281. ISSN 1080-6040.

41. AN, Y.H.; FRIEDMAN, R.J. Prevention of sepsis in total joint arthroplasty. *Journal of Hospital Infection*, 1996. Vol. 33, No. 2, p. 93-108. ISSN 0195-6701.

42. DONLAN, R.M. Biofilms: Microbial life on surfaces. *Emerging Infectious Diseases*, 2002. Vol. 8, No. 9, p. 881-890. ISSN 1080-6040.

43. SOCRANSKY, S.S.; HAFFAJEE, A.D.; CUGINI, M.A.; SMITH, C.; KENT, R.L. Microbial complexes in subgingival plaque. *Journal of Clinical Periodontology*, 1998. Vol. 25, No. 2, p. 134-144. ISSN 0303-6979.

44. COSTERTON, J.W.; STEWART, P.S.; GREENBERG, E.P. Bacterial Biofilms: A Common Cause of Persistent Infections. *Science*, 1999. Vol. 284, No. 5418, p. 1318-1322.

45. VU, B.; CHEN, M.; CRAWFORD, R.J.; IVANOVA, E.P. Bacterial Extracellular Polysaccharides Involved in Biofilm Formation. *Molecules*, 2009. Vol. 14, No. 7, p. 2535-2554. ISSN 1420-3049.

46. HEUKELEKIAN, H.; HELLER, A. Relation between food concentration and surface for bacterial growth. *Journal of Bacteriology*, 1940. Vol. 40, No. 4, p. 547-558. ISSN 0021-9193.

47. ZOBELL, C.E. The effect of solid surfaces upon bacterial activity. *Journal of Bacteriology*, 1943. Vol. 46, No. 1, p. 39-56. ISSN 0021-9193.

48. CHARACKLIS, W.G. Attached microbial growths. II. Frictional resistance due to microbial slimes. *Water Research*, 1973. Vol. 7, No. 9, p. 1249-1258.

49. COSTERTON, J.W.; GEESEY, G.G.; CHENG, K.J. How Bacteria Stick. *Scientific American*, 1978. Vol. 238, No. 1, p. 86-&. ISSN 0036-8733.

50. JONES, H.C.; ROTH, I.L.; SANDERS, W.M. Electron Microscopic Study of a Slime Layer. *Journal of Bacteriology*, 1969. Vol. 99, No. 1, p. 316-&. ISSN 0021-9193.

51. MARSHALL, K.C.; STOUT, R.; MITCHELL, R. Mechanism of the Initial Events in the Sorption of Marine Bacteria to Surfaces. *J Gen Microbiol*, 1971. Vol. 68, No. 3, p. 337-348.

52. DAVEY, M.E.; O'TOOLE, G.A. Microbial biofilms: from ecology to molecular genetics. *Microbiology and Molecular Biology Reviews*, 2000. Vol. 64, No. 4, p. 847-+. ISSN 1092-2172.

53. COSTERTON, J.W.; LEWANDOWSKI, Z.; CALDWELL, D.E.; KORBER, D.R.; LAPPINSCOTT, H.M. Microbial Biofilms. *Annual Review of Microbiology*, 1995. Vol. 49, p. 711-745. ISSN 0066-4227.

54. STOODLEY, P.; SAUER, K.; DAVIES, D.G.; COSTERTON, J.W. BIOFILMS AS COMPLEX DIFFERENTIATED COMMUNITIES. *Annual Review of Microbiology*, 2002. Vol. 56, No. 1, p. 187-209.

55. JASS, J.; SURMAN, S.; WALKER, J. *Medical biofilms : detection, prevention, and control*. Chichester: Wiley, 2003. xxi, 291 p. ISBN 0471988677 : ¹55.00.

56. GRISTINA, A.G.; NAYLOR, P.; MYRVIK, Q. Infections from Biomaterials and Implants - a Race for the Surface. *Medical Progress through Technology*, 1989. Vol. 14, No. 3-4, p. 205-224. ISSN 0047-6552.

57. O'TOOLE, G.A.; KOLTER, R. Flagellar and twitching motility are necessary for Pseudomonas aeruginosa biofilm development. *Molecular Microbiology*, 1998. Vol. 30, No. 2, p. 295-304.

58. TEBBS, S.E.; SAWYER, A.; ELLIOTT, T.S.J. Influence of Surface-Morphology on in-Vitro Bacterial Adherence to Central Venous Catheters. *British Journal of Anaesthesia*, 1994. Vol. 72, No. 5, p. 587-591. ISSN 0007-0912.

59. KAPPELL, G.M.; GROVER, J.P.; CHRZANOWSKI, T.H. Micro-scale surface-patterning influences biofilm formation. *Electronic Journal of Biotechnology*, 2009. Vol. 12, No. 3. ISSN 0717-3458.

60. JANSEN, B.; PETERS, G.; PULVERER, G. Mechanisms and Clinical Relevance of Bacterial Adhesion to Polymers. *Journal of Biomaterials Applications*, 1987. Vol. 2, No. 4, p. 520-543.

61. HOGT, A.H.; DANKERT, J.; FEIJEN, J. Adhesion of coagulase-negative staphylococci to methacrylate polymers and copolymers. *Journal of Biomedical Materials Research*, 1986. Vol. 20, No. 4, p. 533-545.

62. FLETCHER, M.; LOEB, G.I. Influence of Substratum Characteristics on the Attachment of a Marine Pseudomonad to Solid Surfaces. *Appl. Environ. Microbiol.*, 1979. Vol. 37, No. 1, p. 67-72.

63. SCHIERHOLZ, J.M.; BEUTH, J. Implant infections: a haven for opportunistic bacteria. *Journal of Hospital Infection*, 2001. Vol. 49, No. 2, p. 87-93.

64. PASCUAL, A. Pathogenesis of catheter-related infections: lessons for new designs. *Clinical Microbiology & Infection*, 2002. Vol. 8, No. 5, p. 256-264. ISSN 1469-0691.

65. RAAD, I.I.; LUNA, M.; KHALIL, S.-A.M.; COSTERTON, J.W.; LAM, C.; BODEY, G.P. The Relationship Between the Thrombotic and Infectious Complications of Central Venous Catheters. *JAMA: The Journal of the American Medical Association*, 1994. Vol. 271, No. 13, p. 1014-1016.

66. MURGA, R.; MILLER, J.M.; DONLAN, R.M. Biofilm formation by gram-negative bacteria on central venous catheter connectors: Effect of conditioning films in a laboratory model. *Journal of Clinical Microbiology*, 2001. Vol. 39, No. 6, p. 2294-2297. ISSN 0095-1137.

67. BUSSCHER, H.J.; VAN DER MEI, H.C. Physico-Chemical Interactions in Initial Microbial Adhesion and Relevance for Biofilm Formation. *Advances in Dental Research*, 1997. Vol. 11, No. 1, p. 24-32.

68. SAUER, K.; CAMPER, A.K. Characterization of Phenotypic Changes in Pseudomonas putida in Response to Surface-Associated Growth. *J. Bacteriol.*, 2001. Vol. 183, No. 22, p. 6579-6589.

69. GERKE, C.; KRAFT, A.; SÄĽĂŹMUTH, R.; SCHWEITZER, O.; GĂ¶TZ, F. Characterization of theN-Acetylglucosaminyltransferase Activity Involved in the Biosynthesis of the Staphylococcus epidermidisPolysaccharide Intercellular Adhesin. *Journal of Biological Chemistry*, 1998. Vol. 273, No. 29, p. 18586-18593.

70. DAVIES, D.G.; GEESEY, G.G. Regulation of the Alginate Biosynthesis Gene Algc in Pseudomonas-Aeruginosa During Biofilm Development in Continuous-Culture. *Applied and Environmental Microbiology*, 1995. Vol. 61, No. 3, p. 860-867. ISSN 0099-2240.

71. PRIGENT-COMBARET, C.; VIDAL, O.; DOREL, C.; LEJEUNE, P. Abiotic surface sensing and biofilm-dependent regulation of gene expression in Escherichia coli. *Journal of Bacteriology*, 1999. Vol. 181, No. 19, p. 5993-6002. ISSN 0021-9193.

72. WHITELEY, M.; BANGERA, M.G.; BUMGARNER, R.E.; PARSEK, M.R.; TEITZEL, G.M.; LORY, S.; GREENBERG, E.P. Gene expression in Pseudomonas aeruginosa biofilms. *Nature*, 2001. Vol. 413, No. 6858, p. 860-864. ISSN 0028-0836.

73. HARRAGHY, N.; KERDUDOU, S.; HERRMANN, M. Quorum-sensing systems in staphylococci as therapeutic targets. *Analytical and Bioanalytical Chemistry*, 2007. Vol. 387, No. 2, p. 437-444.

74. HODGKINSON, J.T.; WELCH, M.; SPRING, D.R. Learning the Language of Bacteria. *ACS Chemical Biology*, 2007. Vol. 2, No. 11, p. 715-717.

75. HORSWILL, A.; STOODLEY, P.; STEWART, P.; PARSEK, M. The effect of the chemical, biological, and physical environment on quorum sensing in structured microbial communities. *Analytical and Bioanalytical Chemistry*, 2007. Vol. 387, No. 2, p. 371-380.

76. BRANDA, S.S.; VIK, A.; FRIEDMAN, L.; KOLTER, R. Biofilms: the matrix revisited. *Trends in Microbiology*, 2005. Vol. 13, No. 1, p. 20-26.

77. HALL-STOODLEY, L.; STOODLEY, P. Biofilm formation and dispersal and the transmission of human pathogens. *Trends in Microbiology*, 2005. Vol. 13, No. 1, p. 7-10.

78. SUTHERLAND, I.W. Biofilm exopolysaccharides: a strong and sticky framework. *Microbiology-Uk*, 2001. Vol. 147, p. 3-9. ISSN 1350-0872.

79. BOYD, A.; CHAKRABARTY, A.M. Role of alginate lyase in cell detachment of Pseudomonas aeruginosa. *Appl. Environ. Microbiol.*, 1994. Vol. 60, No. 7, p. 2355-2359.

80. GILBERT, P.; EVANS, D.J.; BROWN, M.R.W. Formation and Dispersal of Bacterial Biofilms in-Vivo and in-Situ. *Journal of Applied Bacteriology*, 1993. Vol. 74, p. S67-S78. ISSN 0021-8847.

81. BRADING, M.G.; JASS, J.; LAPPIN-SCOTT, H.M.; COSTERTON, J.W., *Dynamics of bacterial biofilm formation*, in *Microbial biofilms*, H.M. Lappin-Scott and J.W. Costerton, Editors. 1995, Cambridge University Press: Cambridge ; New York. p. xiii,310p. ISBN 0521454123.

82. CHARACKLIS, W.G., *Biofilm processes*, in *Biofilms*, W.G. Characklis and K.C. Marshall, Editors. 1990, Wiley: New York. p. xvii,796p. ISBN 0471826634 : ¹77.65.

83. CERI, H.; OLSON, M.E.; STREMICK, C.; READ, R.R.; MORCK, D.; BURET, A. The Calgary Biofilm Device: New Technology for Rapid Determination of Antibiotic Susceptibilities of Bacterial Biofilms. *J. Clin. Microbiol.*, 1999. Vol. 37, No. 6, p. 1771-1776.

84. LARSEN, T.; FIEHN, N.-E. Resistance of Streptococcus sanguis biofilms to antimicrobial agents. *APMIS*, 1996. Vol. 104, No. 1-6, p. 280-284.

85. VORACHIT, M.; LAM, K.; JAYANETRA, P.; COSTERTON, J.W. Resistance of Pseudomonas pseudomallei growing as a biofilm on silastic discs to ceftazidime and cotrimoxazole. *Antimicrob. Agents Chemother.*, 1993. Vol. 37, No. 9, p. 2000-2002.

86. WILLIAMS, I.; VENABLES, W.A.; LLOYD, D.; PAUL, F.; CRITCHLEY, I. The effects of adherence to silicone surfaces on antibiotic susceptibility in Staphylococcus aureus. *Microbiology*, 1997. Vol. 143, No. 7, p. 2407-2413.

87. WALSH, C. Molecular mechanisms that confer antibacterial drug resistance. *Nature*, 2000. Vol. 406, No. 6797, p. 775-781.

88. ZIMMERLI, W.; WIDMER, A.F.; BLATTER, M.; FREI, R.; OCHSNER, P.E.; FOR THE FOREIGN-BODY INFECTION STUDY, G. Role of Rifampin for Treatment of Orthopedic Implant-Related Staphylococcal Infections: A Randomized Controlled Trial. *JAMA*, 1998. Vol. 279, No. 19, p. 1537-1541.

89. XU, K.D.; MCFETERS, G.A.; STEWART, P.S. Biofilm resistance to antimicrobial agents. *Microbiology*, 2000. Vol. 146, No. 3, p. 547-549.

90. GILBERT, P.; DAS, J.; FOLEY, I. Biofilm Susceptibility to Antimicrobials. *Advances in Dental Research*, 1997. Vol. 11, No. 1, p. 160-167.

91. NICHOLS, W.W.; DORRINGTON, S.M.; SLACK, M.P.E.; WALMSLEY, H.L. Inhibition of Tobramycin Diffusion by Binding to Alginate. *Antimicrobial Agents and Chemotherapy*, 1988. Vol. 32, No. 4, p. 518-523. ISSN 0066-4804.

92. WALTERS, M.C.; ROE, F.; BUGNICOURT, A.; FRANKLIN, M.J.; STEWART, P.S. Contributions of antibiotic penetration, oxygen limitation, and low metabolic activity to tolerance of Pseudomonas aeruginosa biofilms to ciprofloxacin and tobramycin. *Antimicrobial Agents and Chemotherapy*, 2003. Vol. 47, No. 1, p. 317-323. ISSN 0066-4804.

93. DUGUID, I.G.; EVANS, E.; BROWN, M.R.W.; GILBERT, P. Growth-Rate-Independent Killing by Ciprofloxacin of Biofilm-Derived Staphylococcus-Epidermidis - Evidence for Cell-Cycle Dependency. *Journal of Antimicrobial Chemotherapy*, 1992. Vol. 30, No. 6, p. 791-802. ISSN 0305-7453.

94. EVANS, D.J.; ALLISON, D.G.; BROWN, M.R.W.; GILBERT, P. Effect of growth-rate on resistance of Gram-negative biofilms to cetrimide. *Journal of Antimicrobial Chemotherapy*, 1990. Vol. 26, No. 4, p. 473-478.

95. AMORENA, B.; GRACIA, E.; MONZÃŁN, M.; LEIVA, J.; OTEIZA, C.; PÃ©REZ, M.; ALABART, J.-L.; HERNÃˇNDEZ-YAGO, J. Antibiotic susceptibility assay for Staphylococcus aureus in biofilms developed in vitro. *Journal of Antimicrobial Chemotherapy*, 1999. Vol. 44, No. 1, p. 43-55.

96. ANWAR, H.; STRAP, J.L.; CHEN, K.; COSTERTON, J.W. Dynamic Interactions of Biofilms of Mucoid Pseudomonas-Aeruginosa with Tobramycin and Piperacillin. *An-*

*timicrobial Agents and Chemotherapy*, 1992. Vol. 36, No. 6, p. 1208-1214. ISSN 0066-4804.

97. HAUSNER, M.; WUERTZ, S. High Rates of Conjugation in Bacterial Biofilms as Determined by Quantitative In Situ Analysis. *Appl. Environ. Microbiol.*, 1999. Vol. 65, No. 8, p. 3710-3713.
98. GIVSKOV, M.; DE NYS, R.; MANEFIELD, M.; GRAM, L.; MAXIMILIEN, R.; EBERL, L.; MOLIN, S.; STEINBERG, P.D.; KJELLEBERG, S. Eukaryotic interference with homoserine lactone-mediated prokaryotic signalling. *J. Bacteriol.*, 1996. Vol. 178, No. 22, p. 6618-6622.
99. HENTZER, M.; WU, H.; ANDERSEN, J.B.; RIEDEL, K.; RASMUSSEN, T.B.; BAGGE, N.; KUMAR, N.; SCHEMBRI, M.A.; SONG, Z.; KRISTOFFERSEN, P.; MANEFIELD, M.; COSTERTON, J.W.; MOLIN, S.; EBERL, L.; STEINBERG, P.; KJELLEBERG, S.; HOIBY, N.; GIVSKOV, M. Attenuation of Pseudomonas aeruginosa virulence by quorum sensing inhibitors. *EMBO J*, 2003. Vol. 22, No. 15, p. 3803-3815.
100. ENSING, G.T.; ROEDER, B.L.; NELSON, J.L.; VAN HORN, J.R.; VAN DER MEI, H.C.; BUSSCHER, H.J.; PITT, W.G. Effect of pulsed ultrasound in combination with gentamicin on bacterial viability in biofilms on bone cements in vivo. *Journal of Applied Microbiology*, 2005. Vol. 99, No. 3, p. 443-448.
101. JASS, J.; LAPPIN-SCOTT, H.M. The efficacy of antibiotics enhanced by electrical currents against Pseudomonas aeruginosa biofilms. *Journal of Antimicrobial Chemotherapy*, 1996. Vol. 38, No. 6, p. 987-1000.
102. DAROUICHE, RABIH O. Device-Associated Infections: A Macroproblem that Starts with Microadherence. *Clinical Infectious Diseases*, 2001. Vol. 33, No. 9, p. 1567-1572.
103. FRANCOLINI, I.; DONELLI, G.; STOODLEY, P. Polymer Designs to Control Biofilm Growth on Medical Devices. *Reviews in Environmental Science and Biotechnology*, 2003. Vol. 2, No. 2, p. 307-319.
104. BAMBAUER, R.; MESTRES, P.; SCHIEL, R.; SIOSHANSI, P. New Surface-Treatment Technologies for Catheters Used for Extracorporeal Detoxification Methods. *Dialysis & Transplantation*, 1995. Vol. 24, No. 5, p. 228-&. ISSN 0090-2934.
105. PORTOLÉS, M.; REFOJO, M.F.; LEONG, F.-L. Poloxamer 407 as a bacterial abhesive for hydrogel contact lenses. *Journal of Biomedical Materials Research*, 1994. Vol. 28, No. 3, p. 303-309.
106. SHETH, N.K.; FRANSON, T.R.; ROSE, H.D.; BUCKMIRE, F.L.A.; COOPER, J.A.; SOHNLE, P.G. Colonization of Bacteria on Polyvinyl-Chloride and Teflon Intravascular Catheters in Hospitalized-Patients. *Journal of Clinical Microbiology*, 1983. Vol. 18, No. 5, p. 1061-1063. ISSN 0095-1137.
107. SHERERTZ, R.J.; CARRUTH, W.A.; MAROSOK, R.D.; ESPELAND, M.A.; JOHNSON, R.A.; SOLOMON, D.D. Contribution of vascular catheter material to the pathogenesis of infection: The enhanced risk of silicone in vivo. *Journal of Biomedical Materials Research*, 1995. Vol. 29, No. 5, p. 635-645.
108. MAKI, D.G.; STOLZ, S.M.; WHEELER, S.; MERMEL, L.A. Prevention of Central Venous Catheter-Related Bloodstream Infection by Use of an Antiseptic-Impregnated Catheter. *Annals of Internal Medicine*, 1997. Vol. 127, No. 4, p. 257-266.

109. DONELLI, G.; FRANCOLINI, I.; PIOZZI, A.; DI ROSA, R.; MARCONI, W. New polymer-antibiotic systems to inhibit bacterial biofilm formation: A suitable approach to prevent central venous catheter-associated infections. *Journal of Chemotherapy*, 2002. Vol. 14, No. 5, p. 501-507. ISSN 1120-009X.

110. RAAD, I.; DAROUICHE, R.; DUPUIS, J.; ABI-SAID, D.; GABRIELLI, A.; HACHEM, R.; WALL, M.; HARRIS, R.; JONES, J.; BUZAID, A.; ROBERTSON, C.; SHENAQ, S.; CURLING, P.; BURKE, T.; ERICSSON, C. Central Venous Catheters Coated with Minocycline and Rifampin for the Prevention of Catheter-Related Colonization and Bloodstream Infections. *Annals of Internal Medicine*, 1997. Vol. 127, No. 4, p. 267-274.

111. KHARE, M.D.; BUKHARI, S.S.; SWANN, A.; SPIERS, P.; MCLAREN, I.; MYERS, J. Reduction of catheter-related colonisation by the use of a silver zeolite-impregnated central vascular catheter in adult critical care. *Journal of Infection*, 2007. Vol. 54, No. 2, p. 146-150.

112. BRIDGETT, M.J.; DAVIES, M.C.; DENYER, S.P.; ELDRIDGE, P.R. In vitro assessment of bacterial adhesion to Hydromer®-coated cerebrospinal fluid shunts. *Biomaterials*, 1993. Vol. 14, No. 3, p. 184-188.

113. MORRA, M.; CASSINELI, C. Non-fouling properties of polysaccharide-coated surfaces. *Journal of Biomaterials Science-Polymer Edition*, 1999. Vol. 10, No. 10, p. 1107-1124. ISSN 0920-5063.

114. PARK, J.H.; CHO, Y.W.; KWON, I.C.; JEONG, S.Y.; BAE, Y.H. Assessment of PEO/PTMO multiblock copolymer/segmented polyurethane blends as coating materials for urinary catheters: in vitro bacterial adhesion and encrustation behavior. *Biomaterials*, 2002. Vol. 23, No. 19, p. 3991-4000.

115. SCHINABECK, M.K.; LONG, L.A.; HOSSAIN, M.A.; CHANDRA, J.; MUKHERJEE, P.K.; MOHAMED, S.; GHANNOUM, M.A. Rabbit model of Candida albicans biofilm infection: Liposomal amphotericin B antifungal lock therapy. *Antimicrobial Agents and Chemotherapy*, 2004. Vol. 48, No. 5, p. 1727-1732. ISSN 0066-4804.

116. PIOZZI, A.; FRANCOLINI, I.; OCCHIAPERTI, L.; VENDITTI, M.; MARCONI, W. Antimicrobial activity of polyurethanes coated with antibiotics: a new approach to the realization of medical devices exempt from microbial colonization. *International Journal of Pharmaceutics*, 2004. Vol. 280, No. 1-2, p. 173-183.

117. BOWERSOCK, T.L.; WOODYARD, L.; HAMILTON, A.J.; DEFORD, J.A. Inhibition of Staphylococci by vancomycin absorbed on triidodecylmethyl ammonium chloride-coated intravenous catheter. *Journal of Controlled Release*, 1994. Vol. 31, No. 3, p. 237-243.

118. JANSEN, B.; RUITEN, D.; PULVERER, G. In-vitro activity of a catheter loaded with silver and teicoplanin to prevent bacterial and fungal colonization. *Journal of Hospital Infection*, 1995. Vol. 31, No. 3, p. 238-241.

119. JONES, G.L.; RUSSELL, A.D.; CALISKAN, Z.; STICKLER, D.J. A Strategy for the Control of Catheter Blockage by Crystalline Proteus mirabilis Biofilm Using the Antibacterial Agent Triclosan. *European Urology*, 2005. Vol. 48, No. 5, p. 838-845.

120. FOX, S.; WILKINSON, T.S.; WHEATLEY, P.S.; XIAO, B.; MORRIS, R.E.; SUTHERLAND, A.; SIMPSON, A.J.; BARLOW, P.G.; BUTLER, A.R.; MEGSON, I.L.; ROSSI, A.G. NO-loaded Zn2+-exchanged zeolite materials: A potential bifunctional anti-bacterial strategy. *Acta Biomaterialia*. Vol. 6, No. 4, p. 1515-1521.

121. JONES, A. Killer Plastics: Antimicrobial Additives for Polymers. *Plastics Engineering*, 2008. Vol. 64, No. 8, p. 34-+. ISSN 0091-9578.

122. NAKASHIMA, T., SAKAGAMI, Y. AND MATSUO, M. Antibacterial efficacy of cotton fabrics chemically modified by metal salt. *Biocontrol Science*, 2001. Vol. 6, p. 9-15.

123. WILCZYNSKI, M. Anti-microbial porcelain enamels. *Ceramics Engineering and Science Proceedings*, 2000. Vol. 21, p. 81–83.

124. DAVIES, R.L., ETRIS, S. F. The development and functions of silver in water purification and disease control. *Catalysis Today*, 1997. Vol. 36, p. 107-114. ISSN 0920-5861

125. ALEXANDER, J.W. History of the Medical Use of Silver. *Surgical Infections*, 2009. Vol. 10, No. 3, p. 289-292. ISSN 1096-2964.

126. KLASEN, H.J. Historical review of the use of silver in the treatment of burns. I. Early uses. *Burns*, 2000. Vol. 26, No. 2, p. 117-130.

127. KLASEN, H.J. A historical review of the use of silver in the treatment of burns. II. Renewed interest for silver. *Burns*, 2000. Vol. 26, No. 2, p. 131-138. ISSN 0305-4179.

128. SLAWSON, R.M.; VAN DYKE, M.I.; LEE, H.; TREVORS, J.T. Germanium and silver resistance, accumulation, and toxicity in microorganisms. *Plasmid*, 1992. Vol. 27, No. 1, p. 72-79.

129. ZHAO, G.; STEVENS, S.E. Multiple parameters for the comprehensive evaluation of the susceptibility of Escherichia coli to the silver ion. *BioMetals*, 1998. Vol. 11, No. 1, p. 27-32.

130. BALAZS, D.J.; TRIANDAFILLU, K.; WOOD, P.; CHEVOLOT, Y.; VAN DELDEN, C.; HARMS, H.; HOLLENSTEIN, C.; MATHIEU, H.J. Inhibition of bacterial adhesion on PVC endotracheal tubes by RF-oxygen glow discharge, sodium hydroxide and silver nitrate treatments. *Biomaterials*, 2004. Vol. 25, No. 11, p. 2139-2151.

131. Using silver to fight microbial attack. *Plastics, Additives and Compounding*, 2003. Vol. 5, No. 5, p. 32-32.

132. KUMAR, R.; MÜNSTEDT, H. Silver ion release from antimicrobial polyamide/silver composites. *Biomaterials*, 2005. Vol. 26, No. 14, p. 2081-2088.

133. STOBIE, N.; DUFFY, B.; MCCORMACK, D.E.; COLREAVY, J.; HIDALGO, M.; MCHALE, P.; HINDER, S.J. Prevention of Staphylococcus epidermidis biofilm formation using a low-temperature processed silver-doped phenyltriethoxysilane sol-gel coating. *Biomaterials*, 2008. Vol. 29, No. 8, p. 963-969.

134. MELAIYE, A.; YOUNGS, W.J. Silver and its application as an antimicrobial agent. *Expert Opinion on Therapeutic Patents*, 2005. Vol. 15, No. 2, p. 125-130.

135. RUSSELL, A.D.; HUGO, W.B.; AYLIFFE, G.A.J. *Principles and practice of disinfection, preservation, and sterilisation*. 3rd ed. Oxford: Blackwell Science, 1999. x,826p. ISBN 0632041943 : No price.

136. DEMLING, R.H. The role of silver in wound healing - Part 1: Effects of silver on wound management. *Wounds-a Compendium of Clinical Research and Practice*, 2001. Vol. 13, No. 1, p. 4-15. ISSN 1044-7946.

137. CHOPRA, I. The increasing use of silver-based products as antimicrobial agents: a useful development or a cause for concern? *Journal of Antimicrobial Chemotherapy*, 2007. Vol. 59, No. 4, p. 587-590.

138. PARIKH, D.V.; FINK, T.; RAJASEKHARAN, K.; SACHINVALA, N.D.; SAWHNEY, A.P.S.; CALAMARI, T.A.; PARIKH, A.D. Antimicrobial silver/sodium carboxymethyl cotton dressings for burn wounds. *Textile Research Journal*, 2005. Vol. 75, No. 2, p. 134-138.

139. ÜLKÜR, E.; ONCUL, O.; KARAGOZ, H.; YENIZ, E.; ÇELIKÖZ, B. Comparison of silver-coated dressing (Acticoat(TM)), chlorhexidine acetate 0.5% (Bactigrass®), and fusidic acid 2% (Fucidin®) for topical antibacterial effect in methicillin-resistant Staphylococci-contaminated, full-skin thickness rat burn wounds. *Burns*, 2005. Vol. 31, No. 7, p. 874-877.

140. PANÁČEK, A.; KVÍTEK, L.; PRUCEK, R.; KOLÁŘ, M.; VEČEŘÉVÁ, R.; PIZÚROVÁ, N.; SHARMA, V.K.; NEVĚČNÁ, T.; ZBOŘIL, R. Silver Colloid Nanoparticles:Synthesis, Characterization, and Their Antibacterial Activity. *The Journal of Physical Chemistry B*, 2006. Vol. 110, No. 33, p. 16248-16253.

141. ATIYEH, B.S.; COSTAGLIOLA, M.; HAYEK, S.N.; DIBO, S.A. Effect of silver on burn wound infection control and healing: Review of the literature. *Burns*, 2007. Vol. 33, No. 2, p. 139-148.

142. RUPP, M.E.; FITZGERALD, T.; MARION, N.; HELGET, V.; PUUMALA, S.; ANDERSON, J.R.; FEY, P.D. Effect of silver-coated urinary catheters: Efficacy, cost-effectiveness, and antimicrobial resistance. *American Journal of Infection Control*, 2004. Vol. 32, No. 8, p. 445-450.

143. SAMUEL, U.; GUGGENBICHLER, J.P. Prevention of catheter-related infections: The potential of a new nano-silver impregnated catheter. *International Journal of Antimicrobial Agents*, 2004. Vol. 23, No. SUPPL. 1.

144. STRATHMANN, M.; WINGENDER, J. Use of an oxonol dye in combination with confocal laser scanning microscopy to monitor damage to Staphylococcus aureus cells during colonisation of silver-coated vascular grafts. *International Journal of Antimicrobial Agents*, 2004. Vol. 24, No. 3, p. 234-240.

145. OHASHI, S.; SAKU, S.; YAMAMOTO, K. Antibacterial activity of silver inorganic agent YDA filler. *Journal of Oral Rehabilitation*, 2004. Vol. 31, No. 4, p. 364-367.

146. DUBAS, S.T.; KUMLANGDUDSANA, P.; POTIYARAJ, P. Layer-by-layer deposition of antimicrobial silver nanoparticles on textile fibers. *Colloids and Surfaces A: Physicochemical and Engineering Aspects*, 2006. Vol. 289, No. 1-3, p. 105-109.

147. CHEN, C.-Y.; CHIANG, C.-L. Preparation of cotton fibers with antibacterial silver nanoparticles. *Materials Letters*, 2008. Vol. 62, No. 21-22, p. 3607-3609.

148. RAVINDRA, S.; MURALI MOHAN, Y.; NARAYANA REDDY, N.; MOHANA RAJU, K. Fabrication of antibacterial cotton fibres loaded with silver nanoparticles via "Green Approach". *Colloids and Surfaces A: Physicochemical and Engineering Aspects*, 2010. Vol. 367, No. 1-3, p. 31-40.

149. SHATERI KHALIL-ABAD, M.; YAZDANSHENAS, M.E. Superhydrophobic antibacterial cotton textiles. *Journal of Colloid and Interface Science*. Vol. 351, No. 1, p. 293-298.

150. CHOU, W.L.; YU, D.G.; YANG, M.C. The preparation and characterization of silver-loading cellulose acetate hollow fiber membrane for water treatment. *Polymers for Advanced Technologies*, 2005. Vol. 16, No. 8, p. 600-607.

151. DAVIES, R.L.; ETRIS, S.F. The development and functions of silver in water purification and disease control. *Catalysis Today*, 1997. Vol. 36, No. 1, p. 107-114.

152. RAI, M.; YADAV, A.; GADE, A. Silver nanoparticles as a new generation of antimicrobials. *Biotechnology Advances*. Vol. 27, No. 1, p. 76-83.

153. LE, A.-T.; HUY, P.T.; TAM, P.D.; HUY, T.Q.; CAM, P.D.; KUDRINSKIY, A.A.; KRUTYAKOV, Y.A. Green synthesis of finely-dispersed highly bactericidal silver nanoparticles via modified Tollens technique. *Current Applied Physics*. Vol. 10, No. 3, p. 910-916.

154. SHAHVERDI, A.R.; FAKHIMI, A.; SHAHVERDI, H.R.; MINAIAN, S. Synthesis and effect of silver nanoparticles on the antibacterial activity of different antibiotics against Staphylococcus aureus and Escherichia coli. *Nanomedicine: Nanotechnology, Biology and Medicine*, 2007. Vol. 3, No. 2, p. 168-171.

155. SHEIKH, N.; AKHAVAN, A.; KASSAEE, M.Z. Synthesis of antibacterial silver nanoparticles by [gamma]-irradiation. *Physica E: Low-dimensional Systems and Nanostructures*, 2009. Vol. 42, No. 2, p. 132-135.

156. KORA, A.J.; MANJUSHA, R.; ARUNACHALAM, J. Superior bactericidal activity of SDS capped silver nanoparticles: Synthesis and characterization. *Materials Science and Engineering: C*, 2009. Vol. 29, No. 7, p. 2104-2109.

157. SHARMA, V.K.; YNGARD, R.A.; LIN, Y. Silver nanoparticles: Green synthesis and their antimicrobial activities. *Advances in Colloid and Interface Science*, 2009. Vol. 145, No. 1-2, p. 83-96.

158. KIM, J.S.; KUK, E.; YU, K.N.; KIM, J.-H.; PARK, S.J.; LEE, H.J.; KIM, S.H.; PARK, Y.K.; PARK, Y.H.; HWANG, C.-Y.; KIM, Y.-K.; LEE, Y.-S.; JEONG, D.H.; CHO, M.-H. Antimicrobial effects of silver nanoparticles. *Nanomedicine: Nanotechnology, Biology and Medicine*, 2007. Vol. 3, No. 1, p. 95-101.

159. SAINT, S.; ELMORE, J.G.; SULLIVAN, S.D.; EMERSON, S.S.; KOEPSELL, T.D. The efficacy of silver alloy-coated urinary catheters in preventing urinary tract infection: a meta-analysis. *The American Journal of Medicine*, 1998. Vol. 105, No. 3, p. 236-241.

160. LEE, W.-I.; YOUNG, R.-L. Defects and degradation in ZnO varistor. *Applied Physics Letters*, 1996. Vol. 69, No. 4, p. 526-528.

161. HENDRIKSE, K.G.; MCGILL, W.J.; REEDIJK, J.; NIEUWENHUIZEN, P.J. Vulcanization of chlorobutyl rubber. I. The identification of crosslink precursors in compounds containing ZnO/ZnCl<SUB><FONT SIZE='-1'>2</FONT></SUB>. *Journal of Applied Polymer Science*, 2000. Vol. 78, No. 13, p. 2290-2301. ISSN 1097-4628.

162. PILLAI, S.C.; KELLY, J.M.; MCCORMACK, D.E.; O'BRIEN, P.; RAMESH, R. The effect of processing conditions on varistors prepared from nanocrystalline ZnO. *Journal of Materials Chemistry*, 2003. Vol. 13, No. 10, p. 2586-2590.

163. GUO, H.; ZHOU, J.; LIN, Z. ZnO nanorod light-emitting diodes fabricated by electrochemical approaches. *Electrochemistry Communications*, 2008. Vol. 10, No. 1, p. 146-150.

164. CALESTANI, D.; ZHA, M.; MOSCA, R.; ZAPPETTINI, A.; CAROTTA, M.C.; DI NATALE, V.; ZANOTTI, L. Growth of ZnO tetrapods for nanostructure-based gas sensors. *Sensors and Actuators B: Chemical*. Vol. 144, No. 2, p. 472-478.

165. SHAHEEN, W.M.; DERAZ, N.-A.M.; SELIM, M.M. Effect of ZnO doping on surface and catalytic properties of manganese oxides supported on alumina. *Materials Letters*, 2002. Vol. 52, No. 1-2, p. 130-139.

166. KLABUNDE, K.J.; STARK, J.; KOPER, O.; MOHS, C.; PARK, D.G.; DECKER, S.; JIANG, Y.; LAGADIC, I.; ZHANG, D. Nanocrystals as Stoichiometric Reagents with Unique Surface Chemistry. *The Journal of Physical Chemistry*, 1996. Vol. 100, No. 30, p. 12142-12153.

167. GREENE, L.E.; LAW, M.; TAN, D.H.; MONTANO, M.; GOLDBERGER, J.; SOMORJAI, G.; YANG, P. General Route to Vertical ZnO Nanowire Arrays Using Textured ZnO Seeds. *Nano Letters*, 2005. Vol. 5, No. 7, p. 1231-1236.

168. HUANG, H.; YANG, S.; GONG, J.; LIU, H.; DUAN, J.; ZHAO, X.; ZHANG, R.; LIU, Y.; LIU, Y. Controllable Assembly of Aligned ZnO Nanowires/Belts Arrays. *The Journal of Physical Chemistry B*, 2005. Vol. 109, No. 44, p. 20746-20750.

169. DING, Y.; GAO, P.X.; WANG, Z.L. Catalyst-Nanostructure Interfacial Lattice Mismatch in Determining the Shape of VLS Grown Nanowires and Nanobelts: A Case of Sn/ZnO. *Journal of the American Chemical Society*, 2004. Vol. 126, No. 7, p. 2066-2072.

170. LIU, B.; ZENG, H.C. Hydrothermal Synthesis of ZnO Nanorods in the Diameter Regime of 50 nm. *Journal of the American Chemical Society*, 2003. Vol. 125, No. 15, p. 4430-4431.

171. YU, H.; ZHANG, Z.; HAN, M.; HAO, X.; ZHU, F. A General Low-Temperature Route for Large-Scale Fabrication of Highly Oriented ZnO Nanorod/Nanotube Arrays. *Journal of the American Chemical Society*, 2005. Vol. 127, No. 8, p. 2378-2379.

172. LUCAS, M.; MAI, W.; YANG, R.; WANG, Z.L.; RIEDO, E. Aspect Ratio Dependence of the Elastic Properties of ZnO Nanobelts. *Nano Letters*, 2007. Vol. 7, No. 5, p. 1314-1317.

173. WANG, Z.; QIAN, X.-F.; YIN, J.; ZHU, Z.-K. Large-Scale Fabrication of Tower-like, Flower-like, and Tube-like ZnO Arrays by a Simple Chemical Solution Route. *Langmuir*, 2004. Vol. 20, No. 8, p. 3441-3448.

174. JANG, J.-M.; KIM, C.-R.; RYU, H.; RAZEGHI, M.; JUNG, W.-G. ZnO 3D flower-like nanostructure synthesized on GaN epitaxial layer by simple route hydrothermal process. *Journal of Alloys and Compounds*, 2008. Vol. 463, No. 1-2, p. 503-510.

175. LI, L.; PAN, S.; DOU, X.; ZHU, Y.; HUANG, X.; YANG, Y.; LI, G.; ZHANG, L. Direct Electrodeposition of ZnO Nanotube Arrays in Anodic Alumina Membranes. *The Journal of Physical Chemistry C*, 2007. Vol. 111, No. 20, p. 7288-7291.

176. HU, J.Q.; LI, Q.; WONG, N.B.; LEE, C.S.; LEE, S.T. Synthesis of Uniform Hexagonal Prismatic ZnO Whiskers. *Chemistry of Materials*, 2002. Vol. 14, No. 3, p. 1216-1219.

177. WANG, Z.L.; KONG, X.Y.; ZUO, J.M. Induced Growth of Asymmetric Nanocantilever Arrays on Polar Surfaces. *Physical Review Letters*, 2003. Vol. 91, No. 18, p. 185502.

178. PAN, Z.W.; MAHURIN, S.M.; DAI, S.; LOWNDES, D.H. Nanowire Array Gratings with ZnO Combs. *Nano Letters*, 2005. Vol. 5, No. 4, p. 723-727.

179. LEE, J.S.; ISLAM, M.S.; KIM, S. Photoresponses of ZnO nanobridge devices fabricated using a single-step thermal evaporation method. *Sensors and Actuators B: Chemical*, 2007. Vol. 126, No. 1, p. 73-77.

180. ZONG, X.; WANG, P. Effect of UV irradiation on the properties of ZnO nanorod arrays prepared by hydrothermal method. *Physica E: Low-dimensional Systems and Nanostructures*, 2009. Vol. 41, No. 5, p. 757-761.

181. CLAVEL, G.; WILLINGER, M.G.; ZITOUN, D.; PINNA, N. Solvent Dependent Shape and Magnetic Properties of Doped ZnO Nanostructures. *Advanced Functional Materials*, 2007. Vol. 17, No. 16, p. 3159-3169. ISSN 1616-3028.

182. ZANG, C.H.; LIU, Y.C.; ZHAO, D.X.; ZHANG, Y.S. Growth and optical properties of ZnO microwells by chemical vapor deposition method. *Physica B: Condensed Matter*, 2009. Vol. 404, No. 2, p. 315-319.

183. PETERSEN, J.; BRIMONT, C.; GALLART, M.; CRÉGUT, O.; SCHMERBER, G.; GILLIOT, P.; HÖNERLAGE, B.; ULHAQ-BOUILLET, C.; REHSPRINGER, J.L.; LEUVREY, C.; COLIS, S.; SLAOUI, A.; DINIA, A. Optical properties of ZnO thin films prepared by sol-gel process. *Microelectronics Journal*, 2009. Vol. 40, No. 2, p. 239-241.

184. EILERS, H.; TISSUE, B.M. Synthesis of nanophase ZnO, Eu2O3, and ZrO2 by gas-phase condensation with cw-CO2 laser heating. *Materials Letters*, 1995. Vol. 24, No. 4, p. 261-265.

185. SUN, Y.; FUGE, G.M.; ASHFOLD, M.N.R. Growth of aligned ZnO nanorod arrays by catalyst-free pulsed laser deposition methods. *Chemical Physics Letters*, 2004. Vol. 396, No. 1-3, p. 21-26.

186. WANG, Y.; ZHANG, J.; CHEN, X.; LI, X.; SUN, Z.; ZHANG, K.; WANG, D.; YANG, B. Morphology-controlled fabrication of polygonal ZnO nanobowls templated from spherical polymeric nanowell arrays. *Journal of Colloid and Interface Science*, 2008. Vol. 322, No. 1, p. 327-332.

187. YANG, Y.; WANG, X.; SUN, C.; LI, L. Photoluminescence of ZnO nanorod-TiO<sub>2</sub> nanotube hybrid arrays produced by electrodeposition. *Journal of Applied Physics*, 2009. Vol. 105, No. 9.

188. KRISHNAKUMAR, T.; PINNA, N.; KUMARI, K.P.; PERUMAL, K.; JAYAPRAKASH, R. Microwave-assisted synthesis and characterization of tin oxide nanoparticles. *Materials Letters*, 2008. Vol. 62, No. 19, p. 3437-3440.

189. BARTELS, H.A. The effect of eugenol and oil of cloves on the growth of micro.overddot.organisms. *American Journal of Orthodontics and Oral Surgery*, 1947. Vol. 33, p. 458-465.

190. SAWAI, J., KOJIMA, H., IGARASHI, H., HASHIMOTO, A., SHOJI, S. AND; SHIMIZU, M. Evaluation of Growth Inhibitory Effect of Ceramics Powder Slurry on Bacteria by Conductance Method. *JOURNAL OF CHEMICAL ENGINEERING OF JAPAN*, 1995. Vol. 28, p. 288-293. ISSN 0021-9592.

191. YIAMSAWAS, D., BOONPAVANITCHAKUL, K., KANGWANSUPAMONKON, W., *Synthesis and Characterization of ZnO Nanostructures with Antimicrobial Properties*, in *2008 International Conference on Nanoscience and Nanotechnology*. 2008, Ieee: New York. p. 133-136.

192. SAWAI, J.; SAITO, I.; KANOU, F.; IGARASHI, H.; HASHIMOTO, A.; KOKUGAN, T.; SHIMIZU, M. Mutagenicity test of ceramic powder which have growth inhibitory effect on bacteria. *J. Chem. Eng. Japan*, 1995. Vol. 28, p. 352-354.

193. YAMAMOTO, O. Influence of particle size on the antibacterial activity of zinc oxide. *International Journal of Inorganic Materials*, 2001. Vol. 3, No. 7, p. 643-646. ISSN 1466-6049.

194. OHIRA T., Y.O., IIDA Y., NAKAGAWA Z. Antibacterial activity of ZnO powder with crystallographic orientation. *Journal of Materials Science: Materials in Medicine*, 2008. Vol. 19, p. 1407-1412. ISSN 0957-4530.

195. ZHANG L., D.Y., POVEY M., YORK D. ZnO nanofluids – A potential antibacterial agent. *Progress in Natural Science*, 2008. Vol. 18, p. 939–944.

196. YAMAMOTO, O., HOTTA, M., SAWAI, J., SASAMOTO, T., KOJIMA, H. Influence of powder characteristic of ZnO on antibacterial activity Effect of specific surface area. *Journal of the Ceramic Society of Japan*, 1998. Vol. 106(10), p. 1007-1011. ISSN 0914-5400.

197. SAWAI, J.; YOSHIKAWA, T. Quantitative evaluation of antifungal activity of metallic oxide powders (MgO, CaO and ZnO) by an indirect conductimetric assay. *Journal of Applied Microbiology*, 2004. Vol. 96, No. 4, p. 803-809. ISSN 1365-2672.

198. YAMAMOTO, O.; KOMATSU, M.; SAWAI, J.; NAKAGAWA, Z.-E. Effect of lattice constant of zinc oxide on antibacterial characteristics. *Journal of Materials Science: Materials in Medicine*, 2004. Vol. 15, No. 8, p. 847-851.

199. SAWAI, J.; SHOJI, S.; IGARASHI, H.; HASHIMOTO, A.; KOKUGAN, T.; SHIMIZU, M.; KOJIMA, H. Hydrogen peroxide as an antibacterial factor in zinc oxide powder slurry. *Journal of Fermentation and Bioengineering*, 1998. Vol. 86, No. 5, p. 521-522.

200. YAMAMOTO, O., IIDA, Y. Antifungal Characteristics of Spherical Carbon Materials with Zinc Oxide. *Journal of the Ceramic Society of Japan*, 2003. Vol. 111, p. 614-616. ISSN 0914-5400.

201. YAMAMOTO, O.; SAWAI, J.; HOTTA, M.; KOJIMA, H.; SASAMOTO, T. Growth inhibition of bacteria by MgO-ZnO solid-solution powders - Influence of doping amount of ZnO. *Nippon Seramikkusu Kyokai Gakujutsu Ronbunshi/Journal of the Ceramic Society of Japan*, 1998. Vol. 106, No. 12, p. 1252-1254.

202. SAWAI, J.; KAWADA, E.; KANOU, F.; IGARASHI, H.; HASHIMOTO, A.; KOKUGAN, T.; SHIMIZU, M. Detection of active oxygen generated from ceramic powders having antibacterial activity. *Journal of Chemical Engineering of Japan*, 1996. Vol. 29, No. 4, p. 627-633.

203. SAWAI, J.; KOJIMA, H.; IGARASHI, H.; HASHIMOTO, A.; SHOJI, S.; TAKEHARA, A.; SAWAKI, T.; KOKUGAN, T.; SHIMIZU, M. Escherichia coli damage by ceramic powder slurries. *Journal of Chemical Engineering of Japan*, 1997. Vol. 30, No. 6, p. 1034-1039.

204. ZHANG, L.; JIANG, Y.; DING, Y.; POVEY, M.; YORK, D. Investigation into the antibacterial behaviour of suspensions of ZnO nanoparticles (ZnO nanofluids). *Journal of Nanoparticle Research*, 2007. Vol. 9, No. 3, p. 479-489.

205. SAWAI, J.; IGARASHI, H.; HASHIMOTO, A.; KOKUGAN, T.; SHIMIZU, M. Effect of particle size and heating temperature of ceramic powders on antibacterial activity

of their slurries. *Journal of Chemical Engineering of Japan*, 1996. Vol. 29, No. 2, p. 251-256.

206. STOIMENOV, P.K.; KLINGER, R.L.; MARCHIN, G.L.; KLABUNDE, K.J. Metal Oxide Nanoparticles as Bactericidal Agents. *Langmuir*, 2002. Vol. 18, No. 17, p. 6679-6686.
207. FLOWERS, R.H., III; SCHWENZER, K.J.; KOPEL, R.F.; FISCH, M.J.; TUCKER, S.I.; FARR, B.M. Efficacy of an Attachable Subcutaneous Cuff for the Prevention of Intravascular Catheter-Related Infection: A Randomized, Controlled Trial. *JAMA*, 1989. Vol. 261, No. 6, p. 878-883.
208. RAAD, I. Intravascular-catheter-related infections. *The Lancet*, 1998. Vol. 351, No. 9106, p. 893-898.
209. CALDWELL, D.E.; KORBER, D.R.; LAWRENCE, J.R. Imaging of Bacterial-Cells by Fluorescence Exclusion Using Scanning Confocal Laser Microscopy. *Journal of Microbiological Methods*, 1992. Vol. 15, No. 4, p. 249-261. ISSN 0167-7012.
210. ELLIOTT, T.S.J.; MOSS, H.A.; TEBBS, S.E.; WILSON, I.C.; BONSER, R.S.; GRAHAM, T.R.; BURKE, L.P.; FAROQUI, M.H. Novel approach to investigate a source of microbial contamination of central venous catheters. *European Journal of Clinical Microbiology & Infectious Diseases*, 1997. Vol. 16, No. 3, p. 210-213.
211. RAAD, I.I.; SABBAGH, M.F.; RAND, K.H.; SHERERTZ, R.J. Quantitative tip culture methods and the diagnosis of central venous catheter-related infections. *Diagnostic Microbiology and Infectious Disease*, 1992. Vol. 15, No. 1, p. 13-20.
212. HABASH, M.; REID, G. Microbial biofilms: Their development and significance for medical device-related infections. *Journal of Clinical Pharmacology*, 1999. Vol. 39, No. 9, p. 887-898. ISSN 0091-2700.
213. GREEN, R.J.; DAVIES, M.C.; ROBERTS, C.J.; TENDLER, S.J.B. Competitive protein adsorption as observed by surface plasmon resonance. *Biomaterials*, 1999. Vol. 20, No. 4, p. 385-391.
214. SHERERTZ, R.J.; RAAD, I.I.; BELANI, A.; KOO, L.C.; RAND, K.H.; PICKETT, D.L.; STRAUB, S.A.; FAUERBACH, L.L. Three-year experience with sonicated vascular catheter cultures in a clinical microbiology laboratory. *J. Clin. Microbiol.*, 1990. Vol. 28, No. 1, p. 76-82.
215. MAKI, D.G.; WEISE, C.E.; SARAFIN, H.W. A Semiquantitative Culture Method for Identifying Intravenous-Catheter-Related Infection. *New England Journal of Medicine*, 1977. Vol. 296, No. 23, p. 1305-1309.
216. NICKEL, J.C.; COSTERTON, J.W.; MCLEAN, R.J.C.; OLSON, M. Bacterial biofilms: Influence on the pathogenesis, diagnosis and treatment of urinary tract infections. *J. Antimicrob. Chemother.*, 1994. Vol. 33, No. suppl_A, p. 31-41.
217. TRAUTNER, B.W.; DAROUICHE, R.O. Catheter-Associated Infections: Pathogenesis Affects Prevention. *Arch Intern Med*, 2004. Vol. 164, No. 8, p. 842-850.
218. O´GRADY, N.P.; ALEXANDER, M.; DELLINGER, E.P.; GERBERDING, J.L.; HEARD, S.O.; MAKI, D.G.; MASUR, H.; MCCORMICK, R.D.; MERMEL, L.A.; PEARSON, M.L.; RAAD, I.I.; RANDOLPH, A.; WEINSTEIN, R. Guidelines for the Prevention of Intravascular Catheter Related Infections. *Infection Control and Hospital Epidemiology*, 2002. Vol. 23, No. 12, p. 759-769.

219. NOIMARK, S.; DUNNILL, C.W.; WILSON, M.; PARKIN, I.P. The role of surfaces in catheter-associated infections. *Chemical Society Reviews*, 2009. Vol. 38, No. 12, p. 3435-3448. ISSN 0306-0012.

## CURRICULUM VITAE

**Name:** Michal Machovský

**Date of birth:** 1982, April 09

**Place of birth:** Nový Jičín

**Permanent address:** U hřiště 362, Nový Jičín 741 01, Czech Republic

**Nationality:** Czech

**Affiliation:** Polymer Centre, Faculty of technology, Tomas Bata University in Zlin, Náměstí T. G. Masaryka 275, 762 72 Zlín, Czech Republic
Phone: (+420)-57-603-8049
E-mail: machovsky@ft.utb.cz

**Education:**

2001 – 2004 – Faculty of Technology, Tomas Bata University in Zlin
Bc. (BSC.) degree in study programme Chemistry and Materials Technology
Bachelor thesis: Využití termické analýzy pro charakterizaci plastů

2004 – 2006 – Department of Physics and Materials Engineering
Faculty of Technology, Tomas Bata University in Zlin
Ing. (MSc.) degree in study programme Chemistry and Materials Technology
Master thesis: Optická měření difuzních procesů v biopolymerech

2006 - Polymer Centre, Faculty of Technology, Tomas Bata University in Zlin
PhD student in the doctoral programme Chemistry and Materials Technology

## LIST OF PAPERS

**Journal articles:**

1. MACHOVSKY, M.; KURITKA, I.; BAZANT, P.; PASTOREK, M.; SAHA, P. Formation mechanism of ZnO particles prepared by microwave assisted hydrothermal synthesis under mild pH condition. *manuscript in preparation for Crystal Growth and Design.*
2. MACHOVSKY, M.; KURITKA, I.; BAZANT, P.; VESELA, D.; SAHA P.; Antibacterial performance of ZnO based fillers with mesoscale structured morphology in model medical PVC composites. *submitted to Materials Science and Engineering C: Materials for biological applications.*
3. BAZANT, P.; KURITKA, I.; HUDECEK, O.; MACHOVSKY, M.; MRLIK, M.; SEDLACEK, T. Microwave assisted synthesis of Ag/ZnO hybrid filler, preparation and characterization of antibacterial PVC composites made from the same. *accepted to Polymer composites.*
2. MACHOVSKY, M.; KURITKA I.; SEDLAK J.; PASTOREK M. Hexagonal ZnO porous plates prepared from microwave synthesized layered zinc hydroxide sulphate via thermal decomposition. *Materials Research Bulletin, 2013.* http://dx.doi.org/10.1016/j.materresbull.2013.06.018
5. HUBACKOVA, J.; DVORACKOVA M.; STLOUKAL, P.; MOKREJS P.; KUPEC J.; ALEXY, P.; BUGAJ, P.; MACHOVSKY M.; KOUTNY, M. Influence of various starch types on PCL/starch blends anaerobic biodegradation. *Polymer Testing,* 2013. doi: 10.1016/j.polymertesting.2013.05.008.
6. MERCHAN, M.; SEDLARIKOVA, J.; VESEL, A.; MACHOVSKY, M.; SEDLARIK, V.; SAHA, P. Antimicrobial Silver Nitrate-doped Polyvinyl Chloride Cast Films: Influence of Solvent on Morphology and Mechanical Properties. *International Journal of Polymeric Materials and Polymeric Biomaterials,* 2013, vol. 62, no. 2, p. 101-108. ISSN 0091-4037.
7. POLASKOVA, M.; CERMAK, R.; VERNEY, V.; PONIZIL, P.; COMMEREUC, S.; GOMES, M. F. C.; PADUA, A. A. H.; MOKREJS, P.; MACHOVSKY, M. Preparation of microfibers from wood/ionic liquid solutions. *Carbohydrate Polymers,* 2013, vol. 92, no. 1, p. 214-217. ISSN 0144-86178.
8. MACHOVSKY, M.; KURITKA, I.; KOZAKOVA, Z. Microwave assisted synthesis of nanostructured Fe3O4/ZnO microparticles. *Materials Letters,* 2012, vol. 86, p. 136-138. ISSN 0167-577X.
9. OLEJNIK, R.; SLOBODIAN, P.; RIHA, P.; MACHOVSKY, M. Increased sensitivity of multiwalled carbon nanotube network by PMMA functionalization to vapors with affine polarity. *Journal of Applied Polymer Science,* 2012, vol. 126, no. 1, p. 21-29. ISSN 0021-8995.

10. GREGOROVA, A.; MACHOVSKY, M.; WIMMER, R. Viscoelastic Properties of Mineral-Filled Poly(lactic acid) Composites. *International Journal of Polymer Science,* 2012. ISSN 1687-9422.

11. HUSAROVA, L.; MACHOVSKY, M.; GERYCH, P.; HOUSER, J.; KOUTNY, M. Aerobic biodegradation of calcium carbonate filled polyethylene film containing pro-oxidant additives. *Polymer Degradation and Stability,* 2010, vol. 95, no. 9, p. 1794-1799. ISSN 0141-3910.

12. MERCHAN, M.; SEDLARIKOVA, J.; SEDLARIK, V.; MACHOVSKY, M.; SVOBODOVA, J.; SAHA, P. Antibacterial Polyvinyl Chloride/Antibiotic Films: The Effect of Solvent on Morphology, Antibacterial Activity, and Release Kinetics. *Journal of Applied Polymer Science,* 2010, vol. 118, no. 4, p. 2369-2378. ISSN 0021-8995.

13. POLASKOVA, M.; SOWE, M.; KURITKA, I.; SEDLACEK, T.; MACHOVSKY, M.; SAHA, P. Medical-Grade Polyvinyl Chloride Modified with Crystal Violet and Montmorillonite. *International Journal of Polymer Analysis and Characterization,* 2010, vol. 15, no. 1, p. 18-26. ISSN 1023-666X.

14. HRABALOVA, M.; GREGOROVA, A.; WIMMER, R.; SEDLARIK, V.; MACHOVSKY, M.; MUNDIGLER, N. Effect of Wood Flour Loading and Thermal Annealing on Viscoelastic Properties of Poly(lactic acid) Composite Films. *Journal of Applied Polymer Science,* 2010, vol. 118, no. 3, p. 1534-1540. ISSN 0021-8995.

15. KOZAKOVA, Z.; BAZANT, P.; MACHOVSKY, M.; BABAYAN, V.; KURITKA, I. Fast Microwave-Assisted Synthesis of Uniform Magnetic Nanoparticles. *Acta Physica Polonica A,* 2010, vol. 118, no. 5, p. 948-949. ISSN 0587-4246.

**Conference proceedings:**

1. MACHOVSKY, M.; KRATOSOVA, G.; DELORT, A-M.; KOUTNY, M. Microorganisms on the surface of filled low density polyethylene film containing prooxidant additives; scanning electron microscopy survey. *First Congress of the Federation for Environmental Research - Interactions between physico-chemical and microbiological processes in the environment*, Clermont-Ferrand, France, 22-24th October 2008.

2. OTGONZUL, O.; MACHOVSKY, M.; SEDLARIK, V.; KITANO, T.; SAHA, P. Structure properties of partially biodegradable polyamide/polyester polymer blend. *22nd International symposium on polymer analysis and characterization (ISPAC)*, Zlin, Czech Republic, 22-24th June, 2009.

3. POLASKOVA, M.; SOWE, M.; KURITKA, I.; SEDLACEK, T.; MACHOVSKY, M. Medical grade polyvinyl chloride modified with crystal violet and montmorillonite.*22nd International symposium on polymer analysis and characterization (ISPAC)*, Zlin, Czech Republic, 22-24th June, 2009.

4. MRACEK, A.; LEHOCKY, M.; GRULICH, O.; MACHOVSKY, M.; VELEBNY, V. The plasma treatment modification of hyaluronan thin films. *2nd International Conference on Advanced Plasma Technologies (ICAPT) with 1st International Plasma Nanoscience Symposium*, Piran, Slovenia, 29th September-2nd October,2009.
5. MACHOVSKY, M.; BAZANT, P.; KURITKA, I. Novel additives for antimicrobial polymer systems. *Konference Plastko*, Zlin, Czech Republic, 13-14th April, 2010.
6. SLOBODIAN, P.; RIHA, P.; OLEJNIK, R.; PETRAS, D.; MACHOVSKY, M.; SAHA, P. Electromechanical sensors based on carbon nanotube networks. *Fourth International Conference on Sensing Technology (ICST)*, Lecce, Italy, 3-5th June, 2010.
7. KOZAKOVA, Z.; BAZANT, P.; MACHOVSKY, M.; BABAYAN, V.; KURITKA, I. Fast microwave synthesis of uniform magnetic nanoparticles. *14th Czech and Slovak Conference on Magnetism*, Kosice, Slovakia, 6-9th July, 2010.
8. KALENDOVA, A.; KOVAROVA, L.; MALAC, J.; MACHOVSKY, M.; GERARD, J. F. Morphological Study of PVC/Montmorillonite Nanocomposites. In *Nanocon 2010, 2nd International Conference*. 2010. p. 47-52. ISBN 978-80-87294-19-2.
9. BAZANT, p.; KOZAKOVA, Z.; HUDECEK, O.; MACHOVSKY, M. PASTOREK, M.; KURITKA I. Composite material based on hybrid micro-sized Ag-ZnO filler for antibacterial applications. In *Nanocon 2011*, Brno, Czech Republic, 21-23th September, 2011. ISBN 978-80-87294-23-9, p. 459-464.
10. BAZANT, P., MACHOVSKY, M., KURITKA, I., KUCHARCZYK, P., GREGOROVA, A., SEDLARIK, V. *Microwave-assisted synthesis of ZnO/Ag antimicrobial submicro-particles on bio-template*. International Conference on Advanced Plasma Technologies (ICAPT 2011), Strunjan, Slovenia, 11-13th April, 2011. ISBN 978-961-92989-3-0, p. 96-99.
11. BAZANT, P.; KURITKA, I.; MACHOVSKY, M.; SEDLACEK, T.; PASTOREK, M. Microwave assisted synthesis of Ag-ZnO particles and their antibacterial properties. *Mathematical Methods and Techniques in Engineering and Environmental Science*, Catania, Italy, 3rd-5th September, 2011. ISBN 978-1-61804-046-6, p. 341-346.
12. KALENDOVA, A.; ZYKOVA, J.; MATEJKA, V.; MACHOVSKY, M.; PASTOREK, M.; MALAC, J. PVC Kaolinite/Urea Hybrids. In *Nanocon 2011*. 2011. p. 266-270. ISBN 978-80-87294-27-7.
13. KALENDOVA, A.; ZYKOVA, J.; MATEJKA, V.; MACHOVSKY, M.; MALAC, J. PVC Inorganic hybrids based on kaolinite/urea intercalates. *The Fifth International Conference on Quantum, Nano and Micro Technologies (ICQNM 2011)*, Nice/Saint Laurent du Var, France, 21-27th August, 2011. ISBN 978-1-61208-151-9, p. 109-113.

14. KOZAKOVA, Z.; MACHOVSKY, M.; BABAYAN, V.; PASTOREK, M.; KURITKA, I. Influence of Synthesis Parameters on the Growth Process of Magnetic Nanoparticles Synthesized by Microwave-Assisted Solvothermal Method. In *Nanocon 2011*. 2011. p. 280-286. ISBN 978-80-87294-27-7.

15. KUCHARCZYK, P.; SEDLARIK, V.; KITANO, T.; MACHOVSKY, M.; BARAK, M.; KOUTNY, M.; STLOUKAL P.; SAHA, P. Characterization of Partially Biodegradable Polylactide/Poly(methyl methacrylate) blends as potential biomaterials. *4th WSEAS International Conference on Engineering Mechanics, Structures, Engineering Geology, EMESEG'11, 2nd International Conference on Geography and Geology 2011, WORLD-GEO'11, 5th International Conference on EDEB'11*, Corfu Island, Greece, 14-16th July, 2011. ISBN 978-1-61804-022-0, p. 341-346.

16. MACHOVSKY, M.; BAZANT, P.; KOZAKOVA, Z.; PASTOREK, M.; ZLEBEK, P.; KURITKA, I. Open Vessel Microwave-Assisted Synthesis of Ag/Zno Hybrid Fillers with Antibacterial Activity. In *Nanocon 2011*. 2011. p. 628-634. ISBN 978-80-87294-27-7.

17. MACHOVSKY, M.; KURITKA, I.; SAHA, P. Rapid microwave-assisted synthesis of twinned hexagonal ZnO microparticles. *Mathematical Methods and Techniques in Engineering and Environmental Science*, Catania, Italy, 3rd-5th September, 2011. ISBN 978-1-61804-046-6, p. 415-419.

18. SEDLAK, J.; BAZANT, P.; KOZAKOVA, Z.; MACHOVSKY, M.; PASTOREK, M.; KURITKA, I. Nanostructured Zinc Oxide Microparticles with Various Morphologies. In *Nanocon 2011*. 2011. p. 305-309. ISBN 978-80-87294-27-7.

19. BAZANT, P.; KOZAKOVA, Z.; KURITKA, I.; MACHOVSKY, M. Microwave assisted hydrothermal synthesi of Ag-ZnO nano-micro structures: comparison of closed and open vesel reaktor influence on nitrate solution preparation route. In *Nanocon* 2012. 2012. ISBN: 978-80-87294-32-1

20. MUNSTER, L.; KLOFAC, J.; SEDLAK, J.; BAZANT, P.; MACHOVSKY, M.; KURITKA, I. Microwave assisted modification of bio-template by Ag-ZnO sub-microparticles. In *Nanocon* 2012. 2012. ISBN: 978-80-87294-32-1

## APPENDIX – PAPERS INCLUDED TO THE THESIS

**Paper I.**

MACHOVSKY, M.(50 %); KURITKA, I.; BAZANT, P.; PASTOREK, M.; SAHA, P. Formation mechanism of ZnO particles prepared by microwave assisted hydrothermal synthesis under mild pH condition. *Manuscript in preparation to be submitted to Crystal Growth and Design*

# Formation Mechanism of ZnO Particles Prepared by Microwave Assisted Hydrothermal Synthesis under Mild pH Condition

MACHOVSKY MICHAL[1,2], KURITKA IVO[1,2,*], BAZANT PAVEL[1,2], PASTOREK MIROSLAV[1,3], SAHA PETR[1,2],

[1]Centre of Polymer Systems, University Institute, Tomas Bata University in Zlin, Nad Ovcirnou 3685, 760 01 Zlin, CZECH REPUBLIC

[2]Polymer Centre, Faculty of Technology, Tomas Bata University in Zlin, Nam. T. G. Masaryka 275, 762 72 Zlin, CZECH REPUBLIC

[3]Department of Polymer Engineering, Faculty of Technology, Tomas Bata University in Zlin, Nam. T. G. Masaryka 275, 762 72 Zlin, CZECH REPUBLIC

* Corresponding author: kuritka@ft.utb.cz, tel. +420 576 038 049

**Abstract:**

Twinned frustum ZnO microparticles were successfully prepared via a microwave-assisted hydrothermal method using zinc acetate dihydrate and hexamethylenetetramine as reactants. In order to understand the evolution process, time-lapse characterization by powder X-ray diffraction (XRD), scanning electron microscopy (SEM), thermogravimetric analysis (TGA), and attenuated total reflection Fourier transform infrared spectroscopy (ATR-FTIR) was performed. Collected data suggested that the mechanism of transformation proceeds in three stages involving formation of layered zinc hydroxy acetate tetrahydrate as the intermediate product followed by its transformation to the zinc oxide and then by further maturation of zinc oxide particles.

## 1 Introduction

Zinc Oxide (ZnO) is a versatile, multifunctional material which has accompanied human beings for over thousands years in a wide range of applications, and could be reasonable considered to be a mature engineering material. Its use has shifted during the time from medical ointments, facial powders, paint pigmentation, ceramics, to sunscreens, catalysts, or rubbers and plastics additive. The renewed interest in a last few decades has been driven by emergence of many prospective advanced applications, such as field-effect transistors, piezoelectric devices, chemical and biological sensors, field emitters, transparent conductors, ultraviolet light emitting devices, solar cells, etc [1, 2].

Technological importance of ZnO stems from wide direct band gap ($E_g$ ~ 3.37 eV) at room temperature, large exciton binding energy (~ 60 meV), and electrical and optical properties that can be further easily modified. Besides, the absence of a centre of symmetry in wurtzite ZnO crystal structure and partial polar characteristics are responsible for piezoelectric and pyroelectric properties [3, 4]. ZnO also possesses excellent thermal, chemical, and high-energy radiation stability, and is considered to be bio-compatible and bio-safe [5].

Based on the outstanding physico-chemical properties, a lot of efforts have been devoted to ZnO synthesis and characterization. Due to intrinsic features of ZnO crystal structure, a large variety of nano- and microstructures have been successfully prepared, constituting probably the richest family of structures among all inorganic materials. At ambient temperature and pressure, ZnO crystallizes preferentially in a wurtzite structure with a hexagonal lattice that has two interconnecting sub-lattices of $Zn^{2+}$ and $O^{2-}$ with the zinc ion surrounded by tetrahedral oxygen ions and vice versa. This tetrahedral coordination gives rise to crystal faces of different surface energies, among them polar basal plane $\langle 0001 \rangle$ and two non-polar planes $\langle 01\bar{1}0 \rangle$, $\langle 2\bar{1}\bar{1}0 \rangle$ are fast growing. Although growth habit of wurtzite ZnO is mainly determined by internal structure, it could be altered by tuning the relative growth rates at various crystal faces by changing external condition. The ability to control crystal growth is a matter of considerable interest because the optical, physico-chemical, electrical, or antibacterial properties of ZnO crystals are intimately dependent on the crystal morphology. [3]

Physical or “dry” methods, such as chemical vapour deposition (CVD), radio frequency (RF) magnetron sputtering, molecular beam epitaxy (MBE), or pulsed laser deposition (PLD), have been originally employed for fabrication of high quality single crystals and epitaxial layers of ZnO thin films, allowing realization of ZnO-based electronic and optoelectronic devices.
such as javelins [6], bipyramids [7], disks, rods, spindles, flowers [8], stars [9], cages [10], tetrapods [11], dumbbells [12]. Unfortunately, these “dry” physical processes require and harsh synthesis conditions, preventing them from being used for large-scale production and wide applications.

The physical and chemical properties of nanomaterials vary as a function of size, shape and surface chemistry. Thus, new synthetic strategies are vital for the development of novel nanomaterials. Generally, the synthesis methods for ZnO nanostructures can be divided into two groups: wet-chemical/solution based and physical techniques based [33]. Physical techniques, such as vapor–liquid–solid (VLS), vapor solid and chemical vapor deposition
(CVD) in addition to thermal evaporation, typically require high temperatures and pressures as well as particular substrates and result in low product yield. These methods produce highquality ZnO nanostructures; however, the methods are energy and cost intensive. Wet-chemical/solution based methods include hydrothermal/ solvothermal processes, solution–liquid–solid (SLS) and capping agents/surfactant-assisted synthesis. Zinc readily forms hydroxy and ammonia complexes and these methods are based on the hydrolysis of such complexes at elevated or room temperatures. Further, the growth direction can be controlled with various additives in these methods. Amine compounds are often used to direct growth in the c-direction, whereas citrate inhibits c-direction growth and directs the crystal shape into thicker rods or even plates. Thus, wet-chemical/solution based methods provide convenient, facile manipulation, potential for scale-up and a lower temperature pathway for the fabrication of the desired ZnO nanostructures [28,33]. Among them, the hydrothermal technique is a low temperature and relatively simple process, but it requires long reaction times (from a few hours to several days).

Microwave-assisted heating has been gaining importance in synthetic chemistry because of its unique effects, such as rapid and selective heating, higher reaction rates, increased product yields, and energy savings. As the microwave field applied to dielectric materials mainly induces the rotation of polarized dipoles in molecules which generates heat due to molecular inner friction. The presence of an electric field also leads to orientation effects of dipolar molecules and hence reduces the activation energy (entropy term) in the Arrhenius equation.

It is believed that due to the lower activation energy, faster nucleation and growth took place in the reaction solution [13]

As a matter of fact, the number of papers dedicated to microwave-assisted synthesis of inorganic nanomaterials is growing rapidly. However, the mechanism of formation and transformation of these different forms is often still poorly understood. [14]

## 2 Experimental

Zinc acetate dihydrate $Zn(CH_3COO)_2.2H_2O$ (ZAD) and hexamethylenetetramine $(CH_2)_6N_4$ (HMT) were analytical grade, purchased from PENTA (Czech Republic), and used as received without further purification. Demineralised water with a conductivity of 15.0 $\mu Scm^{-1}$ was used for experiments.

All experiments were performed in the microwave open vessel system MWG1K-10 (RADAN, Czech Republic; 1.5 kW, 2.45 GHz) based on modification of a domestic oven by drilling a hole on the ceiling for external cooler and equipped with external MW power source. The system was operated in continuous mode (with zero idle time), the power was set to maximum. The temperature of the reaction system was monitored by an industrial contactless thermometer (Raytek CM, Germany). In a typical synthesis process, 10.98 g of ZAD and 7.01g of HMT were dissolved in 100 mL and 50 mL of demineralised water, respectively. Obtained solutions were mixed together in a reaction bottle and exposed to microwave irradiation. After that, the system was left to cool down naturally. The white precipitate was filtered (0.23µm pore size membrane), washed thoroughly several times with demineralised water and dried in an laboratory oven at 40°C for 24 hours. The MW exposition time for each synthesis was chosen from the range of 2 to 60 minutes to cover the timescale of particle formation process completely. Hence, a series of 11 samples described in Table 1 was prepared by repeated synthesis under conditions indicated above.

The pH-meter Lab 870 (Shott Instruments, Germany) was used for pH monitoring of the reaction mixture prior MW exposure and post synthesis after cooling down before filtering.

Room temperature powder X-ray diffraction (XRD) analysis for crystal phase identification was conducted by the multi-purpose X-ray diffractometer PANalytical X´Pert PRO MPD (The Netherlands) with a Cu-Kα X-ray source ($\lambda$ = 1.5418 Å) in the diffraction angle range 5-85° 2θ. Although the used diffractometer was not equipped with a monochromator to remove Cu-Kα2 radiation and had not installed any Göbel mirror to improve the resolution and the

accuracy of the line position, the peak broadening still can give some useful information even without the knowledge of the instrumental broadening function and the use of Scherer equation. The apparent FWHM values were obtained by fitting Lorentzian peaks into the observed lines without the correction for instrument response. The peak at the $2\theta = 6.6°$ did not show any splitting, similarly, the resolution of the peak at 32.6° was to low as well; hence they were fitted by single Lorentzian function only. The results did not differ significantly from direct estimation of the FWHM value from enlarged graphical representation of the data. On the other hand, the peaks at wider angles 34.3°, 36.2° and 56.2° are split enough due to Kα1 and Kα2 doublet so that they allowed meaningful fitting procedure by two Lorentzian peaks. In these cases, the FWHM of the peak corresponding to the Kα1 was taken into consideration. The FWHM of the second peak in each doublet had almost the same value but estimated with larger uncertainty.

The morphology and structure were characterized by a scanning electron microscope Vega II/LMU (Tescan, Czech Republic) operated at acceleration voltage 5 kV. Thermogravimetric analysis (TGA) was carried out by a SETSYS Evolution 1200 (SETARAM, France) thermogravimeter at a heating rate 20°C $min^{-1}$ in flowing air (30 sccm). Fourier transform infrared (FTIR) spectra were measured on Nicolet iS10 FT-IR spectrometer (Thermo Fisher Scientific Inc., NicoletCZ s.r.o., Czech Republic) equipped with an attenuated total reflectance (ATR) accessory utilizing a diamond crystal.

## 3 Results and discussion

Although a large amount of research papers is devoted to the hydrothermal synthesis of ZnO even with the assistance of MWs, the reaction mechanism is still a mater of vivid discussion and controversial interpretations can be found in the literature. Below discussed original results of instrumental analysis can be elaborated together with the available literature and summarised into a description of the reaction mechanism and ZnO material growth model and implications towards further use of the described synthesis method.

### *3.1 Apparent synthesis stages*

MW irradiation enables very fast and uniform heating of the reaction media. Temperature monitoring as well as visual observation of boil intensity and vapour condensation in external cooler confirmed a steep increase of temperature during the first minute of heating of reaction mixture by MW. The maximum temperature was reached after 1.5 minute and then the reflux

was stabilized, boiling intensity and temperature remained unchanged excepting small fluctuations until MW switched off. Therefore, the first product was collected after 2 minutes which corresponds to the stabilization of the energy transfer processes in the system. To obtain better understanding of the product formation mechanism, a series of time dependent experiments was performed. Data on reaction time, yield and appearance of obtained products are given in Table 1. Three distinctive steps – synthesis stages – can be readily seen and identified according to yield versus time dependence and experienced process behaviour.

**Table 1** Overview of the synthesis conditions, obtained products, yield and apparent reaction stages

| Sample code | Synthesis time [min] | Weight of sample [g] | Comments on obtained product appearance and macroscopically experienced properties | Synthesis stage |
|---|---|---|---|---|
| S2 | 2 | 1.646 | filtration speed – slow<br>filtration cake – thick and soft<br>water wettability – good | I |
| S3 | 3 | 1.627 | | |
| S4 | 4 | 1.567 | | |
| S5 | 5 | 1.393 | filtration speed – relatively fast,<br>filtration cake – medium thickness,<br>water wettability – poor | II |
| S6 | 6 | 1.311 | | |
| S7 | 7 | 0.529 | filtration speed – very fast,<br>filtration cake – thin,<br>water wettability – poor | III |
| S8 | 8 | 0.527 | | |
| S9 | 9 | 0.534 | | |
| S10 | 10 | 0.415 | | |
| S20 | 20 | 0.665 | | |
| S60 | 60 | 0.558 | | |

*3.2 The pH value and the reaction mixture chemistry*

The pH value of the reaction mixture is a key factor to the synthesis of ZnO materials from solution by precipitation methods. It was monitored discontinuously outside the MW

apparatus at the laboratory temperature. It was measured after mixing of the source solutions and before filtration of the cooled reaction mixture for each sample. The pH value was 6.5 immediately after mixing of the reaction solutions and remained 6.3 in all cooled reaction mixtures which testifies that the reaction mixture is a buffer system whose capacity was not consumed even after one hour of the reaction.

To understand growth mechanism of prepared ZnO microparticles solution chemistry must be understand first. The ZnO crystal habit growth is usually considered to consist of repeated linkages of $Zn(OH)_2^{4-}$ growth units. However, this behaviour cannot be generalized for all possible cases.

The ZAD was used as a source of $Zn^{2+}$. It dissolves readily in water yielding a clear solution. For aqueous solution of a salt, the pH value can differ from neutral depending on hydrolysis degree of cations and/or anions in water. For aqueous solution of ZAD, the pH gradually decreases with increase of the ZAD concentration, suggesting that the $Zn^{2+}$ ions hydrolyze more than $CH_3COO^-$ ions [15]. At a given concentration, $Zn^{2+}$ can form various hydroxycomplexes, the stability of these is dependent on pH and temperature of the solution. Under acidic conditions, positively charged metal $Zn^{2+}$ ions or $Zn(OH)^+$ are possible species, whereas uncharged hydroxycomplex $Zn(OH)_2$ is prevailing form under neutral and moderately basic conditions. Negatively charged hydroxycomplexes $Zn(OH)_3^-$ and $Zn(OH)_4^{2-}$ are than expected to be formed at alkaline condition. As the pH value of used ZAD aqueous solution is 6.1, $Zn^{2+}$ and $Zn(OH)^+$ can be expected to be predominating species.

Similarly as ZAD, HMTA dissolved in water readily as well. Hexamethylenetatramine (HMTA), also known as hexamine or methenamine, is a highly water soluble, non-ionic tetradentane cyclic tertiary amine. The use of HMTA as a precipitating agent has been widely reported in literature; however, the exact role of HMTA is still somewhat misunderstood. It is of general acceptance that HMTA acts as a source of $OH^-$ and that HMTA is sensitive to elevated temperature and slowly decomposes to ammonia and formaldehyde in boiling water solutions according the equation:

$$C_6H_{12}N_4 + 10H_2O \leftrightarrow 6CH_2O + 4NH_4^+ + 4OH^-$$

The continual decomposition of HMTA means that the reaction solution will contain ammonium ions and formaldehyde in addition to the starting material and zinc complexes $Zn(NH_3)_4^{2+}$, $Zn(NH_3)_3^{2+}$, $Zn(NH_3)_2^{2+}$ and $Zn(NH_3)^{2+}$ can be present in the reaction mixture in dependence on the value of pH.

*3.3 Morphology of the products*

SEM images in Figure 1 present the morphology evolution of the product in time-lapse record mode. Detailed images of examples of structures formed in various stages of the process are shown in Figure 2. At first sight, the morphology varied from plate-like to twinned particle-like with the increase of reaction time and three stages of the morphology development can be distinguished in accordance with macroscopic observation. Samples collected after 2, 3, and 4 minutes of synthesis exhibit plate-like structure (S2-S4) which correlates with slow filtration and other characteristic feature of the first identified synthesis step (I). Large layered agglomerates of platelets are randomly oriented and twisted. On closer inspection, the plates are rectangular in shape with dimensions of about one to ten micrometers and thickness of several tens of nanometers lying on each other rather than being entangled together. Although two dimensional platelets are predominant for short reaction time, proper examination revealed that seeds of three-dimensional structures assembled from plates are rarely present in the product. In order to understand the mechanism of particle formation, different stages of transformation from plate-like structure to twinned hexagonal prisms individual particle development are captured.

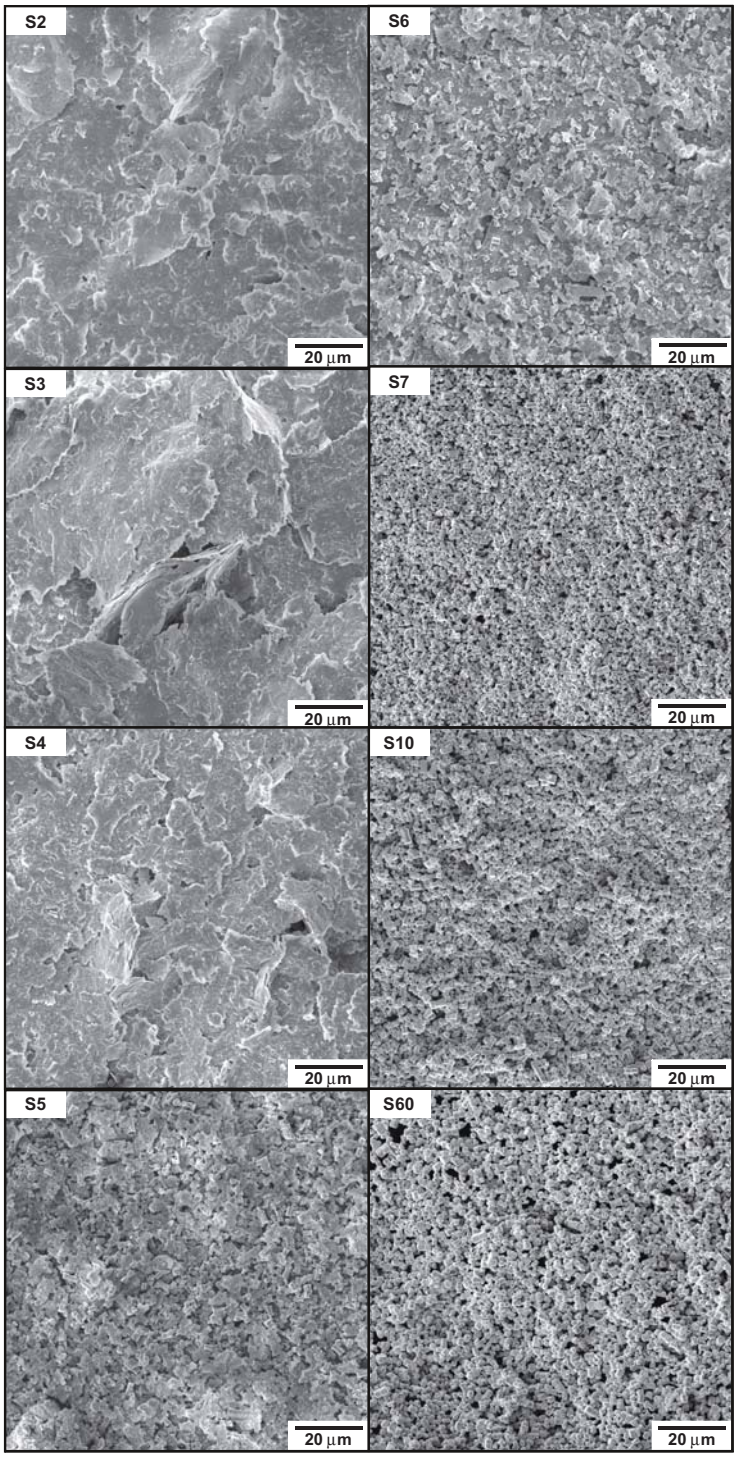


Fig. 1 SEM time-lapse study of the synthesis product morphology – general overview at low magnification. Labelling of images is identical with the sample codes.

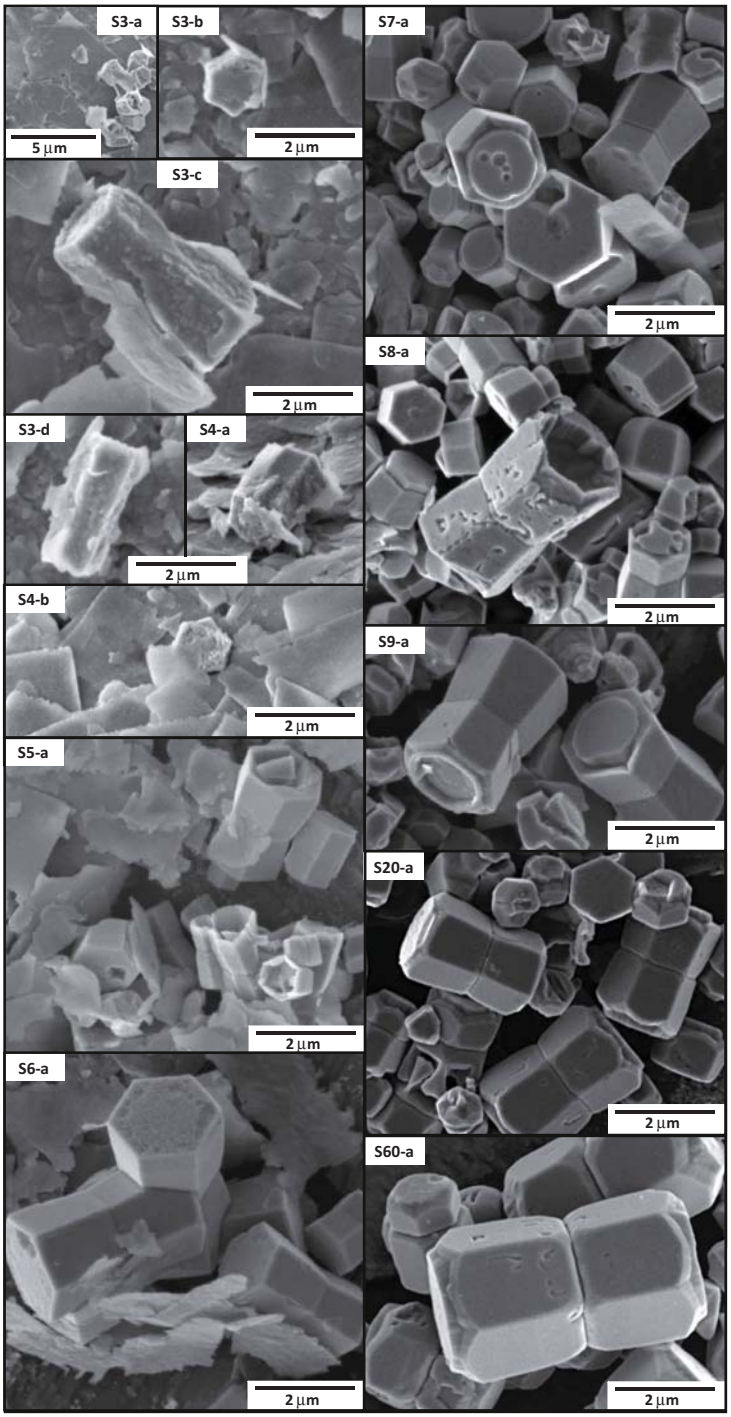


Fig. 2 SEM time-lapse study of the synthesis product morphology – selected details. Labelling of images is identical with the sample codes, the small letter denotes different detailed images captured for the same material. For more description see text.

Both rectangular shape of plates and morphology of crystallite seeds can be seen in detail in Figure 2. Image S3-a illustrates pieces of plates overlapping each other either in right-angled direction or rotated by 45° yielding octagonal symmetry with very first small particles close to the right border of the picture with obvious hexagonal symmetry motives yet not fully regular shapes. The image S3-b show adherence (sticking) of the platelets to the side facets of the seed particle evidencing thus important mechanism of the particle growth which becomes more observable in images S3-c, d and in S4-a. The particle in S3-c has already developed typical shape of twinned hexagonal frustums joined by their apical bases with a narrowing (resembling waist) in the middle part of the particle, the place where the grain boundary of twinned particles is clearly observable in all other following images. The inspection on S4-b confirms the presence of rectangular plates and seed of hexagonal shape in the sample S4.

While the plate-like morphology prevailed for the first development stage and particle seeds were rare, the proportion between plates and 3D structure inverted during second stage (II) of the synthesis in fifth and sixth minute. The size of plates for samples S5 and S observable in Figure 1 markedly decreased in comparison with the previous stages. The increase of seed concentration proceeds along with conversion of plates into twinned particles. Images S5-a, S6-a in Figure 2 document the formation of twinned frustums at the expense of plates on a larger scale as well as the change in size and shape of the plates with irregular borders. Hollow structures in the right lower corner of the image S5-a must be pointed out. It seems that the jacket of the hexagonal frustum particle is created by adherence of plates. It is clearly seen, that the platelets adhere to the surface of newly forming particle and that the volume of the frustums is created by attaching of plates to the trapezoidal facets by wrapping, rolling and compacting the platelets around the frustums. On the other hand, the internal space (cavity) must be filled subsequently by another mechanism. Some structural rebuilt occurs as evident from regular hexagonal or rhombic shapes of cavities in frustums bases if present. Intermediate shape of twinned particle for the second reaction stage (II) is exemplified in the last image window (S6-a) in the left column in the Figure 2. The twinned frustum has well defined shape with sharp edges, flat bases and a narrowing in the middle part where the grain boundary a commissure is clearly visible. However, the intermediate step keeps some residual characteristics of the I stage, i.e. rests of plates, and overlap into the next stage, as some particle with a disc cap can be seen in the image S7-a.

The last step (III) of synthesis is characterized by presence of fully developed three dimensional particles in the sample S7 and higher as obvious from particulate appearance of

their images in Figure 1 and in agreement with experienced fast filtration. Only rare single remaining plate is visible in the right lower corner of the detailed image S7-a in Figure 2. There are no rests of plates visible in images S8-a and higher. The final compacting and densification of the particles is characterised by capping the frustums with discs at the broader ends of the frustums, followed by gradual reshaping of the particles by erosion of the frustums base edges and especially cusps. Initial phase of the disc cap formation is shown in the image S9-a and following stages are characterised by growth of the caps together with progressive erosion of the edges. It is reasonable to expect, that the discs grow at the expenses of eroded edges.

A maturation phase of particle formation process is expected for the last reaction stage (III) as the yield of product remains nearly constant for high reaction times and the particles seems to be bigger (compare images S7, S10 and S60 in Figure 1) with time. Most likely, the bigger particles grow at the expenses of the smaller ones. Eroded polygonal rests of particles are observable among well developed twinned particles in Figure 2, images S9-a, S20-a and S60-a.The particles in the last stage (S60) have slightly lower aspect ratio, are slightly bigger and they are more likely of the shape of twinned hexagonal prisms with disc caps and "V" shaped notches in the prism edges, rather than the shape of twinned frustums derived from hexagonal pyramids typical for the intermediate (II) stage of synthesis.

*3.4 XRD analysis of crystalline phase structure*

The powder X-ray diffractograms of the as-synthesized product sampled at various time are shown in Figure 3. No diffraction peaks that can be ascribed directly to the residues of the ZAD and HMTA were observed. Moreover, neither monohydrate nor anhydrous zinc acetate diffraction patterns were manifested, which testifies that reactive paths of ZnO formation involving zinc acetate recrystallization in any of its lower hydratation stages are not present in this system. In next, no diffraction patterns typical for zinc hydroxide $Zn(OH)_2$ were observed.

XRD patterns shown in Figure 3 changed with increasing synthesis time, similarly as observed in SEM morphology investigation. In the early stage of synthesis (samples S2, S3 and S4), two groups of diffraction peaks were manifested in diffractograms. The low angle region of diffraction pattern is dominated by three distinct peaks at $2\theta = 6.6°$, 13.3° and 20.0° with the most intense one at 6.6°. In general, similar XRD patterns are typical for layered materials exhibiting sharp reflections at low angle and relatively weak reflections at high

degree angle. Based on the experimental conditions and chemicals used, compound that belongs to the rich family of layered double hydroxides (LDH) and hydroxy double salts (HDS) should be expected [16]. Literature survey revealed that similar XRD pattern were reported elsewhere [17-19] and assigned to the layered basic zinc acetate (LBZA), a rich family of compounds with idealised composition $Zn_5(OH)_8(CH_3COO)_2.nH_2O$. The value of *n* was reported 1.5 in [20], 2 in [21], 3 in [22] and 4 in [19]. Generally, the variability in stoichiometry of these compounds was reported as typical including fractional coefficients [17, 23]. Although the exact crystal structure of LBZA has not been unambiguously determined yet, it is considered as variation of the hypothetical brucite-like layered structure of $Mg(OH)_2$, in which $Zn^{2+}$ cations occupied both octahedral and tetrahedral coordination sites in the ratio 3/2. The resulting structural unit is a positively charged complex layer of $[Zn_3^{oct}(OH)_8Zn_2^{tet}(H_2O)_2]^{2+}$, and acetate anions are intercalated between layers in order to balance the charge and control interlayer distance [23]. The mode of interaction of acetate anions is not clear yet and is still a matter of vivid discussion. Although there are more reasonable arguments for free acetate anions in the interlayer gallery space (see references above) than for its direct unidentate bonding to a zinc atom in the hydroxide slab [15], the peculiarity of reintercalation of exchangeable of interlayer anions by acetate ions in LDHs which is reported in [24] testifies for its more complicated role and it seems that the exact acetate coordination depends on the route of LBZA preparation. A more detailed look into this issue is given in following sections dealing with infrared absorption spectra and thermogravimetry.

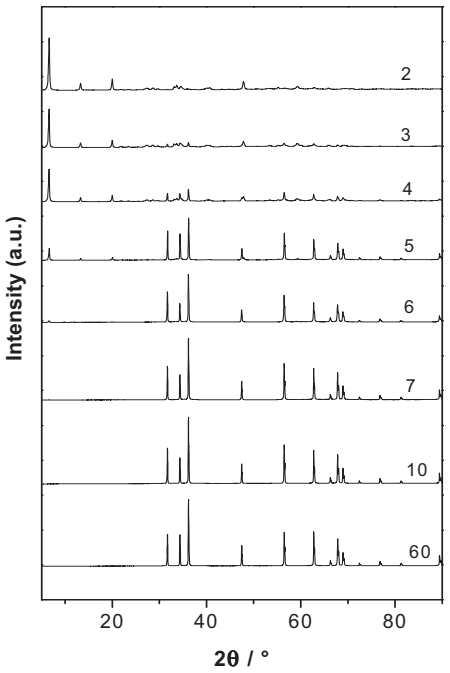


Fig. 3 X-Ray diffractograms recorded for samples S2 to S60,

The first peak from the left (in the low angle region) in the diffractogram of the sample S2 at the $2\theta$ position 6.6° correspond to the 001 diffraction of the layered LBZA phase and the peaks at $2\theta$ = 13.3° and 20.0° can be unambiguously assigned to the second and third order reflection reflections of the same set of planes. A distance of 1.34 nm fits perfectly to the well known Bragg condition for these diffraction lines. In accordance with [19, 20, 25], the three peaks testify for development of regular LBZA structure with interlayer space large enough for bilayer arrangement of free acetate ions and, moreover, enough space for two additional water molecules per structural unit, hence the n value can be expected even as high as 4 in [19]. On the other hand, no diffraction peak was found at the 9.3° which is the position typical for second order 001 reflection for bilayered basic zinc acetate (BLBZA) which can be synthesised under lower temperatures (below 60°C) and similar mild pH conditions [15, 17]. Another example is described by Cui et al. in [18] however its bilaminarity remained uncovered by the authors as they registered a reflection at 8.9°, interpreted it as the first order reflection corresponding to 0.99 nm interlayer distance and did not pay any further attention to this fact in their article hence describing their product like LBZA although it could be more appropriately identified as BLBZA, similarly as in work of Song et al. in [17].

The wide angle region in the diffractogram of the sample S2 comprised diffraction peaks of low intensity which can be explained as *hk*0 reflections. According to their relative broadness, the material can be assessed as manifesting structural disorder of twisted and/or translated against each other brucite-like sheets. However, judging according to the shape of the diffraction lines only, the perfection of the material seems to be lower than that observed for very well developed BLBZA reported in [17] but much better than observed for LBZAs published in [15, 20].

First appearance of peaks belonging to hexagonal wurtzite ZnO phase (JCDD PDF-2 entry 01-079-0207) was noticed in the diffractogram of the sample S3. With increasing synthesis time, the intensity of peaks related to ZnO crystalline phase become higher, whereas the intensity of peaks of LBZA phase declined sharply. Figure 3 shows the development of the most characteristic peak intensities for LBZA and ZnO. Typical patterns for ZnO are manifested for samples S2 and S3 in a trace level only, while for sample S4 their presence among other peaks becomes clearly visible. The ZnO manifestation overbalances the LBZA reflections lines for sample S5. The intensities of these peaks for samples S5 and higher do not differ markedly from the relative peak proportions of the pattern stored in the database which testifies for very small growth anisotropy of ZnO during the second and third stage of the synthesis, if any. Reasonable appearance of the ZnO diffraction pattern for S4 can be considered as the end of the first reaction stage and the beginning of the second reaction stage. On the other hand, the last manifestation of most intensive diffraction line for LABZA at 6.6° was observed for sample S6, thus confining the intermediate stage (from S4 to S6) in agreement with morphological observations yet the macroscopic characteristics of the sample S4 fitted more into the first stage as shown in Table 1.

The last stage of synthesis starts from S7 where no traces of the lines intensities corresponding to LBZA were observed at any position. The part of the series of samples from from S7 to S60 is characteristic by exclusive presence of ZnO crystalline phase and gradual maturation of developed particles is expected.

A more detailed insight into the growth mechanism can be obtained with the analysis of full width at half maximum (FWHM) for selected representative peaks in recorded diffractograms. The results are summarised in Table 2.

The 001 diffraction for LBZA material does not exhibit any shift of its maximum position within the 0.05° precision interval, which means that there is not any reasonable change of the interlayer distance over the synthesis time. The decrease of the respective FHWM of the 001 peak with time can be explained with the increase of crystallite dimension in the direction of

the *c* axis which means, that during the synthesis the number of stacking layers increases from a very small number of several layers at the beginning up to at least tens of layers [20]. This is in agreement with observed rolling and compacting of the synthesised plates. The final increase of the LBZA 001 peak FWHM value for the S6 sample where it was lastly observable testifies for exhausting of the LBZA and presence of very small amount of the material possibly in form of only some remaining LBZA layers in stacks otherwise almost transformed into ZnO.

The most intensive peak 101 for ZnO phase at 36.2° was analysed together with the 110 diffraction line at 56.5° to obtain information about the growth tendencies for ZnO particle. The position of peaks do not exhibit any change as it can be expected for wurtzite structure where no intercalation is possible. The peak corresponding to the 100 reflection appeared in S3 sample as the first well developed peak among all ZnO belonging diffraction lines, while the first noticed increase of signal intensity at the position of the peak 101 for sample S3 was too broad and of too low intensity to be analysed. The nuclei of ZnO must be very small and they were not observed in SEM images. The FWHM of the 101 peak for sample S4 gave rather an estimation of a range of values than one precise value. The obtained range 0.15-0.19° testifies for very small size of crystallites which gradually increases with the synthesis time. Saturation can be observed between $7^{th}$ and $10^{th}$ minute (S7, S10) which means that the growing particles exceeded the critical size where the ability of the used apparatus to distinguish the manifestation of the Scherer equation holds on. Slightly different trend can be observed for the peak 110. It starts to be noticeable in diffractograms for the material S4 which is later than for the former peaks. In next, the dependence of its FWHM has a maximum for S6 which testifies not only for growth anisotropy of the nuclei but also for a rearrangement of their growth imparting reduction of nuclei dimension in the respective direction. Identical behaviour was observed for the peak corresponding to the 002 diffraction line. It is noteworthy, that the maximum of FWHM for 110 and 002 peaks of ZnO coincides with the final increase of FWHM for the peak 001 of LBZA just before the LBZA vanishes from the system being totally converted to ZnO.

Table 2 Analysis of positions and apparent FWHM of selected peaks in diffractograms of prepaed materials.

| Peak identification | | Sample | | | | | | | |
|---|---|---|---|---|---|---|---|---|---|
| | | S2 | S3 | S4 | S5 | S6 | S7 | S10 | S60 |
| 001 LBZA | peak position / $2\theta°$ | 6.6 | 6.6 | 6.6 | 6.6 | 6.6 | n.a. | n.a. | n.a. |
| | FWHF | 0.23 | 0.21 | 0.20 | 0.18 | 0.24 | n.a. | n.a. | n.a. |
| 100 ZnO | peak position / $2\theta°$ | n.a. | 31.7 | 31.7 | 31.7 | 31.7 | 31.7 | 31.7 | 31.7 |
| | FWHF | n.a. | 0.20 | 0.18 | 0.14 | 0.14 | 0.13 | 0.13 | 0.13 |
| 101 ZnO | peak position / $2\theta°$ | n.a. | 36.2 | 36.2 | 36.2 | 36.2 | 36.2 | 36.2 | 36.2 |
| | FWHF | n.a. | n.a. | >0,15[a] | 0.13 | 0.13 | 0.10 | 0.09 | 0.09 |
| 110 ZnO | peak position / $2\theta°$ | n.a. | n.a. | 56.5 | 56.5 | 56.5 | 56.5 | 56.5 | 56.5 |
| | FWHF | n.a. | n.a. | n.a. | 0.13 | 0.15 | 0.10 | 0.10 | 0.10 |
| 002 ZnO | peak position / $2\theta°$ | n.a. | n.a. | 34.3 | 34.4 | 34.3 | 34.3 | 34.3 | 34.3 |
| | FWHF | n.a. | n.a. | n.a. | 0.12 | 0.13 | 0.10 | 0.09 | 0.09 |

[a] range 0.15-0.19

*3.5 Infrared spectroscopic study*

FTIR spectra were collected with the use of the ATR technique with the diamond crystal. Therefore, the recorded spectra are more sensitive to the surface composition than it would be in transmission mode. The spectra and spectral band assignments of collected samples are presented in Figure 3. Obtained spectra show strong correlation with the observed reaction

stages. Pure ZnO has week absorption bands in the regions from 560 and 550 $cm^{-1}$ and from 520 to 500 $cm^{-1}$, a significant and very strong band centred at about 450 $cm^{-1}$, and six other weak bands at lower frequencies [26]. On the other hand, it is virtually invisible at higher wavenumbers in mid-infrared region creating thus a large spectroscopic window. Hence, the composition of the material obtained in the first reaction step can be analyzed in detail and its decomposition during the second growth stage can be clearly followed too. For the final stage, obtained spectra are relatively poor and flat with some residual peaks only, which point towards possible occurrence of imperfections or defects on the surface of prepared ZnO particles that stem from original precursors.

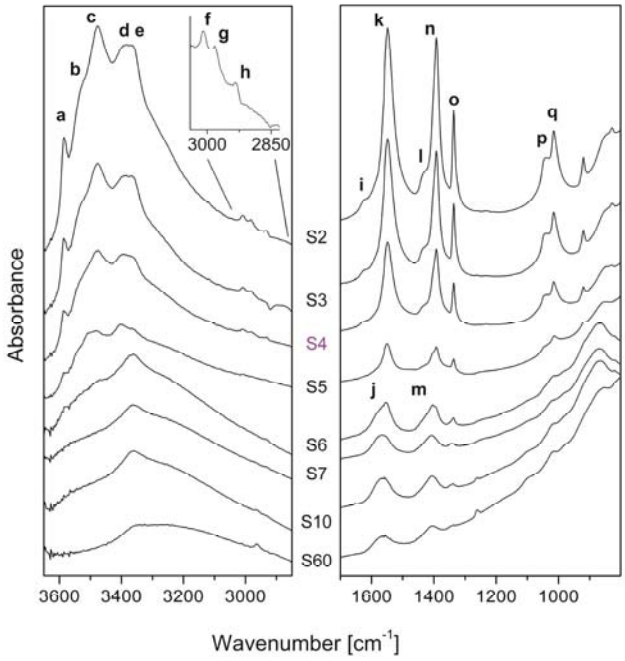


Fig. 4 ATR-FTIR absorption spectra of prepared products. The spectra are labelled according to the sample codes.

In the left panel of the Figure 4, there are manifested five relatively well-resolved bands superimposed on a broad peak for sample S2 in the O-H stretching vibration region from 3600 to 2800 $cm^{-1}$. The band loses the resolution and intensity with the increasing time of synthesis. The sharp band (a) observed at 3585 $cm^{-1}$ may be assigned to stretching vibrations of insulated OH group, which is not involved in any hydrogen bonding. This spectral band disappears within the second stage of material growth and its intensity correlates well with the

decrease of spectral intensity (i) in between 1620-1630 $cm^{-1}$, where the $OH^-$ deformation vibration mode of the hydroxide slab in layered material is manifested. It has been revealed by Wang Y. et al [15] that this band (i) increases in the IR absorption spectrum with the development of the layered structure from ZAD with the phase transformation through BLBZA to LBZA and these authors extrapolated out of their measured data this gradual replacement of acetate ion by hydroxyl one as the mechanism giving arise to $Zn(OH)_2$ followed by final ZnO formation which seems to be a reasonable hypothesis within the framework of their observations. However, in our case, this is not appropriate explanation of the reaction mechanism. Neither XRD nor this FTIR study confirmed occurrence of $Zn(OH)_2$ phase at any reaction stage. Moreover, it can be seen, that the band (i) vanishes much faster than (k) and (n) bands which are ascribed to acetate carboxyl group (see further discussion in this section).

The second most pronounced among prominent OH peaks is centred at 3475 $cm^{-1}$ (c) dominates the whole spectrum with its highest absorbance and has a clearly distinguishable band in its left shoulder at approximately 3535 $cm^{-1}$ (b). These spectral bands disappear in the second stage of material development as well. However, they lose the resolution faster than the intensity and merge into one broad peak which disappears totally in the third stage of material growth.

In next, a doublet of peaks (d) and (e) at positions 3393 $cm^{-1}$ and 3363 $cm^{-1}$, respectively, is attributed to OH stretching vibration as well. The peak at 3393 $cm^{-1}$ follows trend observed for previously described bands. The peak at 3363 $cm^{-1}$ is present in almost all spectra and does not disappear completely even during the maturation of the material after one hour, although XRD diffractograms show presence of ZnO crystalline phase only. Hence, these residual hydroxyls are associated with the defect structure of the particles surface.

The well defined shape of (b, c, d and e) peaks is most likely a manifestation of the structural order in prepared LBZA material in the first stage. The frequencies are lowered by different bonding configurations of hydroxyls in the crystalline structure, but the resulting bands are sharp, similarly as in case of intermolecular hydrogen bonding. These observations testify together with the wide angle XRD patterns for high quality of prepared crystalline LBZA phase during our experiments.

Finally, a very broad peak from 3600 $cm^{-1}$ to 2800 $cm^{-1}$ underlying all above described sharper bands may be assigned to vibrations of hydroxyl groups involved in significant hydrogen bonding with the omnipresent water. A plausible explanation is that the broad absorption band can be attributed to both physically (water, $H_2O$) and chemically (–OH

groups) bonded water to the surface of particles, especially this can be expected in the second and third reaction stage. In both cases, the frequencies could be reasonably dumped by hydrogen bonding and other interactions so the observed wavenumbers are dispersed and shifted towards lower values. The maximum of this broad band cannot be estimated unambiguously; therefore it is not indicated directly by a letter in the graph panels.

C-H stretching vibration bands of the interlayer acetate anion are observed at 3010 $cm^{-1}$, 2980 $cm^{-1}$, and 2932 $cm^{-1}$, see bands (f), (g) and (h) in the enlarged graph inset. These three peaks are typical for asymmetric (f and g) and symmetric (h) stretching vibrations of C-H on $sp^3$ hybridized carbon in $CH_3$ group; however, all three values are slightly shifted towards higher wavenumbers than typical for aliphatic hydrocarbons. The frequencies are raised due to carboxylic substituent as observed for acetate salts. [26]

Other significant absorption bands can be found below 1800 $cm^{-1}$ as shown in the right panel in Figure 4 The two most intense bands in spectra belongs to asymmetric stretch band ($\nu_{as}(COO^-)$) at 1548 $cm^{-1}$ (k) and symmetric stretch band ($\nu_s(COO^-)$) 1392 $cm^{-1}$ (n). The difference $\Delta\ \nu_{as-s}$ of 156 $cm^{-1}$ is related to the coordination state of the acetate anion with the metal cation [27] and is identical within the error caused by resolution with the difference observed for sodium acetate 155 $cm^{-1}$ [19]. Obviously, the acetate ion is not in bidentate coordination as in zinc acetate which has the $\Delta\ \nu_{as-s}$ value 91 $cm^{-1}$ [28]. This indicates that the acetate anions exist in such bonding configuration, that the bond character is almost purely ionic, hence it is not directly bonded to Zn atom where more covalent character would be an appropriate expectation. It suggest that the acetate anion is not directly attached to the matrix cation in $Zn_5(OH)_8(Ac)_2.4H_2O$ but interacts with it via hydrogen bonding. [19] Similarly, the elsewhere reported difference $\Delta\ \nu_{as-s}$ of 160 $cm^{-1}$ was interpreted as the evidence for free acetate anion and consequent completion of tetrahedral Zn sites by water molecules in other paper [25]. Different way of approaching to very similar observations is in [15] where the authors compares unidentate, bridging and bidentate coordinations of acetate anion, suggesting that $\Delta\ \nu_{as-s}$ of about 160-150 $cm^{-1}$ is related either to unidentate or to bridging coordination with zinc cations, as the difference of $\Delta\ \nu_{as-s}$ between unidentate and bridging coordination type is very small. However, our observed $\Delta\ \nu_{as-s}$ of 156 $cm^{-1}$ is closer to the value of 157 $cm^{-1}$ reported for unidentate coordination in LBZA than 151 for bridging coordination of carboxyl ion in BLBZA. On the other hand, it seems that presence of intercalated water and possible hydrogen bonding involvement in damping of vibrations makes the interpretation difficult in spite of the argumentation cogency in [19]. Observed $\Delta\ \nu_{as-s}$ shifts are relatively small and some ambiguity is there the acetate-zinc bonding

assgnement, comparison with XRD results discussed above and, somewhat surprisingly, with analysis of stoichiometry of prepared compounds which was examined by thermogravimetric study can contribute to the solution of this question, therefore the discussion on this issue continues in the next section.

The intensities of bands (k) and (n) decrease with the increase of reaction time and a new pair of peaks (j) and (m) appears at the position 1564 $cm^{-1}$ and 1406 $cm^{-1}$, respectively. The transition time is between fifth and seventh minute of synthesis which coincides with the passage from the second growth stage the third one. The very slight, but distinguishable shift towards higher frequencies together with a small increase of $\Delta\ \nu_{as\text{-}s}$ (158 $cm^{-1}$) value testifies for slight increase of ionic character of the interaction acetate anion with cation matrix in the zinc material. The coordination type remains unchanged whether it is unidentate or free anion and the low intensity of observed peaks suggests low concentration of acetate ions. According to XRD observation, the material has purely ZnO crystalline structure in the third stage of development. Therefore, it can be deduced that acetate ions are located at the surface of particles or in their pores if any.

The bands at 1435 $cm^{-1}$ (l), 1336 $cm^{-1}$ (o) and 1043 $cm^{-1}$ (p) and 1016 $cm^{-1}$ (q) are ascribed to various deformation vibration modes of -$CH_3$ group ( l – asymmetric in plane bending, o – symmetric in plane bending, and p – rocking mode). [25, 26] $CH_3$ group is a constituent group of the acetate ion and the time evolution of these peaks correlates with the decrease of intensities at 1548 and 1392 $cm^{-1}$ testifying thus the decrease of acetate amount in prepared materials. Similarly as for $COO^-$ group, some residual spectral densities at these wavenumbers are observable even in mature samples.

The bands at wavenumbers lower than 1000 $cm^{-1}$ can be ascribed to various vibrations of C-C and H-O-H without the need of being studied further in detail.

*3.6 Thermogravimetric analysis*

Thermogravimetric analysis (TGA) of prepared material was conducted in dynamic air atmosphere in order to clarify stoichiometry of composition of samples with respect to the ZnO content. The material decomposes by evolution of volatile products or products of oxidation according to other above discussed structural investigations and assumptions based on used materials; the analysed samples must contain zinc formally in (II+) oxidation state being coordinated by groups with high content of oxygen in (-II) oxidation state containing

hydrogen and carbon too. The rest of the material can be composed of water, acetyl, hydroxyl or carbonate moieties. Hence, the final product of heating of any such sample in oxidative atmosphere must be ZnO, if its decomposition temperature is not exceeded. The results of TG analysis are shown in Figure 4. Three main decomposition steps were observed for S2 material. As the reaction time increases, the total mass loss decreases with the steepest change between samples S4 and S5 which generally correlates with the second synthesis stage. The theoretical mass loss for LBZA identified by XRD based upon the formula $Zn_5(OH)_8(CH_3CO_2)_2.4H_2O$ is 37.7 % if the char contains pure ZnO only. Observed total mass loss for S2 was 37.1 % which is in agreement with theoretical predicted value for the tetrahydrate, although the amount of intercalated water could slightly vary. The first (A) and second (B) decomposition steps are overlapped and their separation was made at the position of the first valley on the -dTG curve. According to stoichiometric formula of the layered tetrahydrate, the total mass loss corresponding to the loss of four water molecules from the interlayer galleries per structural unit would be 11.03 %. The second decomposition step can be considered as dehydroxylation connected with the evolution of other four water molecules [19]. Among them, three $H_2O$ molecules can be evolved at the expenses of hydroxyl groups attached to zinc atoms, the fourth $H_2O$ molecule can be formed from two acetates while leaving acetanhydride in the solid phase. The total weight loss connected with these first two decomposition steps would be 22.06 %. This is in agreement with observation for S2 sample, where the mass loss was 22.2 %. Other interpretations of mechanisms for the second step of thermal decomposition of $Zn_5(OH)_8(CH_3CO_2)_2.4H_2O$ were published in the literature too. The second decomposition step was attributed to the collapse of the interlayer structure releasing a variety of products generated by multiple reaction mechanisms [29]. The third major decomposition step (C) is clearly separated on the –dTG curve and is followed by a small feature at the temperature nearly 400°C (D). The liberation of acetate groups can proceed as the release of molecular acetic acid and acetone [30-32], or other various organic compounds resulting from pyrolytical transformations of acetate anion catalysed by ZnO containing inorganic matrix [29] According to the literature [19], the last step is caused by volatilization of acetanhydride with theoretical mass loss of 15.63%. The acetate group may be lost as $CO_2$ and $H_2O$ under air atmosphere through the reaction with oxygen as well. Our experimental value of the weight loss in the third step is 14.8%. The slightly pronounced high temperature feature observed in the right shoulder of the peak C on -dTG curve cannot be interpreted so straightforwardly as the major peaks. At the final stage (D) of thermal decomposition, residual species can be evolved from the moieties embedded in collapsed layered structure of the

material with the total mass los about 0.7 %. Although no evolved gas analysis was made during this study, the observed weight losses and temperature maxima for the three major decomposition steps of S2 material are most compatible with observation and interpretation of Biswick et al [19].

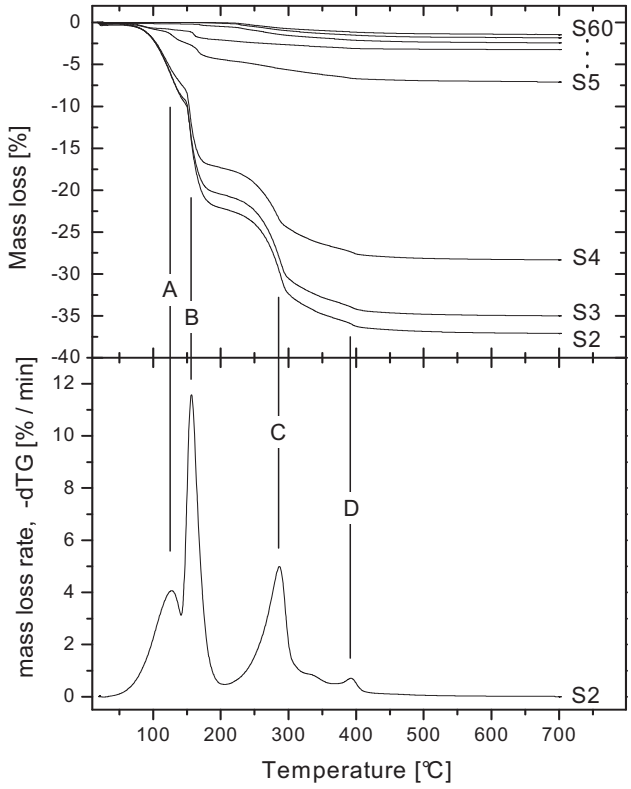


The total mass loss for S3 was 35.0 %. For trihydrate and dihydrate, the expected weight loss would be 35.93, and 34.06 %, respectively. The mass loss for the first two steps was 20.5 % (8.6 + 11.9 %). The third step corresponded with the mass loss of 14.5 %. These values fit best to the stoichiometry of trihydrate form of zinc hydroxy acetate (LBZA), where the release of 7.$H_2O$ would correspond to mass loss of 19.86 % and the acetanhydride would make 16.07 %, both together 35.93 %. However, the stoichiometric coefficient of intercalated water needs not to be necessarily an integer. Hence, initial formation of tetrahydrate and

successive loss of intercalated water is deduced for the first synthesis stage. With the decreasing content of hydrate water would the weight loss corresponding to the first two decomposition steps decrease and the mass loss for the third step would relatively increase. Such behaviour was not observed for materials S4 and S5. The corresponding TGA curves on Fig. 4 show rather overall flattening of signal than changing proportion between major steps. It is a manifestation of ZnO presence in material as the ZnO phase does not contribute significantly to observed weight losses, hence the observed pattern resemble mixing of the layered material with ZnO which should be virtually undetectable by TGA over this temperature range. It means in next, that monohydrate or anhydrate forms are most likely not present in the obtained product, which confirms the structural formula $[Zn_3^{oct}(OH)_8Zn_2^{tet}(H_2O)_2]^{2+}$ of the positively charged hydroxide slabs, as the two water molecules there must be bonded strongly that those two located in the interlayer space. It seems, that this complex unit balanced by two acetate counterions is that what is often indicated by the formula $Zn_5(OH)_8(CH_3COO)_2.2H_2O$ used elsewhere. Moreover, XRD analysis discussed above did not reveal any reasonable decrease of the interlayer distance of prepared LBZA phase with increasing synthesis time. This corresponds with the structural model involving two water molecules in direct coordination with zinc ions and free acetate anions stacked in two layers in the interlayer gallery of the LBZA thus being the main contributors to the interlayer spacing while the intercalation water molecules do not influence the distance too much. The IR absorption study discussed above supports this model strongly as well. To summarize briefly in other words, LBZA compound comprised in the S2 sample is actually a dihydrate and the chemical formula should be better written as $[Zn_3(OH)_8Zn_2(H_2O)_2](CH_3CO_2)_2.2H_2O$ rather than $Zn_5(OH)_8(CH_3CO_2)_2.4H_2O$ forcing an improper notion of the compound being a tetrahydrate. Consistently, the formula $[Zn_3(OH)_8Zn_2(H_2O)_2](CH_3CO_2)_2$ has to be used instead of wrong $Zn_5(OH)_8(CH_3COO)_2.2H_2O$ as this compound is not a hydrate in strict sense of that term at all.

According to this TG analysis, the second stage of synthesis can be centred between fourth and fifth minute of reaction time (materials S4 and S5) which is in agreement with the results of other instrumental analyses above. TGA curves for materials S6 keep some step-like structure resembling the three step decomposition, but the weight losses are almost negligible. The triad of TGA curves for materials S7 to S60 shows only minor decrease of weight caused by decomposition of surface impurities and dehydration of surface located hydroxyl groups. It can be straightforwardly concluded with respect to the results of all other analyses performed

on these samples that maturation and densification of the particles proceed with the increasing synthesis time from S7 to S60 which corresponds to the third stage of material synthesis.

**Conclusions**

ZnO with specific morphology of twinned frustums can be obtained through a MW assisted synthesis with all its advantages. The reaction time is shortened from tens of hours up to tens of minutes in comparison with conventional hydrothermal methods. Moreover, if needed, the developed method allows synthesizing well crystallized LBZA material in even shorter synthesis time too just by stopping the procedure in its early stage after 2 minutes.

The use of zinc acetate salt contributes to a robust buffer system formation during the synthesis. Although HMTA serves as source of hydroxyl anions and ammonium cations, the hydroxyl groups are built in the structure of the precursor LBZA during its formation formation while ammonium cations and acetate ions induce the buffering effect of a weak acid – weak base salt solution. The mechanism of ZnO formation does not involve neither ZnOH nor direct ZnO formation as observed for single source methods or for ZnCl. It is the intermediate product LABZA, which is subsequently transformed into ZnO.

Imparting the understanding of the reaction and crystal growth mechanisms and further development of the MW assisted solvothermal methods of ZnO synthesis will contribute to the environmental sustainability due to the enormous decrease of the synthesis time, energy and possibly material savings as well as it will conduce to the development of high performance functional materials.

**Acknowledgment**

This article was written with the support of the Operational Programme ‘Education for Competitiveness’ co-funded by the European Social Fund (ESF) and the national budget of the Czech Republic, within the project ‘Advanced Theoretical and Experimental Studies of Polymer Systems’ (reg. number: CZ.1.07/2.3.00/20.0104).

This article was written with the support of Operational Programme ‘Research and Development for Innovations’ co-funded by the European Regional Development Fund (ERDF) and the national budget of the Czech Republic, within the ‘Centre of Polymer Systems’ project (reg. number: CZ.1.05/2.1.00/03.0111).

**References**


[1] C. Jagadish, S.J. Pearton, Zinc oxide bulk, thin films and nanostructures : processing, properties and applications, Elsevier, Amsterdam ; London, 2006.

[2] A. Moezzi, A.M. McDonagh, M.B. Cortie, Zinc oxide particles: Synthesis, properties and applications, Chem. Eng. J. (Lausanne), 185 1-22.

[3] H. Morkoç, Ü. Özgür, Zinc oxide : fundamentals, materials and device technology, Wiley-VCH, Weinheim, 2009.

[4] S. Baruah, J. Dutta, Hydrothermal growth of ZnO nanostructures, Science and Technology of Advanced Materials, 10 (2009).

[5] U. Ozgur, Y.I. Alivov, C. Liu, A. Teke, M.A. Reshchikov, S. Dogan, V. Avrutin, S.J. Cho, H. Morkoc, A comprehensive review of ZnO materials and devices, J. Appl. Phys., 98 (2005).

[6] S.C. Padmanabhan, D. Ledwith, S.C. Pillai, D.E. McCormack, J.M. Kelly, Microwave-assisted synthesis of ZnO micro-javelins, J. Mater. Chem., 19 (2009) 9250-9259.

[7] N. Wang, X. Cao, Q.Y. Wu, R. Zhang, L. Wang, P.G. Yin, L. Guo, Hexagonal ZnO Bipyramids: Synthesis, Morphological Evolution, and Optical Properties, J. Phys. Chem. C, 113 (2009) 21471-21476.

[8] R.C. Pawar, J.S. Shaikh, A.A. Babar, P.M. Dhere, P.S. Patil, Aqueous chemical growth of ZnO disks, rods, spindles and flowers: pH dependency and photoelectrochemical properties, Solar Energy, 85 1119-1127.

[9] Z.W. Peng, G.Z. Dai, P. Chen, Q.L. Zhang, Q. Wan, B.S. Zou, Synthesis, characterization and optical properties of star-like ZnO nanostructures, Mater. Lett., 64 898-900.

[10] L. Castaneda, Synthesis and characterization of ZnO micro- and nano-cages, Acta Mater., 57 (2009) 1385-1391.

[11] D. Calestani, M. Zha, R. Mosca, A. Zappettini, M.C. Carotta, V. Di Natale, L. Zanotti, Growth of ZnO tetrapods for nanostructure-based gas sensors, Sensors and Actuators B: Chemical, 144 472-478.

[12] Q.J. Yu, C.L. Yu, H.B. Yang, W.Y. Fu, L.X. Chang, J. Xu, R.H. Wei, H.D. Li, H.Y. Zhu, M.H. Li, G.T. Zou, G.R. Wang, C.L. Shao, Y.C. Liu, Growth of dumbbell-like ZnO microcrystals under mild conditions and their photoluminescence properties, Inorg. Chem., 46 (2007) 6204-6210.

[13] C.O. Kappe, D. Dallinger, S.S. Murphree, Practical microwave synthesis for organic chemists : strategies, instruments, and protocols, Wiley-VCH, Weinheim, 2009.

[14] I. Bilecka, M. Niederberger, Microwave chemistry for inorganic nanomaterials synthesis, Nanoscale, 2 1358-1374.

[15] Y. Wang, Y.H. Li, Z.Z. Zhou, X.H. Zu, Y.L. Deng, Evolution of the zinc compound nanostructures in zinc acetate single-source solution, Journal of Nanoparticle Research, 13 (2011) 5193-5202.

[16] G.G. Carbajal Arizaga, K.G. Satyanarayana, F. Wypych, Layered hydroxide salts: Synthesis, properties and potential applications, Solid State Ionics, 178 (2007) 1143-1162.

[17] R.Q. Song, A.W. Xu, B. Deng, Q. Li, G.Y. Chen, From layered basic zinc acetate nanobelts to hierarchical zinc oxide nanostructures and porous zinc oxide nanobelts, Adv. Funct. Mater., 17 (2007) 296-306.

[18] Q.Y. Cui, K. Yu, N. Zhang, Z.Q. Zhu, Porous ZnO nanobelts evolved from layered basic zinc acetate nanobelts, Appl. Surf. Sci., 254 (2008) 3517-3521.

[19] T. Biswick, W. Jones, A. Pacula, E. Serwicka, J. Podobinski, Evidence for the formation of anhydrous zinc acetate and acetic anhydride during the thermal degradation of zinc hydroxy acetate, Zn(5)(OH)(8)(CH(3)CO(2))(2)center dot 4H(2)O to ZnO, Solid State Sci., 11 (2009) 330-335.

[20] L. Poul, N. Jouini, F. Fievet, Layered hydroxide metal acetates (metal = zinc, cobalt, and nickel): Elaboration via hydrolysis in polyol medium and comparative study, Chem. Mater., 12 (2000) 3123-3132.

[21] H. Morioka, H. Tagaya, J.I. Kadokawa, K. Chiba, Studies on layered basic zinc acetate, J. Mater. Sci. Lett., 18 (1999) 995-998.

[22] A. Kawai, Y. Sugahara, I.Y. Park, K. Kuroda, C. Kato, Preparation of Zinc Oxide Powders from Two in: S.B. Hirano, G.L. Messing, H. Hausner (Eds.) Ceramic powder science IV: 4th International conference on ceramic powder processing science : Selected papers, American Ceramic Society, Westerville, Ohio, 1991, pp. 75-94.

[23] E. Hosono, S. Fujihara, T. Kimura, H. Imai, Growth of layered basic zinc acetate in methanolic solutions and its pyrolytic transformation into porous zinc oxide films, J. Colloid Interface Sci., 272 (2004) 391-398.

[24] S.P. Newman, W. Jones, Comparative Study of Some Layered Hydroxide Salts Containing Exchangeable Interlayer Anions, J. Solid State Chem., 148 (1999) 26-40.

[25] E.S. Jang, J.H. Won, Y.W. Kim, Z. Cheng, J.H. Choy, Synthesis of porous and nonporous ZnO nanobelt, multipod, and hierarchical nanostructure from Zn-HDS, J. Solid State Chem., 183 (2010) 1835-1840.

[26] G. Socrates, Infrared and Raman characteristic group frequencies : tables and charts, 3rd ed. ed., Wiley, Chichester, 2001.
[27] K. Nakamoto, Infrared and Raman spectra of inorganic and coordination compounds, 6th ed., Wiley Hoboken, N.J., Oxford, 2009.
[28] E. Kandare, J.M. Hossenlopp, Hydroxy double salt anion exchange kinetics: Effects of precursor structure and anion size, J. Phys. Chem. B, 109 (2005) 8469-8475.
[29] E. Kandare, J.M. Hossenlopp, Thermal degradation of acetate-intercalated hydroxy double and layered hydroxy salts, Inorg. Chem., 45 (2006) 3766-3773.
[30] A. Jimenez-Lopez, E. Rodriguez-Castellon, P. Olivera-Pastor, P. Maireles-Torres, A.A.G. Tomlinson, D.J. Jones, J. Roziere, Layered basic copper anion exchangers: chemical characterisation and X-ray absorption study, J. Mater. Chem., 3 (1993) 303-307.
[31] N. Masciocchi, E. Corradi, A. Sironi, G. Moretti, G. Minelli, P. Porta, Preparation, Characterization, andab initioX-Ray Powder Diffraction Study of Cu2(OH)3(CH3COO)Â·H2O, J. Solid State Chem., 131 (1997) 252-262.
[32] R. Rojas, C. Barriga, M. Angeles Ulibarri, P. Malet, V. Rives, Layered Ni(ii)-Zn(ii) hydroxyacetates. Anion exchange and thermal decomposition of the hydroxysalts obtained, J. Mater. Chem., 12 (2002) 1071-1078.

**Paper II.**

MACHOVSKY, M.(50 %); KURITKA I.; SEDLAK J.; PASTOREK M. Hexagonal ZnO porous plates prepared from microwave synthesized layered zinc hydroxide sulphate via thermal decomposition. *Materials Research Bulletin, 2013.*

http://dx.doi.org/10.1016/j.materresbull.2013.06.018

Materials Research Bulletin xxx (2013) xxx–xxx

Contents lists available at SciVerse ScienceDirect

Materials Research Bulletin

journal homepage: www.elsevier.com/locate/matresbu

# Hexagonal ZnO porous plates prepared from microwave synthesized layered zinc hydroxide sulphate via thermal decomposition

Michal Machovsky [a,b,*], Ivo Kuritka [a,b], Jakub Sedlak [a,b], Miroslav Pastorek [a,c]

[a] Centre of Polymer Systems, University Institute, Tomas Bata University in Zlin, Nad Ovcirnou 3685, 760 01 Zlin, Czech Republic
[b] Polymer Centre, Faculty of Technology, Tomas Bata University in Zlin, Nam. T.G. Masaryka 275, 762 72 Zlin, Czech Republic
[c] Department of Polymer Engineering, Faculty of Technology, Tomas Bata University in Zlin, Nam. T.G. Masaryka 275, 762 72 Zlin, Czech Republic

ARTICLE INFO

*Article history:*
Received 26 February 2013
Received in revised form 27 May 2013
Accepted 10 June 2013
Available online xxx

*Keywords:*
A. Layered compounds
A. Oxides
C. X-ray diffraction
C. Thermogravimetric analysis (TGA)
C. Infrared spectroscopy

ABSTRACT

Layered zinc hydroxide sulphate (ZHS) was prepared by microwave-assisted hydrothermal precipitation of zinc sulphate monohydrate with hexamethylenetetramine. Under ambient conditions, the structure of ZHS determined by X-ray diffraction (XRD) was found to be a mixture of zinc hydroxide sulphate pentahydrate $Zn_4SO_4(OH)_6{\cdot}5H_2O$ and tetrahydrate $Zn_4SO_4(OH)_6{\cdot}4H_2O$. Fourier transform infrared (FTIR) spectroscopy was used for characterization of the prepared materials. Based on the interpretation of ZHS's thermal decomposition profile obtained by thermogravimetric analysis, ZnO of high purity was prepared by calcination at 900 °C for 2 h. The structure of the resulting ZnO was confirmed by the XRD. The morphology examination by scanning electron microscopy revealed a porous mesh-like ZnO structure developed from the ZHS precursor at the expense of mass removal due to the release of water and sulphate during the calcination.

© 2013 Elsevier Ltd. All rights reserved.

## 1. Introduction

Layered materials consisting of stacked two-dimensional charged layers with nano-dimensional interlayer spacing occupied by water molecules and charged chemical species compatible to those layers have attracted considerable attention from both academia and industry. The interest in these materials mostly stems from their ability to exchange interlayer cations/anions by various organic and inorganic molecules of the same charge, giving rise to rich intercalation chemistry. A great variety of layered materials that have exchangeable cations balancing negatively charged layers such as cationic clays or metal phosphates and phosphonates are known for a long time and can be widely found in nature. In contrast, the family of layered materials that possess anion-exchange properties is comparatively rare [1,2].

Among them, layered double hydroxides (LDH) and layered hydroxide salts (LHS) which comprise positively charged metal hydroxide layers with exchangeable charge-balancing anions and water molecules in the interlayer galleries are regarded as the most representative members of anionic layered materials.

LDH can be described by the general formula: $[M^{2+}_{1-x}M^{3+}_x(OH)_2]^{x+}(A^{m-})_{x/m}{\cdot}nH_2O$, where $M^{2+}$ and $M^{3+}$ are divalent and trivalent metal cations, respectively, A is a counter-ion with $m^-$ charge, and $(x)$ is the stoichiometric coefficient within the range from 0.1 to 0.5. Layered hydroxide salts (LHS) are structurally similar to LDH, possessing the generic formula $M^{2+}(OH)_{2-x}(A^{m-})_{x/m}{\cdot}nH_2O$. The identities of cations and interlayer anions together with the value of the stoichiometric coefficient may be varied over a wide range, allowing a plethora of materials with vastly different properties to be prepared towards the intended application [3,4].

In this respect, a variety of LDH and LHS have been successfully synthesized. Various approaches have been employed for the synthesis of both LDH and LSH. Among them, solution based routes such as hydrolysis of salts and oxides or precipitation with alkaline solution are most common [3,5]; however, methods employing other principles such as the mechanochemical synthesis [6] or the structural memory effect [7] can be found in literature as well. These materials are used in a diverse set of application areas such as catalysis, polymer additives, pharmaceutics, water purification, and ion exchangers [8,9] and references therein. Furthermore, both LDH and LHS are regarded as green materials in terms of their stability, inertness and biocompatibility, and research focused on their use in medicine as drug carriers or biomolecule reservoirs is ongoing [10,11]. Besides, LDH and LHS are widely used as precursors for various mixed and single metal oxides.

Here we report on the microwave-assisted hydrothermal synthesis of zinc hydroxide sulphate $Zn_4(OH)_6SO_4{\cdot}nH_2O$ (ZHS), a

* Corresponding author at: Centre of Polymer Systems, University Institute, Tomas Bata University in Zlin, Nad Ovcirnou 3685, 760 01 Zlin, Czech Republic. Tel.: +420 576 038 049; fax: +420 576 031 444.
*E-mail addresses:* machovsky@ft.utb.cz (M. Machovsky), ivo@kuritka.net (I. Kuritka), j1sedlak@ft.utb.cz (J. Sedlak), pastorek@ft.utb.cz (M. Pastorek).

0025-5408/$ – see front matter © 2013 Elsevier Ltd. All rights reserved.
http://dx.doi.org/10.1016/j.materresbull.2013.06.018

member of layered hydroxide salts, by simple precipitation of zinc sulphate monohydrate with hexamethylenetetramine. Although microwaves have been widely used in the modern organic synthesis for almost three decades, it is only recently when microwave-assisted heating has experienced a renaissance in the liquid-phase synthesis of inorganic materials. A unique combination of thermal (kinetic), non-thermal, and specific microwave effects offers several advantages in comparison to conventional heating such as rapid and selective heating, higher reaction rates, increased product yields, an improved reproducibility, and energy savings. Generally, a 10–100-fold reaction rate enhancement can be achieved [12,13]. In the case of our study, the synthesis was completed quickly within 3 min in microwaves. For the sake of illustration, the use of conventional heating sources in the ZHS synthesis instead of microwave prolonged the reaction time to 20 min [14], 45 min [15], or even to 5 h [16].

In the next step, the obtained ZHS powder was used as the precursor for the preparation of ZnO. Due to its unique physicochemical properties, ZnO is regarded as mature engineering material and, as such, covers a broad field of applications ranging from pharmaceutics and medicine, catalysis, rubbers and plastics industry, to optoelectronics and piezoelectric devices, chemical and biological sensing, etc. As the physico-chemical properties are intimately dependent on crystal size, shape, orientation, grain size, etc.; a lot of efforts have been devoted to the synthesis of various ZnO structures [17].

Among them, porous ZnO micro- and nanostructures have received great interest recently, as being shown to possess properties superior to the corresponding solid structures in applications such as catalysis, sensing, and batteries or magnetic devices [18,19]. A variety of methods have been employed for producing porous structures, however, pore directing agents or templates are usually involved and must be subsequently removed by either dissolving or by thermal treatment [20,21].

In this regard, the thermal decomposition of LHS precursors represents an easy way for the preparation of porous 2D ZnO structures that are otherwise difficult to obtain due to ZnO crystal grow habits without any capping or directing agents [22]. LHS precursors that have been used for the preparation of ZnO include zinc hydroxide nitrate $Zn_5OH_8(NO_3)_2{\cdot}2H_2O$ [23], zinc hydroxide chloride $Zn_5(OH_8)Cl_2{\cdot}2H_2O$ [24–26] zinc hydroxide sulphate hemihydrate $Zn_4(OH)_6SO_4{\cdot}0.5H_2O$ [15,16], or zinc hydroxide acetate $Zn_5OH_8(CH_3COO)_2{\cdot}2H_2O$ [27,28].

It has been shown that the microstructure of ZnO obtained by thermal decomposition retains the morphology of the LHS precursor and enables 2D porous ZnO structures to be prepared. Furthermore, apart from using pore-directing agents or templates, the porosity resulted from the release of internally born gaseous side-products [29].

## 2. Experimental

### 2.1. Materials

Zinc sulphate monohydrate $ZnSO_4{\cdot}H_2O$ and hexamethylenetetramine $(CH_2)_6N_4$ were both purchased from PENTA (Czech Republic) and used as received without further purification. Demineralized water with conductivity about $10^{-7}$ S cm$^{-1}$ was used throughout experiments.

### 2.2. Synthesis of zinc hydroxide sulphate

The zinc hydroxide sulphate precursor was synthesized by precipitation of zinc sulphate monohydrate with hexamethylenetetramine. The precipitation reaction was performed in the microwave open vessel system MWG1K-10 (RADAN, Czech Republic; 1.5 kW, 2.45 GHz) operated in a continuous mode (zero idle time, maximum power) with the temperature monitored by an industrial contactless thermometer (Raytek CM, Germany).

The synthesis process was carried out as follows: 0.05 mol of zinc sulphate monohydrate and 0.05 mol of hexamethylenetetramine were dissolved in 100 mL and 50 mL of demineralised water, respectively. The obtained solutions were mixed together in a reaction bottle, placed in microwave oven cavity, and exposed to microwave irradiation immediately. The temperature of the reaction mixture increased steeply during the first 2 min, reaching a maximum of 97 °C at the beginning of the third. It should be noted that the thermometer collected a signal from a certain solid angle which is slightly bigger than the reaction bottle subtends, hence the measured temperature value is only indicative for reaching the maximum temperature, and the mixture was intensively boiling at that point. The microwave system was switched off after 3 min of microwave exposure and left to cool down naturally. The white precipitate was filtered (0.23 μm pore size membrane), washed thoroughly with demineralised water several times and dried in a laboratory oven at 40 °C for 24 h.

### 2.3. Preparation of ZnO

ZnO was obtained by thermal decomposition of dried ZHS precursor powder. ZHS was loaded into an open alumina crucible and heated to 900 °C at a heating rate of 5 °C min$^{-1}$ in a furnace with a static air atmosphere. After reaching the desired temperature, the sample was calcined for 2 h and than left to cool down slowly in a closed oven.

### 2.4. Characterization

Phase compositions of powder samples before and after calcination were characterized by the multi-purpose X-ray diffractometer PANalytical X'Pert PRO MPD (The Netherlands) with a Cu Kα X-ray source (λ = 1.5418 Å) in the diffraction angle

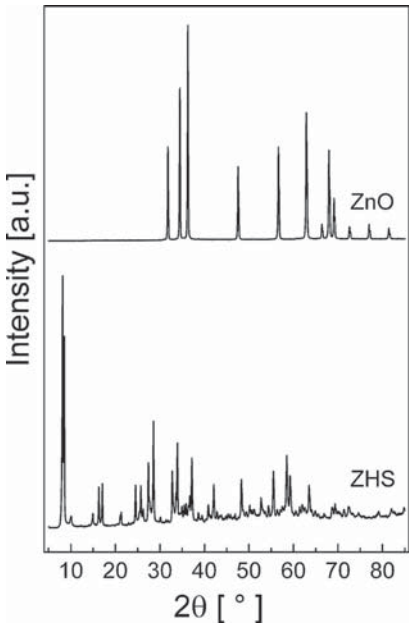


**Fig. 1.** XRD patterns of the precursor (ZHS) and calcined powder (ZnO).

Please cite this article in press as: M. Machovsky, et al., Mater. Res. Bull. (2013), http://dx.doi.org/10.1016/j.materresbull.2013.06.018

range of 5–85° 2$\theta$. The morphology and structure were observed by the scanning electron microscope Vega II/LMU (Tescan, Czech Republic). The thermogravimetric analysis (TGA) was carried out by the thermogravimeter Q500 (TA instruments, United States) in the temperature range from 25 to 850 °C at a heating rate of 10 °C $min^{-1}$ in flowing air (30 sccm). Fourier transform infrared (FTIR) spectra were collected on the Nicolet 6700 FT-IR spectrometer (Thermo scientific, United States) equipped with an attenuated total reflectance (ATR) accessory utilizing a diamond crystal.

## 3. Results and discussion

Powder X-ray diffraction patterns of both zinc hydroxide sulphate (ZHS) and zinc oxide (ZnO) obtained by its calcination are shown in Fig. 1. At the first sight, the X-ray diffractions patterns of ZHS precursor (Fig. 1a) exhibits features typical for a layered structure, with sharp diffraction peaks in the range of small Bragg angles and broader asymmetric diffraction peaks in the range of high angles [3].

A careful analysis of the XRD pattern revealed the presence of two phases of basic zinc sulphate; zinc hydroxide sulphate pentahydrate $Zn_4SO_4(OH)_6{\cdot}5H_2O$ (JCDD PDF-2 entry 00-039-0688), and its lower hydrate, zinc hydroxide sulphate tetrahydrate $Zn_4SO_4(OH)_6{\cdot}4H_2O$ (JCDD PDF-2 entry 00-044-0673). In fact, the multiphase pattern corresponding to basic sulphate with various degrees of hydration is quite common, with the relative composition dependent strongly on the condition of ageing and even on the ambient temperature and humidity.

The interlayer distance can be obtained simply from the Bragg equation for a doublet of peak at 2$\theta$ angles of 8.17° and 8.53°, corresponding to ZHS pentahydrate and tetrahydrate, respectively [30,31]. The calculated decrease of interlayer distance from 10.82 to 10.37 Å is attributed to the loss of one water molecule per structural unit. These values are almost identical with those reported elsewhere where a structural model can be found [31].

The powder XRD pattern for material obtained from ZHS calcinated at 900 °C for 2 h shown in Fig. 1b corresponds well to the hexagonal wurtzite ZnO structure (JCDD PDF-2 entry 01-079-0207) with no other phase detected. In this regard, the calcination temperature and time were found to be sufficient for converting the ZHS precursor to ZnO completely.

The scanning electron micrographs of precursor ZHS powder are shown in Fig. 2a and b. It consists of hexagonal sheets, bimodal in particle size distribution with one fraction being about 1 μm and the second approximately 10 μm. The sheets thickness can be estimated to be in order of several tens of nanometers from higher resolution image in Fig. 2b. The morphology of ZnO obtained by calcination can be seen in Fig. 2c and d. At first sight, the release of volatile products during the calcination process resulted in the formation of a mesh-like ZnO structure. The triclinic ZHS nanosheets crystal lattice parameters are similar to the hexagonal cell of the ZnO wurtzite structure, moreover, the ZHS hemihydrate cell is pseudohexagonal, which results in a topotactic conversion of the precursor into the newly born ZnO grains keeping their orientation along *c*-axes. The porous structure is developed at the expense of mass removal due to the release of water and sulphate

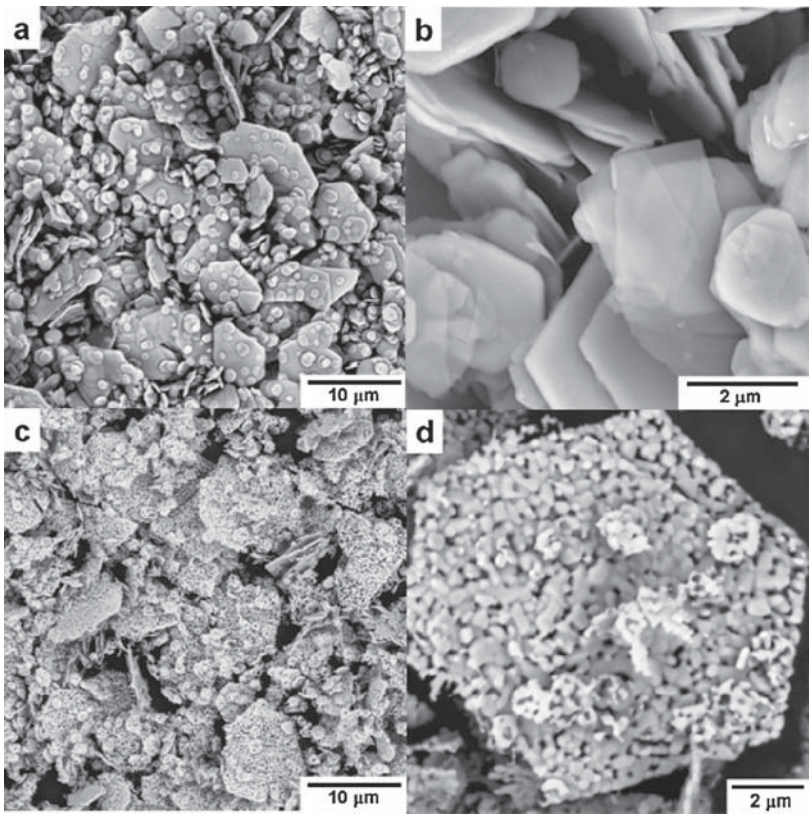


**Fig. 2.** SEM images of the precursor (ZHS – a, b) and calcined powder (ZnO – c, d).

Please cite this article in press as: M. Machovsky, et al., Mater. Res. Bull. (2013), http://dx.doi.org/10.1016/j.materresbull.2013.06.018

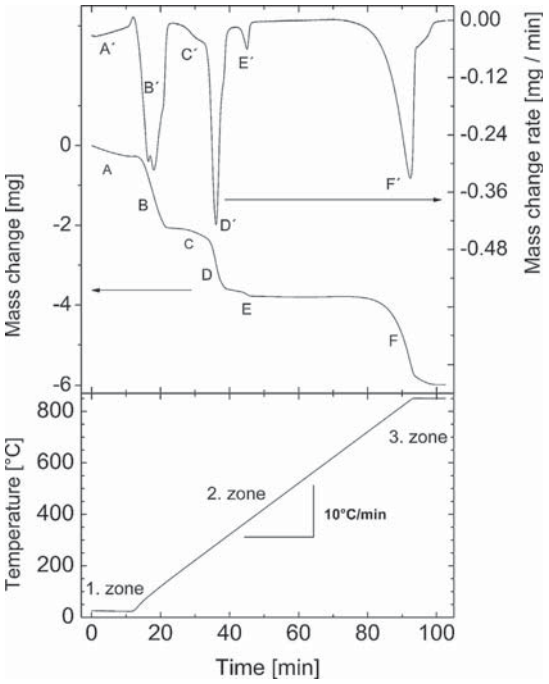


**Fig. 3.** TG analysis of the precursor (ZHS) material. The lower graph panel shows temperature programme divided into three zones: (1) isothermal at laboratory temperature 23 °C, (2) linear heating at 10 °C $min^{-1}$, and (3) isothermal at 850 °C. The upper graph window shows TGA curve with steps labelled by capital letters, the downwards peaks of the first derivative associated to the right are correspondingly labelled by primed capitals.

during annealing due the sintering of ZnO crystals after the decomposition, with the overall morphology of LHS being retained but the crystals are very small as can be seen in Fig. 2d [32].

However, a slight decrease in dimension can be expected due to the mass losses during the dehydration and dehydroxylation during calcination of the precursors [33].

The thermal analysis confirmed the composition of the prepared precursor material; however, the stoichiometry of the $ZHS{\cdot}5H_2O$ and $ZHS{\cdot}4H_2O$ compounds cannot be derived straightforwardly from the TGA curve record. As it can be seen in Fig. 3, the material loss mass in the dynamic air-flow atmosphere even at isothermal conditions (25 °C). Hence, the initial balance equilibration and thus the precise estimation of the initial sample weight were somewhat problematic and the curve was plotted on the raw data unit (mg) instead of the weight loss fraction (%). First derivative of the mass change, i.e. mass change rate, enhanced the resolution of decomposition steps. Isothermal drying was manifested as the step A on the TGA curve during the first 10 min. The deliberation of physically adsorbed and intercalated water with the maximum release rate at 98 °C (step B) was accelerated by the start of heating with a rate of 20 °C. According to the literature, the $ZHS{\cdot}5H_2O$ can be precipitated from the solution. Discrete lower hydrates, namely tetra- and tri-hydrates, could be prepared by dehydration of the pentahydrate, either thermally or by drying over desiccants; the monohydrate could only be prepared by dehydration of the higher hydrates over desiccants; the hemihydrate and anhydrate could only be prepared by thermal dehydration [31]. Therefore, the steps A and B ending at 160 °C are ascribed to a consecutive formation of lower hydrates from the starting material by a process requiring a small amount of energy only. The less pronounced step C corresponds to the loss of hemihydrate water. The following steps are associated with the dehydroxylation of the basal hydroxide layers in two stages, i.e. step D at 282 °C and E at 372 °C. The final mass loss step F corresponds to the decomposition of sulphate groups solely.

The stoichiometry of the thermal decomposition process can be assessed with the aid of the unambiguity of the last step F, where $SO_3$ is released from sulphate groups and disproportionate to $SO_2$

**Table 1**
Analysis of thermogravimetric data for ZHS. For details see text.

| Decomposition step | Maximum weight loss rate temperature [°C] | Weight loss [mg] | Deliberated gas | Stoichiometry | Comment |
|---|---|---|---|---|---|
| A | n/a | 0.27 | $H_2O$ | > 1/2 | *Physically adsorbed and intercalated water (pentahydrate)* |
| B | 98 | 1.80 | | >3 and 1/2 | Sum slightly > 4 *(tetrahydrate)* |
| C | 250 | 0.24 | | 1/2 | *3½ intercalated water and ½ for hemihydrate step* |
| D | 282 | 1.32 | | 2 and 2/3 | Sum = 3 |
| E | 372 | 0.16 | | 1/3 | *Three $H_2O$ are equivalent to $(OH)_6$ in the structural formula of ZHS* |
| F | 844 | 2.18 | $SO_3$ ($SO_2 + 1/2O_2$) | 1 | Unity *One $SO_3$ is equivalent to one $SO_4^{2-}$ group in the structural formula of ZHS* |

and $O_2$ according to Eqs. (1) and (2)

$$SO_3 \rightarrow SO_2 + 1/2O_2, \quad (1)$$

$$2SO_3 \rightarrow 2SO_2 + 2O_2. \quad (2)$$

As the amount of $SO_3$ is proportional to the amount of sulphate groups in the starting material in the ratio of 1:1, the sudoku of stoichiometry can be calculated. It is obvious that all decomposition steps at lower temperatures (from A up to E) are associated with the evolution of water molecules. Stoichiometric ratios in Table 1 were calculated from the observed mass losses with the help of $SO_3$ and $H_2O$ molar masses, and the decomposition of the material can be described by the following consecutive equations adopted from [34].

Steps A and B

$$Zn_4(SO_4)(OH)_6{\cdot}xH_2O \rightarrow Zn(SO_4)\cdot 3Zn(OH)_2{\cdot}1/2H_2O + (x-1/2)H_2O, \quad (3)$$

where $x$ is 4 or 5.

Step C corresponds to the hemihydrate dehydration and to the anhydride ZHS formation

$$Zn(SO_4)\cdot 3Zn(OH)_2{\cdot}1/2H_2O \rightarrow Zn(SO_4)\cdot 3Zn(OH)_2{\cdot}1/2H_2O$$

The intermediate structure between steps D and E was not revealed, thus, both steps are described by one summary equation

$$2[Zn(SO_4)\cdot 3Zn(OH)_2] \rightarrow 5ZnO + Zn_3O(SO_4)_2 + 6H_2O$$

The final step F is described as follows:

$$Zn_3O(SO_4)_2 \rightarrow 3ZnO + 2SO_2 + O_2$$

According to the thermogravimetric analysis, ZnO was prepared in bigger amounts (20 g) from the parental ZHS by calcination at 900 °C. The calcination time was set to 2 h assuring a complete conversion of the starting material in static air atmosphere. The amount of the prepared ZnO was 59% with respect to the initial batch weight, which is in good agreement with the theoretical content of ZnO in the ZHS pentahydrate (59.22%) and confirms suitability of this process to be scaled-up easily.

FTIR ATR spectra of the precursor and of the prepared ZnO are shown in Fig. 4. The crystal structure of ZHS has two main layers consisting of six- and four-coordinated zinc atoms and sulphates ($SO_4^{2-}$ tetrahedrons) separated by an intermediate layer of intercalation water molecules [30]. Although the MW enhanced synthesis proceeds very fast and such extreme conditions may be considered as non-suitable for a regular crystal phase development and growth, there can be identified seven very well resolved hydroxyl group vibration modes at the wavenumbers 3631, 3542, 3504, 3426, 3297, 3237 and 3172 $cm^{-1}$, the eighth band is located within the right shoulder of the hydroxyl absorption peak at 3054 $cm^{-1}$. Isolated absorption bands testify for a high structural order in the vicinity of each hydroxyl group bound either in hydroxide slabs or even in intercalated water. In this region, stretching vibration modes of hydroxo-complexes Zn–O–H can be expected. Asymmetric and symmetric stretching vibrations of H–O–H are observed too as confirmed by the presence of concomitant bands at 1700–1600 $cm^{-1}$. The stretching vibration bands of water molecules can be shifted to lower wavenumbers, but without losing their sharpness which again testifies for a highly ordered hydrogen bonding. A manifestation of lattice bonded water as well as aquo-complexes can be expected. A strong broad absorption between 1700 and 1600 $cm^{-1}$ can be associated with bending modes of hydration water or with physically adsorbed water molecules. Bending vibrations of hydroxo-complexes are not manifested near 1600 but close to 1200 $cm^{-1}$ where a sharp band is observed at 1161 $cm^{-1}$, however if the OH group is a part of a bridging hydroxo-complex, the bending vibration mode is even more shifted close to 950 $cm^{-1}$ as manifested by a sharp peak observed at 958 $cm^{-1}$. The four bands emerging in the region limited by these two hydroxo-complex deformation modes (1116, 1076, 1045 and 1022 $cm^{-1}$) can be ascribed to the sulphate group which points towards lowering of sulphate anion symmetry, as four IR active stretching bands may be expected for bidentate or bridging coordination [35], the latter is appropriate for the ZHS structure. The same number of the sulphate ion deformation vibration modes can be found at lower wavenumbers [35]; however, wagging, twisting and rocking modes of H–O–H that

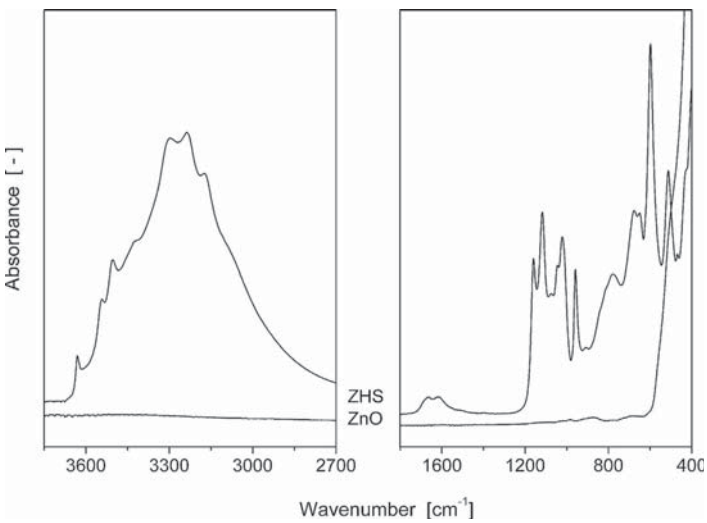


**Fig. 4.** FTIR spectra of the precursor (ZHS – upper curve, magnified 2× in the left panel window) and calcined powder (ZnO – lower curve).

can be found only in coordinated water molecules, but not in lattice bound water, are manifested in the region 910–650 $cm^{-1}$ as well. Thus, seven bands in total were identified at the positions 910, three peaks at 875, 838 and 809 hidden in the left shoulder of the 781 peak, 677 and 652 $cm^{-1}$. Lattice (or crystal) water vibration modes are expected to be observable below 600 $cm^{-1}$ at 597, 513, 469 and 428 $cm^{-1}$. However, the exact assignment of all features in the region below 1000 $cm^{-1}$ would be speculative without a model calculation and the X-ray monocrystal structure analysis. No peaks for HMTA were found confirming thus the precursor's purity from the organic moieties. Moreover, the $CO_2$ absorption manifested as carbonate vibration bands in IR spectra was not observed, which confirms the precursor's stability at the ambient condition [30,36–40].

The infrared absorption spectrum of the prepared ZnO shows the typical strong band at the position of about 450 $cm^{-1}$. According to the literature [36], pure ZnO has week absorption bands in the regions from 560 to 550 $cm^{-1}$ and from 520 to 500 $cm^{-1}$, a significant and a very strong band centred at about 450 $cm^{-1}$. In our case, the weak bands merged with the strong one and they are slightly visible in the edge of the large peak. No water, sulphate or organic contaminations are manifested in the spectra of the calcined product.

## 4. Conclusion

An extremely fast synthesis yielding high quality crystalline layered zinc hydroxide sulphate was developed. The use of microwave energy speeds up the reaction starting from zinc sulphate and the hexamethylenetetramine water solution to be completed within 3 min. The structure of the prepared product was unambiguously assigned to zinc hydroxide sulphate pentahydrate $Zn_4SO_4(OH)_6{\cdot}5H_2O$ and tetrahydrate $Zn_4SO_4(OH)_6{\cdot}4H_2O$. The bonding configuration of the sulphate anion was identified as a bridging coordination type from the well-resolved IR absorption spectra.

The precursor was further successfully converted into a porous ZnO mesh-like structure by calcination at 900 °C. The thermal decomposition process was elucidated in a detailed TG study and the stoichiometry of the prepared ZHS hydrate was confirmed, too. The observed hexagonal porous plates kept the original shape of the precursor's crystals, which testifies for the prevailing topotactic conversion mechanism. Moreover, it was demonstrated that the preparation of hexagonal ZnO porous plates can be performed in a larger scale.

## Acknowledgments

This article was written with the support of the Operational Programme 'Education for Competitiveness' co-funded by the European Social Fund (ESF) and the national budget of the Czech Republic, within the project 'Advanced Theoretical and Experimental Studies of Polymer Systems' (reg. number: CZ.1.07/2.3.00/20.0104).

This article was written with the support of Operational Programme 'Research and Development for Innovations' co-funded by the European Regional Development Fund (ERDF) and the national budget of the Czech Republic, within the 'Centre of Polymer Systems' project (reg. number: CZ.1.05/2.1.00/03.0111).

## References

[1] M. Rajamathi, G.S. Thomas, P.V. Kamath, Proc. Indian Acad. Sci.: Chem. Sci. 113 (2001) 671–680.
[2] S.H. Hwang, Y.S. Han, J.H. Choy, Bull. Korean Chem. Soc. 22 (2001) 1019–1022.
[3] G.G. Carbajal Arizaga, K.G. Satyanarayana, F. Wypych, Solid State Ionics 178 (2007) 1143–1162.
[4] S.P. Newman, W. Jones, J. Solid State Chem. 148 (1999) 26–40.
[5] M.R. Othman, Z. Helwani, Martunus, W.J.N. Fernando, Appl. Organomet. Chem. 23 (2009) 335–346.
[6] N. Thomas, Mater. Res. Bull. 47 (2012) 3568–3572.
[7] M.Z.b. Hussein, M.Y. Ghotbi, A.H. Yahaya, M.Z. Abd Rahman, Mater. Chem. Phys. 113 (2009) 491–496.
[8] F.Z. Zhang, X. Xiang, F. Li, X. Duan, Catal. Surv. Asia 12 (2008) 253–265.
[9] D.G. Evans, D.A. Xue, Chem. Commun. (2006) 485–496.
[10] J. Zhang, F. Zhang, L. Ren, D.G. Evans, X. Duan, Mater. Chem. Phys. 85 (2004) 207–214.
[11] J.M. Oh, T.T. Biswick, J.H. Choy, J. Mater. Chem. 19 (2009) 2553–2563.
[12] I. Bilecka, M. Niederberger, Nanoscale 2 (2010) 1358–1374.
[13] C.O. Kappe, D. Dallinger, S.S. Murphree, Practical Microwave Synthesis for Organic Chemists: Strategies, Instruments, and Protocols, Wiley-VCH, Weinheim, 2009 .
[14] X.D. Gao, X.M. Li, W.D. Yu, F. Peng, C.Y. Zhang, Mater. Res. Bull. 41 (2006) 608–611.
[15] E. Darezereshki, M. Alizadeh, F. Bakhtiari, M. Schaffie, M. Ranjbar, Appl. Clay Sci. 54 (2011) 107–111.
[16] L.H. Xue, X.T. Mei, W.X. Zhang, L.X. Yuan, X.L. Hu, Y.H. Huang, K. Yanagisawa, Sens. Actuators B: Chem. 147 (2010) 495–501.
[17] C. Jagadish, S.J. Pearton, Zinc Oxide Bulk, Thin Films and Nanostructures: Processing, Properties and Applications, Elsevier, Amsterdam/London, 2006.
[18] Y. Ren, Z. Ma, P.G. Bruce, Chem. Soc. Rev. 41 (2012) 4909–4927.
[19] J. Zheng, Z.-Y. Jiang, Q. Kuang, Z.-X. Xie, R.-B. Huang, L.-S. Zheng, J. Solid State Chem. 182 (2009) 115–121.
[20] Z. Liu, Z. Jin, W. Li, X. Liu, J. Qiu, W. Wu, Mater. Lett. 60 (2006) 810–814.
[21] J. Jiu, K.-i. Kurumada, M. Tanigaki, Mater. Chem. Phys. 81 (2003) 93–98.
[22] W.J. Li, E.W. Shi, W.Z. Zhong, Z.W. Yin, J. Cryst. Growth 203 (1999) 186–196.
[23] J.R. Huang, Y.J. Wu, C.P. Gu, M.H. Zhai, Y.F. Sun, J.H. Liu, Sens. Actuators B: Chem. 155 (2011) 126–133.
[24] W.X. Zhang, K. Yanagisawa, Chem. Mater. 19 (2007) 2329–2334.
[25] L.-H. Fu, Y.-Y. Dong, M.-G. Ma, S.-M. Li, S.-L. Sun, R.-C. Sun, Mater. Lett. 92 (2013) 136–138.
[26] Q. Zhong, X. Huang, J. Duan, J. Liu, F. Sun, X. He, Mater. Lett. 62 (2008) 188–190.
[27] Q.Y. Cui, K. Yu, N. Zhang, Z.Q. Zhu, Appl. Surf. Sci. 254 (2008) 3517–3521.
[28] E.S. Jang, J.H. Won, Y.W. Kim, Z. Cheng, J.H. Choy, J. Solid State Chem. 183 (2010) 1835–1840.
[29] N. Audebrand, J.-P. Auffrédic, D. Louër, Chem. Mater. 10 (1998) 2450–2461.
[30] N. Boshkov, K. Petrov, S. Vitkova, G. Raichevsky, Surf. Coat. Technol. 194 (2005) 276–282.
[31] I.J. Bear, I.E. Grey, I.E. Newnham, L.J. Rogers, Aust. J. Chem. 40 (1987) 539–556.
[32] S.A. Morin, A. Forticaux, M.J. Bierman, S. Jin, Nano Lett. 11 (2011) 4449–4455.
[33] K. Ada, M. Goekgoez, M. Oenal, Y. Sankaya, Powder Technol. 181 (2008) 285–291.
[34] T. Biswick, W. Jones, A. Pacula, E. Serwicka, J. Podobinski, Solid State Sci. 11 (2009) 330–335.
[35] H.H. Adler, P.F. Kerr, Am. Miner. 50 (1965) 132.
[36] G. Socrates, Infrared and Raman Characteristic Group Frequencies: Tables and Charts, 3rd ed., Wiley, Chichester, 2001.
[37] J.T. Kloprogge, M.L. Weier, L.V. Duong, R.L. Frost, Mater. Chem. Phys. 88 (2004) 438–443.
[38] J.T. Kloprogge, L. Hickey, R.L. Frost, J. Solid State Chem. 177 (2004) 4047–4057.
[39] J.T. Kloprogge, M. Broekmans, L.V. Duong, W.N. Martens, L. Hickey, R.L. Frost, J. Mater. Sci. 41 (2006) 3535–3539.
[40] K. Kakiuchi, E. Hosono, T. Kimura, H. Imai, S. Fujihara, J. Sol-Gel Sci. Technol. 39 (2006) 63–72.

**Paper III.**

MACHOVSKY, M.(50%); KURITKA, I.; BAZANT, P.; VESELA, D.; SAHA P.; Antibacterial Performance of ZnO-based Fillers with Mesoscale Structured Morphology in Model Medical PVC Composites. *submitted to Materials Science and Engineering C: Materials for Biological Applications*

*Manuscript
Click here to view linked References

# Antibacterial Performance of ZnO-based Fillers with Mesoscale Structured Morphology in Model Medical PVC Composites

MACHOVSKY MICHAL[1,2], KURITKA IVO[1,2,*], BAZANT PAVEL[1,2], VESELA DANIELA[1], SAHA PETR[1,2]

[1]Centre of Polymer Systems, University Institute, Tomas Bata University in Zlin, Nad Ovcirnou 3685, 760 01 Zlin, CZECH REPUBLIC

[2]Polymer Centre, Faculty of Technology, Tomas Bata University in Zlin, Nam. T. G. Masaryka 275, 762 72 Zlin, CZECH REPUBLIC

*corresponding author: ivo@kuritka.net , +420 576 038 049

**Abstract**

Three different ZnO-based antibacterial fillers with a different morphology of microparticles structured on a mesoscale were prepared by the use of the microwave assisted synthesis and additional annealing in one case. PVC composites containing 0.5 – 5wt% of ZnO based antibacterial fillers were prepared by melt mixing and characterized by scanning electron microscopy and X-ray diffractometry. Mechanical testing showed no adverse effect either of the used fillers or the applied processing conditions on the prepared material in comparison with the neat medical grade PVC. The surface antibacterial activity of the prepared PVC composites was assessed against *Escherichia coli* ATCC 8739 and *Staphylococcus aureus* ATCC 6538P according to ISO 22196: 2007 (E). All materials at almost all filler loading levels were efficient against both bacteria. The material with the most expanding morphology assuring the largest contact between filler and matrix achieved an excellent level of more than 99.9999 % reduction of viable cells of *E. coli* in comparison to untreated PVC and performed very well against *S. aureus,* too. A correlation between morphology and efficacy of the filler was observed and, as a result, a general rule was formulated which links the proneness of the microparticles to perform well against bacteria to their shape and morphology.

**Keywords**

Zinc oxide; mesoscale; microparticle; nanostructure; antibacterial; composite

## 1. Introduction

Microbial colonization of medical devices' surfaces and the subsequent biofilm formation represents one of the most serious issues in healthcare-associated infection. It is estimated that more than half of nosocomial infections are connected with some type of implanted medical device [1]. A worrying feature of biofilm-based infections is represented by an inherent resistance of bacterial cells growing as a biofilm to antibiotics when compared with planktonic cells. Such inherent resistance may be caused by one or more of the following: delayed penetration of antimicrobial agent through the biofilm matrix, an altered growth rate of biofilm organisms, and other physiological changes due to the biofilm mode of growth [2]. Biofilms antibiotic resistance two or more orders greater in magnitude than those displayed by planktonic bacteria of the same strain depending on the species-drug combination have been reported [3-5]. Therefore, the common antibiotic therapy is often sufficient to kill planktonic cells and those dispersed from the biofilm, but insufficient to kill cells living in the biofilm, and infection symptoms are cyclic in nature. Moreover, as the overuse of antibiotics leads to the prevalence and development of genes encoding antibiotic resistance (GEAR), the rapidly increasing antibiotic resistance to even planktonic cells presents another critical issue [6].

As the bacterial adhesion to surfaces is an essential step for the onset of biofilm formation, medical devices' surfaces that can inhibit initial bacterial attachment by varying the degree of hydrophobicity/hydrophilicity or the surface structure have been proposed [7-9]. However, such surfaces are susceptible to fouling immediately upon contacting physiological fluids, and, despite the fact that the surface energy and other surface related properties may improve the medical device performance, an active antibacterial agent that inhibits bacterial growth is needed. Considerable research has been focused on polymers whose antibacterial activity is conferred via modification of their backbones by grafting of various low or high molecular antibacterial moieties, such as quaternary ammonium groups [10, 11], natural or synthetic peptides [12, 13], halogens, phospho and sulpho groups [14-16].

Although a great variety of approaches have been successfully explored up to now, the majority of antibacterial polymeric materials nowadays are made up by polymer compounding with either organic or inorganic antibacterial agents. Among the latter, metal (Ag, Au, Cu, etc.) [17, 18] and metal oxides (ZnO, $TiO_2$, CuO, CaO, MgO, etc.) nanoparticles or their combination [19, 20] are of particular interest as they have been shown to possess strong antibacterial activity against representatives of both gram-positive as well as gram-negative bacteria strains [21, 22]. In addition, the use of inorganic nanoparticles as antimicrobial agents has several benefits in comparison with the organic antimicrobials, such

as improved stability and low toxicity towards mammalian cells, although the safety issues of nanoparticles application are still a matter of vivid discussions [23].

Nanocomposites made up of inorganic nanoparticles and polymers exhibit an improved performance when compared with their microparticle counterparts, mainly due to a larger surface in comparison to the volume ratio. However, this inevitably leads to an increase in the surface energy and interactions between particles such as van der Waals and electrostatic forces become stronger, causing a tendency to agglomeration. A plethora of chemical and/or physical treatment strategies has been utilized for nanoparticles to reduce the surface energy and, thus to avoid formation of clusters or agglomerates and achieve a uniform particle distribution in the polymer matrix, as documented in reviews [24-27]; nevertheless, these methods are often too sophisticated and cost demanding.

In this article, we report on a different and originally developed concept how to circumvent these unavoidable disadvantages of inorganic nanoparticles by a simple use of relatively large microparticles, yet with nanostructured morphology. Structural nanocomponents impart the beneficial features of the nanosize effects to their assembly on a mesoscale into a bigger particle. The shape of a snowflake inspired this study at the beginning.

Zinc oxide was chosen as the model material of the inorganic antibacterial filler due to its large variability of forms in which it can be prepared and because the antibacterial activity of its nanoparticulate forms is well known and their efficacy as an antibacterial agents is well documented in the literature [28]. Hierarchically, mesoscale structured ZnO microparticles can be prepared relatively simply by precipitation from solutions of zinc salts. We developed a microwave (MW) assisted synthesis improving the classical synthesis methods by shortening the reaction time, material, energy and, therefore, we achieved cost savings for the preparation of various ZnO powders [29]. Three different materials were selected among the possible candidates to be investigated. In first, a two-dimensional zinc hydroxide acetate layered system analogous to nanoclays was obtained; as the second material, twinned ZnO frustums were synthesized and, as the third material with the most complex morphology, mesh-like porous platelets were prepared by a slightly more elaborate method [30].

The antibacterial activity of various polymer additives (namely nanoparticles) is usually evaluated quantitatively or qualitatively against model organisms representing gram negative and gram positive bacteria by estimation of the minimum inhibitory concentration (MIC), minimum bactericidal concentration (MBC), disk diffusion method, growth inhibition method, Halo test, agar or broth dilution techniques. For the function of a plastic medical device, the antibacterial effect of the surface of the plastic component itself has relevancy

rather than the effect of the released species on planktonic cells in its surrounding environment. Therefore, a method to determine the antibacterial efficacy of the surface of a finished plastic article is the best and only option giving reliable data that can be quantitative, qualitative and time related [31]. The standard ISO 22196:2007 (E) [32], formerly JIS Z 2801 [33], meets these criteria and was applied throughout this study.

Lastly, in order to asses the efficacy of synthesized fillers, a model composite material is required, as it is the surface antibacterial activity which is the key performance factor for the medical materials as emphasized above. Plasticized PVC is the most widely used plastic in medical device applications because of its bio- and hemocompatibility, transparency, flexibility, durability, sterilizability and low cost. Typical medical products made thereof include blood bags and tubing, gloves, dialysis equipment, catheters, or device packaging [34, 35]. Therefore, medical grade PVC was used as the polymer matrix for the incorporation of ZnO based antibacterial fillers, and the antibacterial activity on the plastic surface of the prepared composites was evaluated.

## 2. Experimental

### *2.1 Materials*

Zinc sulphate monohydrate $ZnSO_4.H_2O$, zinc acetate dihydrate $Zn(CH_3COO)_2.2H_2O$ and hexamethylenetetramine $(CH_2)_6N_4$ were purchased from PENTA (Czech Republic) and used as received without further purification. Medical grade PVC RB3 was delivered by Modenplast (Italy). Distilled water was used throughout experiments.

### *2.2 Biological materials*

Nutrient Broth w/1% Peptone, Nutrient Agar No. 2, Soyabean Casein Digest Medium, and TWEEN 80 were all supplied by HIMEDIA (India). Lecithin natural was purchased from Mogador (Czech Republic).

### *2.3 Microorganisms*

*Escherichia coli* ATCC 8739 and *Staphylococcus aureus* ATCC 6538P were both obtained from the Czech Collection of Microorganisms (Czech Republic).

### *2.4 Preparation of antibacterial fillers*

As antibacterial fillers, the basic zinc hydroxide acetate (ZHA) and two zinc oxide (ZnO) powders denoted as ZnO **1** and ZnO **2** were prepared.

The synthesis of ZHA was performed in the microwave open vessel system MWG1K-10 (RADAN, Czech Republic; 1.5 kW, 2.45 GHz) operated in a continuous mode (zero idle time, maximum power) with the temperature monitored by an industrial contactless thermometer (Raytek CM, Germany). The synthesis process was carried out as follows; 0.05 M of zinc acetate dihydrate and 0.05 M of hexamethylenetetramine were dissolved in 100 mL and 50 mL of distilled water, respectively. The obtained solutions were mixed together in a reaction bottle, placed into the microwave oven cavity and exposed to microwave irradiation. The temperature of the reaction mixture increases steeply reaching a maximum of 97 °C after approximately 90 s. The microwave system was switched off after 2 minutes of microwave exposure and left to cool down naturally. The white precipitate was filtered (0,23μm pore size membrane), washed thoroughly several times with distilled water and dried in a laboratory oven at 40 °C for 24 hours. As the second filler, ZnO **1** was prepared under the same conditions as ZHA, only the synthesis time was extended from 2 to 10 minutes. Finally, the ZnO powder denoted as ZnO **2** was prepared via two steps method described elsewhere [30]. Briefly, the solution obtained by mixing 0.05 M of the zinc sulphate monohydrate and 0.05 M of hexamethylenetetramine, dissolved in 100 mL and 50 mL of distilled water, respectively, was exposed to microwaves for 10 minutes in the first step. After the filtering and washing procedure had been completed, ZnO **2** powder was obtained by thermal decomposition of the dried zinc hydroxide sulphate precursor by heating to 900 °C at a heating rate of 5 °C/min in a furnace with a static air atmosphere. After reaching the desired temperature, the sample was calcined for 2 hours and than left to cool down slowly in a closed oven.

### *2.5 Preparation of PVC/ZnO composites*

Composites containing 0.5, 1, 2, and 5 wt% of ZHA, ZnO **1** and ZnO **2** were prepared by melt mixing of PVC pellets with an appropriate amount of the prepared filler in a Brabender measuring mixer W50 EHT PL at the temperature of 175 °C. The rotor speed was kept at 20 rpm for first 2 minutes followed by an increase to 50 rpm for another 4 minutes. After this time, a constant torque was reached, suggesting a homogeneous mixing of the filler into the matrix. Then, 1 mm thick sheets were produced by hot press procedure involving preheating at 175 °C for 2 min followed by compressing for 4 min and subsequent cooling under pressure. The neat PVC reference sample was prepared in the same way. The obtained sheets were used as a testing sample for an evaluation of the antibacterial activity and of mechanical properties.

### *2.6 Characterization*

X-ray diffraction (XRD) patterns of the prepared fillers and PVC composites made thereof were recorded by the multi-purpose X-ray diffractometer X´Pert PRO MPD (PANalytical, The Netherlands) with a Cu-Kα X-ray source (λ = 1.5418 Å) in the diffraction angle range of 5-85° 2$\theta$. The morphology of fillers was observed by the scanning electron microscope Vega II/LMU (Tescan, Czech Republic). The scanning electron microscopy examination was also performed on composites fractured surfaces in order to evaluate the degree of homogeneity and to gain insight into the composites' internal structure. Mechanical properties (Young's modulus, tensile strength) of composites were evaluated using the Testometric universal-testing machine M 350-5CT (LABOR machine, Czech Republic) at the crosshead speed of 500 mm/min and a gauge length of 50 mm with a cell-load 1kN, in accordance with ISO 527-2:1996. Tensile tests were repeated on 10 specimens cut for each sample to ensure the reproducibility of the data.

### *2.7 Antibacterial activity testing*

The antibacterial activity of the prepared ZnO/PVC composites was assessed against *Escherichia coli* ATCC 8739 and *Staphylococcus aureus* ATCC 6538P according to ISO 22196: 2007 (E) with a slight modification [32]. Incubator HERAcell 150i (ThermoScientific, USA) was used in this part of the work. For the sake of clarification, a brief description of this standard assay for the evaluation of the antibacterial activity on plastic surfaces is given. First, a test inoculum was prepared by transferring one loop of the pre-incubated bacteria into a small amount 1/500 diluted nutrient broth so that the bacteria concentration was in between $2.5 \times 10^5$ and $10 \times 10^5$ cells /mL. The test specimens (three treated and three untreated specimens) with dimensions of 50 mm x 50 mm x 1 mm were placed in Petri dishes and inoculated by 0.4 mL of the test inoculum. The inoculated specimens' surface was covered with a thin piece of polypropylene film (40 mm x 40 mm) and pressed down gently so that test inoculum spread to the edges. After incubation for 24 h at 35 °C under humid conditions (95 %), the test inoculum remaining on covers polypropylene film and the test specimen was completely recovered by 10 mL of SCDLP broth (prepared by adding 1 g of lecithin and 7 g of polysorbate per liter of Tryptone Soya Broth). The recovered SCDLP broth was 10-fold serial diluted in phosphate-buffered physiological saline and 1 mL of each dilution was placed together with 1 mL of undiluted recovered SCDLP into separate Petri dishes. Then, 15 mL of plate count agar was poured into each Petri dish, swung gently to disperse bacteria and incubated for 48 h at 35 °C under humid conditions (95 %). After incubation, the number of

colonies was counted in the Petri dishes containing from 30 – 300 colonies and the number of viable bacteria recovered was determined according to Eq. 1.

$$N = (100 \times C \times D \times V)/A, \quad (1)$$

where

N is the number of viable bacteria recovered per $cm^2$ per test specimen;

C is the average plate count for the duplicate plates;

D is the dilution factor for the plates counted;

V is the volumeof SCDLP in mL added to the specimen

The results are expressed in terms of the antibacterial activity R, which is defined as the difference in the logarithm of the viable cell count found on an antibacterial-treated sample and on an untreated sample after inoculation with an incubation of bacteria

$$R=(U_t-U_0)-(A_t-U_0)=U_t-A_t, \quad (2)$$

where

R is the antibacterial activity;

$U_0$ is the average of the common logarithm of the number of viable bacteria, in cells/$cm^2$, recovered from the untreated test specimens immediately after inoculation;

$U_t$ is the average of the common logarithm of the number of viable bacteria, in cells/$cm^2$, recovered from the untreated specimens after 24 h;

$A_t$ is the average of the common logarithm of the number of viable bacteria, in cells/$cm^2$, recovered from the treated test specimens after 24 h.

At this point, we have omitted the evaluation of the number of viable bacteria recovered from the untreated test specimens immediately after inoculation because of the extensiveness of the experiments, and the value of the antibacterial activity R was determined simply according to

$$R=U_t-A_t, \quad (3)$$

## 3. Results and discussion

### *3.1 Characterization of the prepared fillers*

Powder XRD patterns of the prepared fillers are shown in Fig. 1. The structure of the sample prepared in 2 minutes via MW-assisted hydrothermal precipitation of ZAD with HMTA exhibits sharp reflections at a low angle and relatively weak reflections at a high degree angle (Figure 1, diffractogram a). In general, XRD patterns with similar features are typical for layered materials, therefore, a compound that belongs to the family of layered double hydroxides (LDH) and hydroxide double salts (HDS) should be expected to be based on the chemicals used. The low angle region of the diffraction pattern is dominated by three distinct peaks at $2\theta = 6.6°$, 13.3° and 20.0° with the most intense one being that at 6.6°. Similar XRD patterns were reported elsewhere [36, 37] as 001 primary, secondary and tertiary order reflections and assigned to the zinc hydroxide acetate (ZHA), a compound with the idealised composition $Zn_5(OH)_8(CH_3COO)_2.nH_2O$. A search-match database analysis for verifying the structure and composition under our experimental conditions indicates the best agreement with the formula $Zn(OH)_{1.58}(CH_3COO)_{0.42}\cdot_{0.31}H_2O$ (JCDD PDF-2 entry 00-056-0569). The diffractogram b in the Figure 1 shows XRD patterns of ZnO **1** prepared under the same conditions as ZHA but with the synthesis time prolonged to 10 minutes. All diffraction peaks observed at $2\theta = 31.7°$, 34.4, 36.2°, 47.5°, 56.5°, 62.7°, 66.3°, 67.8°, 69°, 72.5°, 76.9° and 81.2° are characteristic for the wurtzite ZnO structure (hexagonal phase, space group $P6_{3mc}$) and are in a good agreement with the JCDD PDF-2 entry 01-079-0207. Moreover, the sharpness and narrowness of the diffraction peaks implies a well developed crystalline structure of the synthesized ZnO with no level traces of crystalline impurities detected.

**HERE FIGURE 1**

The powder XRD pattern for the sample denoted as ZnO **2** obtained by calcining of the precursor at 900 °C for 2 hours (Figure 1, diffractogram c) corresponds well to the hexagonal wurtzite ZnO phase (JCDD PDF-2 entry 01-079-0207). Although both samples, i.e. ZnO **1** and ZnO **2,** can be assigned to the hexagonal wurtzite ZnO phase, there are significant differences between the ratios of peaks intensity. Without any microscopic observation, this clearly indicates different morphologies of the prepared fillers.

The morphologies of the prepared fillers can be seen in Figure 2(a-f). In compliance with the XRD patterns interpretation, the ZHA exhibit the two-dimensional plate-like morphology typical for layered materials. At a closer look, the plates are rectangular in shape with dimensions of about one to ten micrometers and a thickness of several tens of nanometers

(Figure 2a,b). The synthesis time increasing from 2 to 10 minutes resulted in the transformation of the ZHA plate-like structure into ZnO particles resembling twinned truncated frustums (sample ZnO **1**) as documented in Figure 2c,d. The higher resolution image shows that ZnO crystal possesses a relatively high degree of imperfection and a broader particle size distribution, with the bigger particles having the length of between 3-4 μm and a diameter of about 2 μm.

**HERE FIGURE 2**

The scanning electron micrographs of the powder denoted as ZnO **2** are shown in Fig. 2e,f. It consists of mesh-like ZnO platelets with a porous morphology developed at the expense of mass removal due to the release of intercalation and structural water and sulphate groups during precursor annealing. The powder is bimodal in the particle size distribution with one fraction being about 1 μm and the second approximately 10 μm. The sheets thickness can be estimated to be in the order of several tens of nanometers from the higher resolution image in Fig. 2f.

***3.2 Characterisation of the prepared composites***

The XRD patterns (diffractograms b,c and d) of the prepared composites as well as the plain PVC matrix (diffractogram a) are shown in Fig. 3. For the sake of brevity, the results are exemplified in samples loaded by 5 wt% of fillers. Due to the absence of the long-range atomic order in amorphous polymers, the XRD patterns of the plain softened PVC sample exhibit only broad scattering peaks. The analysis of diffractogram b in Figure 3 reveals structural changes in the filler ZHA that occurred during the mixing of the filler into the matrix. The almost negligible diffraction line intensity remains at $2\theta = 6.6°$ while a strong and sharp peak raised at $2\theta = 11.9°$ for composite material which points towards a large and well defined change of the basal spacing of the compounded filler in comparison with the free powder ZHA. The shift of the 001 peak corresponds to the decrease in the interlayer distance from 13.4 to 7.4 Å. Such decrease cannot be attributed to the loss of intercalated water molecules only but also the contribution of the loss of an acetate ion per structural unit must be accounted, similarly as can be observed in re-intercalation processes with the use of carboxylic acids with different alkyl chain lengths [38]. Moreover, judging by the values of the full width at the half maximum (FWHM) obtained for both peaks (0.23° for the peak at 6.6° and 0.09° for the peak at 11.9°) even without correction for instrumental broadening, it

can be estimated that the free powder ZHA consists of a smaller number of less ordered crystalline layers in stack than the ZHA compounded into the polymer matrix. In other words, it means that the ZHA powder undergoes a certain compacting of the structure caused by external shear force, pressure and elevated temperature (175°C) which is higher than during synthesis (100°C). On the other hand, the material evidently keeps its layered structure although the presence of the newly created ZnO hexagonal wurtzite phase is clearly indicated by the presence of the characteristic peaks in the diffractogram. ZnO originates at the expense of the water and acetate groups liberation from ZHA, as can be confirmed by the pungent acetic odor released from the samples experienced during the mixing of the filler with PVC matrix. The acetate groups are released more likely as acetic acid, rather than acetanhydride because the temperature of 175°C is quite low and intercalated water molecules are present in excess in the system over acetate groups under elevated pressure [36].

**HERE FIGURE 3**

In contrast to above described ZHA composite, the interpretation of XRD patterns recorded for materials containing ZnO **1** and ZnO **2** fillers (Figure 3, diffractograms c and d respectively) is straightforward. All observed diffraction peaks can be found at the same positions as for original powder materials. However, the differences in ratios of peak intensity testify for an increasing preferential orientation of the fillers which means that a texture was developed during sample preparation. The diffractogram for ZnO **2** is dominated by the 002 reflection as the most intensive line which is unambiguously related to the basal planes perpendicular to the *c*-axis of ZnO crystallites. According to this observation, a parallel alignment of ZnO **2** hexagonal porous plates with the flat sample plane can be expected. A less pronounced orientation effect was observed for ZnO **1** containing material, favoring the 100 reflection line over the line corresponding to the 101 reflection.

The morphology of the prepared composite materials was observed by SEM on freeze fracture surfaces. The images are shown in Fig. 4; the left column shows low magnification images giving an overview of a large area to demonstrate the very good distribution of fillers ZnO **1** and **2 (**images e and g respectively**)**. The ZHA filler (image c) can be identified as white lumps with a bad distribution. A detailed image d in the right column shows a bad dispersion for the material ZHA as no single platelets similar to those in Fig. 2 can be seen. This observation is in agreement with the result of XRD analysis implicating a reasonable compacting of the material. On the other hand, the good dispersion of materials ZnO **1** and **2**

is demonstrated with the aid of images of single particles embedded into the polymer matrix (see image f for ZnO **1** and h for ZnO **2**). The perfect alignment of particles in the direction of the material flow can be seen in the image g, which confirms a strong orientation effect of hot press compression molding manifested in the XRD diffractogram for ZnO **2**. Moreover, the detailed image h exemplifies resistance of the porous platelets against disintegration by shear forces during compounding with a viscous PVC melt. The captured micrographs of neat PVC are shown in images a and b for comparison.

**HERE FIGURE 4**

The addition of small amounts of fillers as active antibacterial additives should not reasonably influence the mechanical properties of the prepared materials. Moreover, the compounding process has to be performed under conditions that do not deteriorate the material properties of the used PVC material in order to maintain the full range of its applicability.
Two basic characteristics, i.e. the Young's modulus and the tensile strength, were chosen to characterize the mechanical performance of the prepared composites according to the ISO 527-7:1996 [39]. The obtained results are summarized in Table 1. The comparison of the neat PVC matrix with all prepared composites showed no adverse effect on the prepared material either of the used fillers or of the applied processing conditions.

**HERE TABLE 1**

### 3.3 Surface antibacterial activity evaluation

A quantitative assessment of the surface antibacterial activity of the prepared composites tested against *Escherichia coli* ATCC 8739 and *Staphylococcus aureus* ATCC 6538P according to ISO 22196: 2007 (E) is summarized in Tables 1.,2. The values for the antibacterial activity were determined but there is no unique absolute pass/fail criterion defined and the assessment of the surface antibacterial performance is an arbitrary matter. The earlier standard JIS Z 2801 preceding the ISO 22196: 2007 (E) specified a value of 2.0 or greater as the demonstrated antibacterial activity. Therefore, most of the prepared composite materials can be categorized as having an imparted antibacterial activity on their surface through compounding with tested fillers. The critical value of 2.0 can be successfully accepted for hygienic and similar applications. On the other hand, the value of 6.0, i.e. the

99.9999 % reduction in cell count against controls, is considered for advanced medical plastics applications [31]. Even with regard to such strict criteria, the ZnO **2** based material can be ranked as having an excellent efficacy against *E. coli* at any used filler concentration and can be classified as performing very well against *S. aureus* at the concentration of 2 wt% or higher. The difference in susceptibility between gram-positive and gram-negative bacteria is often assigned to changes in the interaction mechanisms of ZnO with the bacterial membrane. Gram-positive bacteria have much thicker peptidoglycan cell walls compared with gram-negative bacteria, which results in a decreased susceptibility to the membrane damage induced by ZnO nanoparticles [40].

**HERE TABLE 2**

It is widely recognized that the antibacterial properties of nanoparticles depend on their size, shape, and even morphology and size distribution [41, 42]. However, these findings hold on straightforwardly for nanoparticles suspended in a liquid medium acting against planktonic forms of bacteria. The cell killing mechanism is often ascribed to the mechanical damage of the cell membrane [43] which is not a plausible mechanism for composite systems where the particles are embedded in the continuous polymer matrix. Therefore, another mechanism must be taken into account. Most likely it is the release or generation of active species which can reach the surface of the plastic article and have a localized effect there. In case of ZnO, the release of $Zn^{2+}$ cations or its complex forms is one of the proposed mechanisms [44]. The generation of reactive oxygen species (ROS) is another relevant explanation of ZnO's activity [45], but it requires illumination of the material by light with at least some portion of energy transferred by photons in the UVA region, e.g. the daylight unfiltered by window glass. However, the testing procedures are usually performed in the dark, the cultures of microorganisms being for the main part of the time closed in incubators, the same as it was in our case as well, so the photochemical mechanism cannot be considered as the exclusive cause of the observed antibacterial effect. Presumably, a combination of these two effects imparts the antibacterial activity to the surface of the prepared composites. If so, it can be deduced that the most efficient system will be that one with the largest surface in contact with the polymer matrix, because it is the filler-matrix interface where the active species are entering the continuous polymer matrix. Material ZnO **2** has obviously the best morphological arrangement to expect the biggest effect and, indeed, it was observed. On the other hand, it

must be stressed out that the active species of inorganic antibacterial systems, denoted commonly as non-migrating in contrast to diffusive organics denoted as migrating systems, work at a short distance only, as they either have low diffusivity through the polymer matrix (the case of the cations), or a short lifetime limiting their diffusion length (the case of ROS). Therefore, the distance between particles is the critical parameter, which depends straightforwardly on their concentration and particle shape and it can explain the observed thresholds in the efficacy of compacted ZHA and ZnO **1** material with a low aspect ratio. According to this, it is not only the size of the specific surface area what matters but the specific particle-matrix interface area per unit mass of the composite which can be more likely the key parameter. A particle with rugged, furcated or extended morphology can influence a larger volume of the polymer matrix in proximity of its surface than that one with a compact shape and internal pores. In next, particles with the extended morphology must have smaller distance between particles than compact shape particles at a given concentration in the composite. This can be generalized as follows: The ideal inorganic nanostructured microparticle intended to be used as an antibacterial filler has to have the lowest ratio possible between the envelope and true material density.

**4. Conclusion**

The present study showed that the antibacterial effect of ZnO based materials is strongly dependent on their particle morphology. Although ZnO is strain specific and performed better against representative gram negative bacteria than against gram positive bacteria, the two best composite materials based on the medical grade flexible PVC compounded with the prepared filler ZnO **2** were shown as an excellent antibacterial polymer system with a considerable surface antibacterial activity value higher than 6 against *Escherichia coli* and higher than 5 against *Staphylococcus aureus* which represents, in other words, the $10^6$x and $10^5$x reduction of viable cells respectively, in comparison to untreated PVC. Almost all prepared composite materials were found as efficient for less demanding applications according to the weaker criterion of minimal antibacterial activity being at least 2.

It is noteworthy that the prepared fillers consist of nanostructured particles with the overall particle size greater than one micrometer and behave like common powders which make them unproblematic for mixing with plastics, avoiding all technical difficulties usually related to the nanoparticles. Besides, the filler and the mixing procedure demonstrated no adverse effect on good mechanical properties of the used medical grade PVC. These facts suggest that the

studied ZnO based nanostructured microfillers, namely ZnO **2**, have potential in medical plastics industries as additive materials for PVC medical devices.
As the final conclusion of this pilot study, a general rule for the proneness of the inorganic nanostructured microparticles to be efficient as antimicrobial additives can be formulated. The ideal inorganic nanostructured microparticle intended to be used as antibacterial filler has to have the lowest ratio possible between the envelope and true material density to maximize the particle-matrix interface area and to assure the shortest average distance between particles at the given filler concentration. However, further detailed studies will be needed to confirm the validity of this rule over the large spectrum of possible inorganic antibacterial polymer systems.

**Acknowledgment**
This article was written with the support of the Operational Programme 'Education for Competitiveness' co-funded by the European Social Fund (ESF) and the national budget of the Czech Republic, within the project 'Advanced Theoretical and Experimental Studies of Polymer Systems' (reg. number: CZ.1.07/2.3.00/20.0104).

This article was written with the support of the Operational Programme 'Research and Development for Innovations' co-funded by the European Regional Development Fund (ERDF) and the national budget of the Czech Republic, within the project 'Centre of Polymer Systems' (reg. number: CZ.1.05/2.1.00/03.0111).

**References:**

[1] I. Francolini, G. Donelli, FEMS Immunol. Med. Microbiol., 59 (2010) 227-238.
[2] R.M. Donlan, J.W. Costerton, Clinical Microbiology Reviews, 15 (2002) 167-+.
[3] H. Ceri, M.E. Olson, C. Stremick, R.R. Read, D. Morck, A. Buret, J. Clin. Microbiol., 37 (1999) 1771-1776.
[4] I. Williams, W.A. Venables, D. Lloyd, F. Paul, I. Critchley, Microbiology-Uk, 143 (1997) 2407-2413.
[5] M.J. Ashby, J.E. Neale, S.J. Knott, I.A. Critchley, J. Antimicrob. Chemother., 33 (1994) 443-452.
[6] S. Noimark, C.W. Dunnill, M. Wilson, I.P. Parkin, Chem. Soc. Rev., 38 (2009) 3435-3448.

[7] T. Cao, H. Tang, X. Liang, A. Wang, G.W. Auner, S.O. Salley, K.Y.S. Ng, Biotechnol. Bioeng., 94 (2006) 167-176.
[8] K. Bazaka, M.V. Jacob, R.J. Crawford, E.P. Ivanova, Acta Biomaterialia, 7 (2011) 2015-2028.
[9] A.M.G. Borges, L.O. Benetoli, M.A. Licinio, V.C. Zoldan, M.C. Santos-Silva, J. Assreuy, A.A. Pasa, N.A. Debacher, V. Soldi, Mater. Sci. Eng., C, 33 (2013) 1315-1324.
[10] C. Yao, X. Li, K.G. Neoh, Z. Shi, E.T. Kang, J. Membr. Sci., 320 (2008) 259-267.
[11] H. Bakhshi, H. Yeganeh, S. Mehdipour-Ataei, M.A. Shokrgozar, A. Yari, S.N. Saeedi-Eslami, Mater. Sci. Eng., C, 33 (2013) 153-164.
[12] F. Costa, I.F. Carvalho, R.C. Montelaro, P. Gomes, M.C.L. Martins, Acta Biomaterialia, 7 (2011) 1431-1440.
[13] G. Gao, D. Lange, K. Hilpert, J. Kindrachuk, Y. Zou, J.T.J. Cheng, M. Kazemzadeh-Narbat, K. Yu, R. Wang, S.K. Straus, D.E. Brooks, B.H. Chew, R.E.W. Hancock, J.N. Kizhakkedathu, Biomaterials, 32 (2011) 3899-3909.
[14] E.-R. Kenawy, F.I. Abdel-Hay, A.A. El-Magd, Y. Mahmoud, Reactive and Functional Polymers, 66 (2006) 419-429.
[15] G.J. Gabriel, A. Som, A.E. Madkour, T. Eren, G.N. Tew, Mater. Sci. Eng., R, 57 (2007) 28-64.
[16] A. Munoz-Bonilla, M. Fernandez-Garcia, Prog. Polym. Sci., 37 (2012) 281-339.
[17] M. Rai, A. Yadav, A. Gade, Biotechnology Advances, 27 (2009) 76-83.
[18] J. Ramyadevi, K. Jeyasubramanian, A. Marikani, G. Rajakumar, A.A. Rahuman, Mater. Lett., 71 (2012) 114-116.
[19] M. Machovsky, P. Bazant, Z. Kozakova, M. Pastorek, P. Zlebek, I. Kuritka, Open Vessel Microwave-Assisted Synthesis of Ag/Zno Hybrid Fillers with Antibacterial Activity, Nanocon 2011, Tanger Ltd, Slezska, 2011, pp. 628-634.
[20] A. Amarjargal, L.D. Tijing, H.R. Pant, C.H. Park, C.S. Kim, Current Applied Physics, 12 (2012) 1106-1112.
[21] Y.W. Baek, Y.J. An, Sci. Total Environ., 409 (2011) 1603-1608.
[22] N. Jones, B. Ray, K.T. Ranjit, A.C. Manna, FEMS Microbiol. Lett., 279 (2008) 71-76.
[23] M. Moritz, M.g. Geszke-Moritz, Chem. Eng. J. (Lausanne), 228 (2013) 596-613.
[24] S. Kango, S. Kalia, A. Celli, J. Njuguna, Y. Habibi, R. Kumar, Prog. Polym. Sci., 38 (2013) 1232-1261.
[25] T. Hanemann, D.V. Szabo, Materials, 3 (2010) 3468-3517.

[26] C. Taviot-Gueho, F. Leroux, In situ polymerization and intercalation of polymers in layered double hydroxides, Layered Double Hydroxides, 2006, pp. 121-159.
[27] J. Liu, W.J. Boo, A. Clearfield, H.J. Sue, Mater. Manuf. Processes, 21 (2006) 143-151.
[28] P.J.P. Espitia, N.d.F. Soares, J.S.d.R. Coimbra, N.J. de Andrade, R.S. Cruz, E.A.A. Medeiros, Food and Bioprocess Technology, 5 (2012) 1447-1464.
[29] J. Sedlak, P. Bazant, Z. Kozakova, M. Machovsky, M. Pastorek, I. Kuritka, Nanostructured Zinc Oxide Microparticles with Various Morphologies, Nanocon 2011, Tanger Ltd, Slezska, 2011, pp. 305-309.
[30] M. Machovsky, I. Kuritka, J. Sedlak, M. Pastorek, Mater. Res. Bull., (2013).
[31] A. Jones, Plastics Engineering, 64 (2008) 34-+.
[32] ISO, Geneva, Switzerland, (2007).
[33] JIS, (2001).
[34] V.S. Sastri, Plastics in medical devices : properties, requirements and applications, Elsevier/William Andrew, Norwich, N.Y., 2010.
[35] C.E. Wilkes, J.W. Summers, C.A. Daniels, M.T. Berard, PVC handbook, Hanser, Munich ; Cincinnati, 2005.
[36] T. Biswick, W. Jones, A. Pacula, E. Serwicka, J. Podobinski, Solid State Sci., 11 (2009) 330-335.
[37] E.S. Jang, J.H. Won, Y.W. Kim, Z. Cheng, J.H. Choy, J. Solid State Chem., 183 (2010) 1835-1840.
[38] E. Kandare, J.M. Hossenlopp, J. Phys. Chem. B, 109 (2005) 8469-8475.
[39] ISO, (1996).
[40] P.J.P. Espitia, N.d.F. Soares, R.F. Teofilo, D.M. Vitor, J.S.d.R. Coimbra, N.J. de Andrade, F.B. de Sousa, R.D. Sinisterra, E.A.A. Medeiros, Journal of Nanoparticle Research C7 - 1324, 15 (2013) 1-16.
[41] A.l. Simon-Deckers, S. Loo, M. Mayne-L'hermite, N. Herl -
, Environ. Sci. Technol., 43 (2009) 8423-8429.
[42] A. Stanković, S. Dimitrijević, D. Uskoković, Colloids and Surfaces B: Biointerfaces, 102 (2013) 21-28.
[43] M.J. Hajipour, K.M. Fromm, A. Akbar Ashkarran, D. Jimenez de Aberasturi, I.R.d. Larramendi, T. Rojo, V. Serpooshan, W.J. Parak, M. Mahmoudi, Trends Biotechnol., 30 (2012) 499-511.
[44] K.M. Reddy, K. Feris, J. Bell, D.G. Wingett, C. Hanley, A. Punnoose, Appl. Phys. Lett., 90 (2007).

[45] N. Padmavathy, R. Vijayaraghavan, Science and Technology of Advanced Materials, 9 (2008).

**Table 1.:** Selected mechanical properties of the prepared composites

| Filler content | Filler code | Young's modulus | Tensile strength |
|---|---|---|---|
| [wt.%] | | [Mpa] | [Mpa] |
| 0 | – | 9.4 ± 1.1 | 19.9 ± 0.7 |
| 0.5 | ZHA | 10.5 ± 1.1 | 20.1 ± 0.7 |
| | ZnO **1** | 9.6 ± 1.1 | 20.4 ± 0.7 |
| | ZnO **2** | 9.3 ± 0.9 | 19.9 ± 0.6 |
| 1 | ZHA | 10.4 ± 1.0 | 20.1 ± 0.5 |
| | ZnO **1** | 10.0 ± 1.2 | 20.6 ± 0.5 |
| | ZnO **2** | 9.0 ± 0.9 | 20.3 ± 0.8 |
| 2 | ZHA | 10.4 ± 0.9 | 20.0 ± 0.6 |
| | ZnO **1** | 10.4 ± 1.0 | 21.0 ± 0.3 |
| | ZnO **2** | 10.5 ± 1.2 | 19.5 ± 1.4 |
| 5 | ZHA | 10.6 ± 1.1 | 19.2 ± 0.9 |
| | ZnO **1** | 9.5 ± 1.1 | 20.3 ± 1.1 |
| | ZnO **2** | 10.1 ± 0.5 | 20.3 ± 0.9 |

**Table 2**.: Summary of surface antibacterial activity against *E. coli* and *S. aureus* evaluation for the prepared composite materials.

| Filler content | R – value for *E. coli* | | | R – value for *S. aureus* | | |
|---|---|---|---|---|---|---|
| [wt.%] | [-] | | | [-] | | |
| | Filler code | | | Filler code | | |
| | ZHA | ZnO **1** | ZnO **2** | ZHA | ZnO **1** | ZnO **2** |
| 0.5 | 4.0 | 1.2 | > 6.6 | 1.8 | 0.9 | 0.2 |
| 1 | 4.5 | 3.6 | > 6.6 | 1.8 | 2.4 | 2.3 |
| 2 | 4.6 | 3.5 | > 6.6 | 1.9 | 2.4 | > 5.1 |
| 5 | 5.4 | 5.2 | > 6.6 | 2.5 | 3.3 | > 5.1 |

**Figure captions:**

**Figure 1.:** Powder XRD patterns of the prepared fillers. Labeling of diffractograms: ZHA – a, ZnO **1** – b, ZnO **2** – c.

**Figure 2.**: SEM images of the prepared fillers. The upper row shows ZHA, the middle row shows ZnO **1**, the lower row shows ZnO **2**. For a detailed description of the labels a – f, see the text.

**Figure 3.:** Powder XRD patterns of the prepared composites with 5 wt% filler loading and neat PVC. Labeling of diffractograms: Neat PVC – a, PVC:ZHA – b, PVC:ZnO **1** – c, PVC:ZnO **2** – d.

**Figure 4.**: SEM images of freeze fractured surfaces of the prepared composites with 5wt% filler loading and neat PVC. The upper row shows the morphology of neat PVC, the second row shows ZHA, the third row shows ZnO **1**, the lowest row shows ZnO **2**. For a detailed description of the images labels a – h, see the text.

Figure 1
Click here to download high resolution image

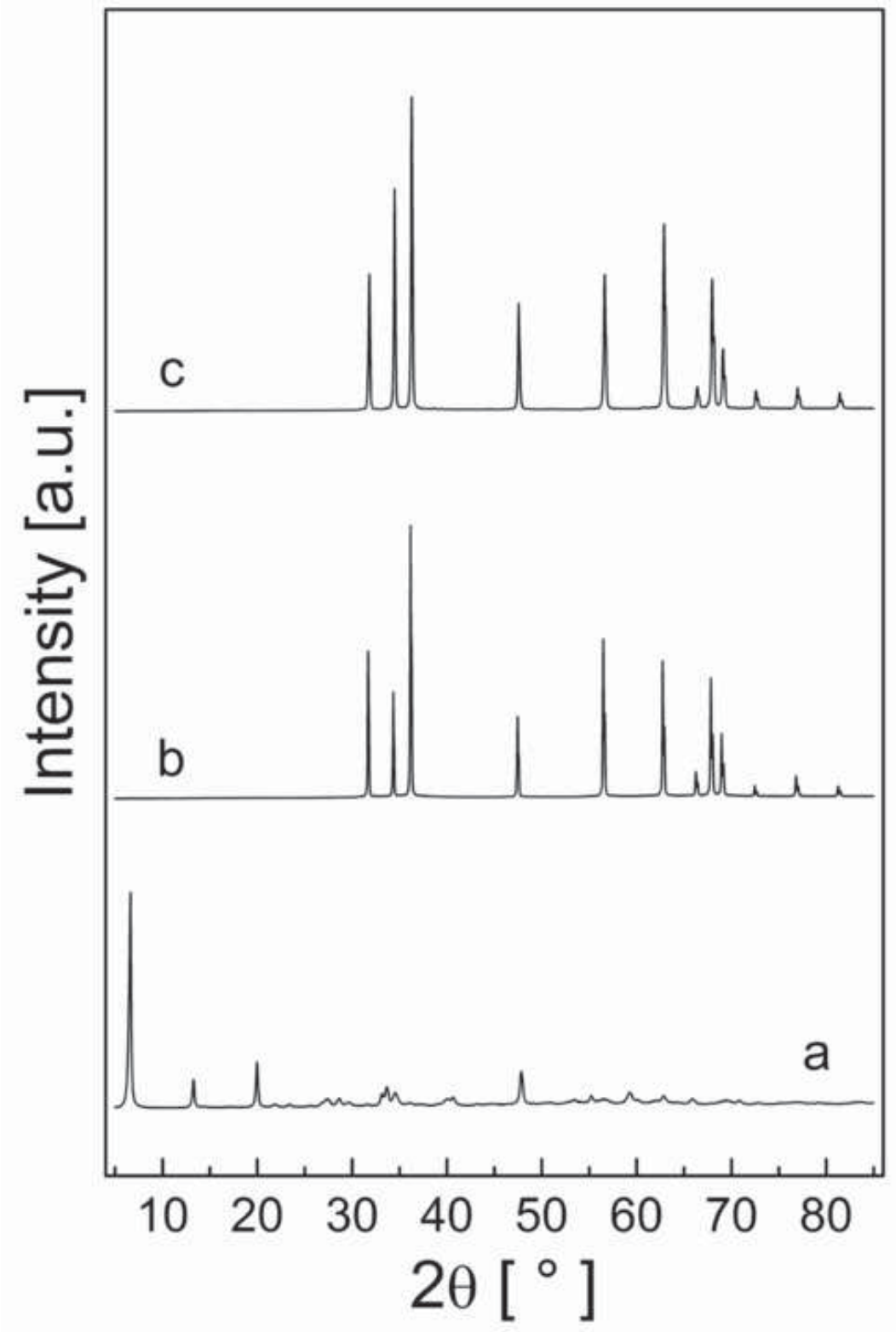

Figure 2
Click here to download high resolution image

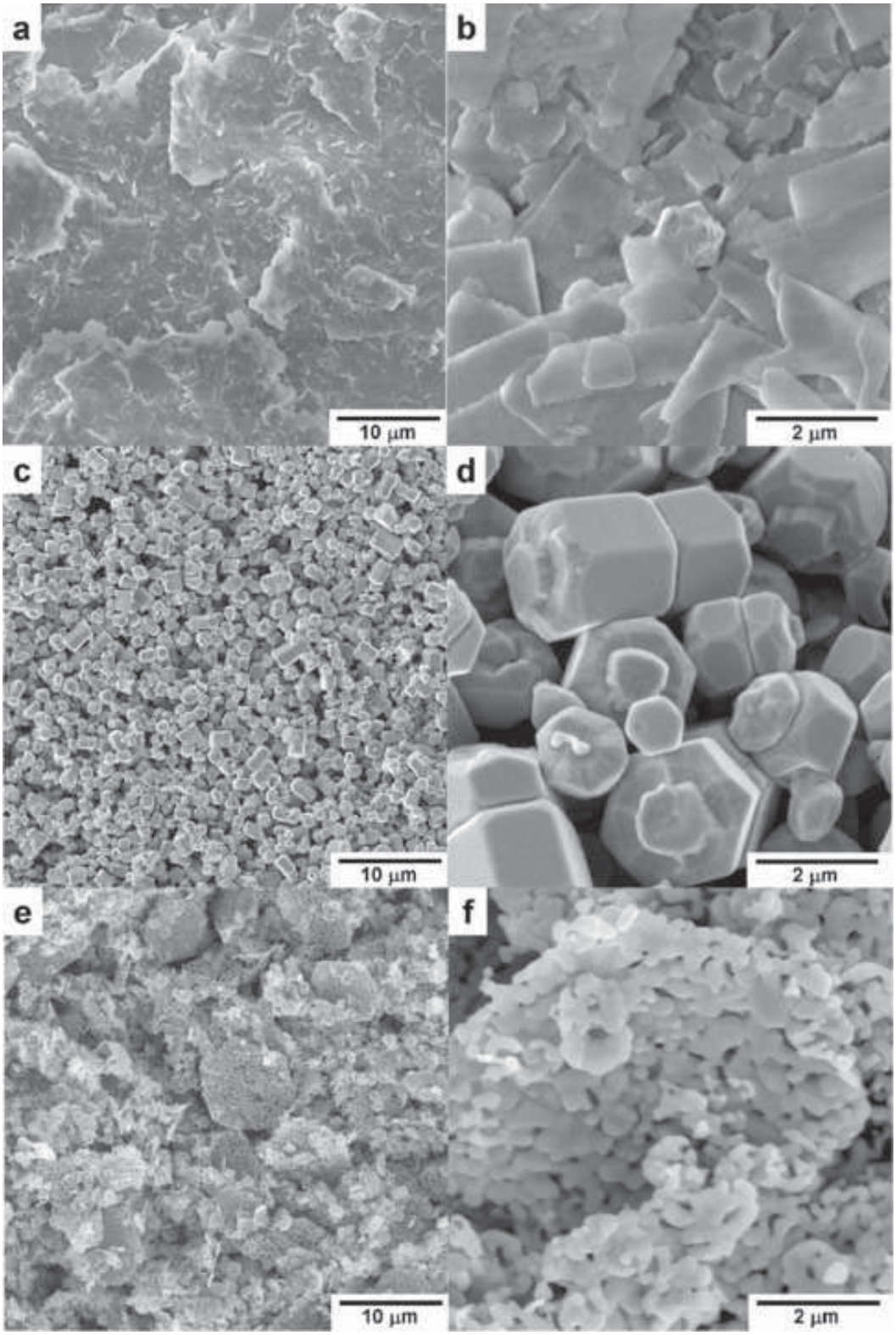

Figure 3
Click here to download high resolution image

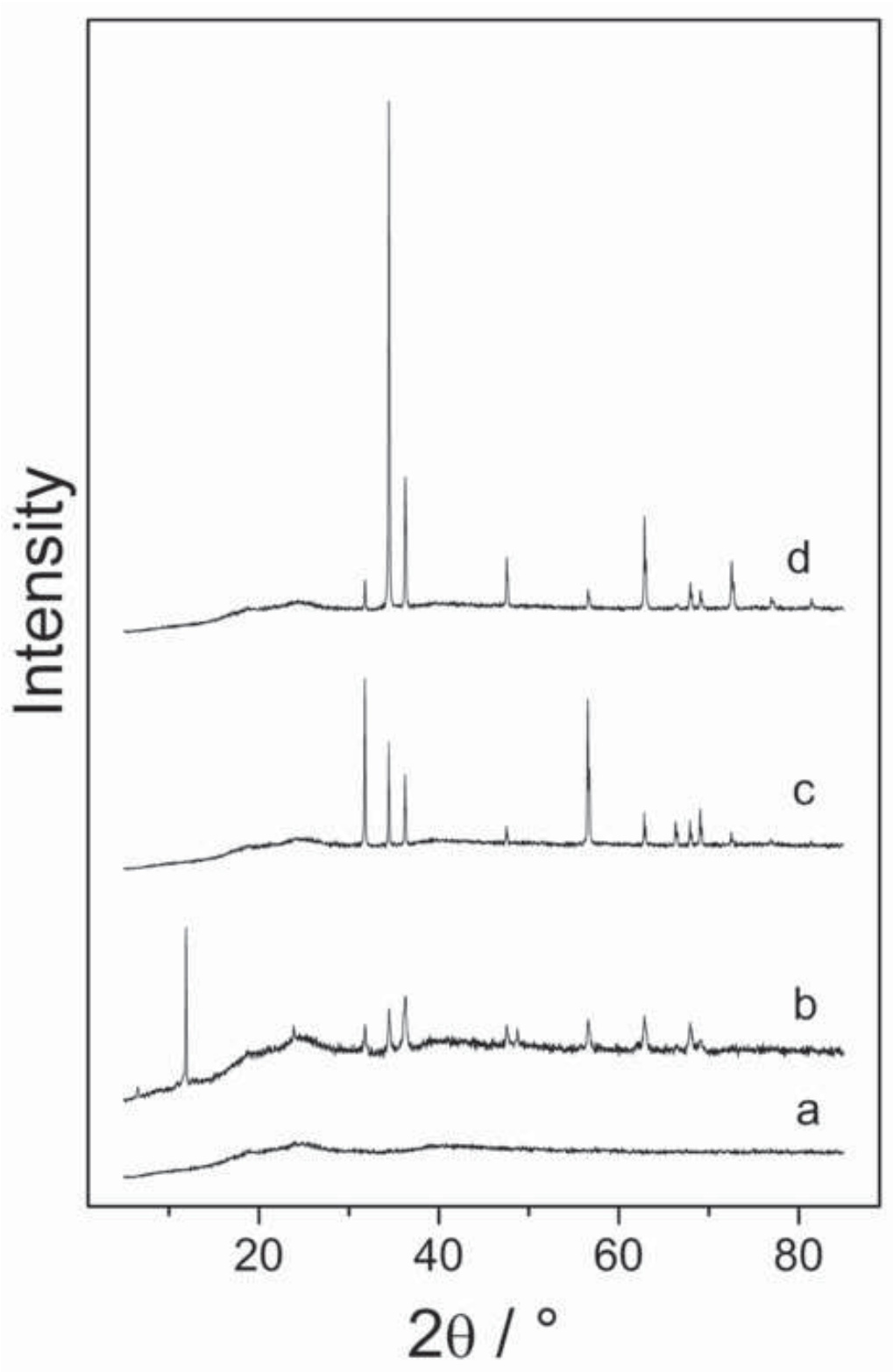

**Figure 4**

**Click here to download high resolution image**

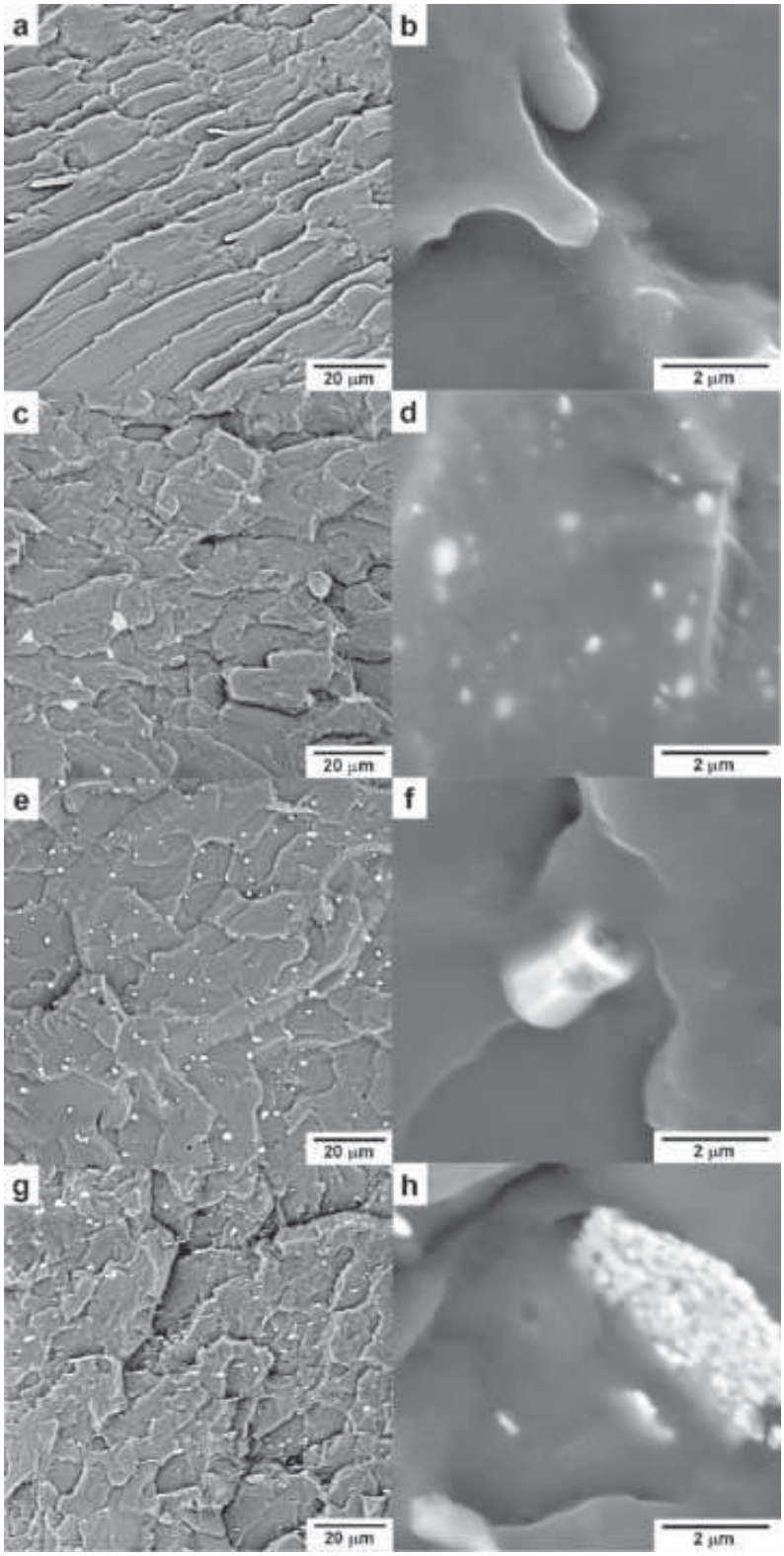

**Paper IV.**

BAZANT, P.; KURITKA, I.; HUDECEK, O.; MACHOVSKY, M.(30%); MRLIK, M.; SEDLACEK, T. Microwave assisted synthesis of Ag/ZnO hybrid filler, preparation and characterization of antibacterial PVC composites made from the same. *Accepted to Polymer composites*

Polymer Composites

# Microwave assisted synthesis of Ag/ZnO hybrid filler, preparation and characterization of antibacterial PVC composites made from the same



| | |
|---|---|
| Journal: | *Polymer Composites* |
| Manuscript ID: | PC-13-0306.R1 |
| Wiley - Manuscript type: | Research Article |
| Date Submitted by the Author: | n/a |
| Complete List of Authors: | Bazant, Pavel; Tomas Bata University in Zlin, Centre of Polymer Systems, University Institute; Tomas Bata University in Zlin, Polymer Centre, Faculty of Technology<br>Kuritka, Ivo; Tomas Bata University in Zlin, Centre of Polymer Systems, University Institute; Tomas Bata University in Zlin, Polymer Centre, Faculty of Technology<br>Hudecek, Ondrej; Tomas Bata University in Zlin, Centre of Polymer Systems, University Institute; Tomas Bata University in Zlin, Polymer Centre, Faculty of Technology<br>Machovsky, Michal; Tomas Bata University in Zlin, Centre of Polymer Systems, University Institute; Tomas Bata University in Zlin, Polymer Centre, Faculty of Technology<br>Mrlik, Miroslav; Tomas Bata University in Zlin, Centre of Polymer Systems, University Institute; Tomas Bata University in Zlin, Polymer Centre, Faculty of Technology<br>Sedlacek, Tomas; Tomas Bata University in Zlin, Centre of Polymer Systems, University Institute; Tomas Bata University in Zlin, Polymer Centre, Faculty of Technology |
| Keywords: | Polymer-matrix-composite, Antibacterial, Hybrid filler, Nanostructure |
| | |



SCHOLARONE™
Manuscripts

# Microwave assisted synthesis of Ag/ZnO hybrid filler, preparation and characterization of antibacterial PVC composites made from the same

Pavel Bazant[a,b,*], Ivo Kuritka[a,b], Ondrej Hudecek[a,b], Michal Machovsky[a,b], Miroslav Mrlik[a,b], Tomas Sedlacek[a,b]

[a] Centre of Polymer Systems, University Institute, Tomas Bata University in Zlin, Nad Ovcirnou 3685, 760 01 Zlin, CZECH REPUBLIC

[b] Polymer Centre, Faculty of Technology, Tomas Bata University in Zlin, Nam. T. G. Masaryka 275, 762 72 Zlin, CZECH REPUBLIC

* *Correspondence to:* Pavel Bazant, Centre of Polymer Systems, University Institute, Tomas Bata University in Zlin, Nad Ovcirnou 3685, 760 01 Zlin, CZECH REPUBLIC

*e-mail:* bazant@uni.utb.cz

For Peer Review

**Acknowledgements**

This article was written with the support of the Operational Program 'Research and Development for Innovations' co-funded by the European Regional Development Fund (ERDF) and the national budget of the Czech Republic, within the Centre of Polymer Systems project (reg. number: CZ.1.05/2.1.00/03.0111).

This article was written with the support of the Operational Program 'Education for Competitiveness' co-funded by the European Social Fund (ESF) and the national budget of the Czech Republic, within the 'Advanced Theoretical and Experimental Studies of Polymer Systems' project (reg. number: CZ.1.07/2.3.00/20.0104).

This work was supported by the Internal Grant Agency of Tomas Bata University in Zlin (grant No. IGA/FT/2013/026).

ABSTRACT:

Hybrid Ag/ZnO (silver/zinc oxide) nano-structured microparticles were obtained via the fast and simple microwave assisted synthesis. The phase structure of filler particles was revealed by X-ray diffraction analysis. Composites with medical-grade PVC were prepared with filler concentration from 1 to 5 wt% . The scanning electron microscopy was used for morphology characterization and elemental analysis of both filler and composites. The mechanical properties of composites and the electrical resistivity were found suitable for medical device application. The excellent surface antibacterial performance of the prepared composite tested according to ISO 22196: (2007) against *E. coli* and *S. Aureus* showed the reliability of the material in the medical application field.

For Peer Review

## 1. Introduction

The bacterial antibiotic resistance has rapidly increased mainly due to the overuse of antibiotics during the past 20 years, especially in hospital environments, thus the treatment of nosocomial infections has become difficult. Among hospital-acquired infections, medical device-related infections (MDI) have been recognized as one of the rapidly growing and significant problems, especially for the insertion of indwelling devices, which come into intimate contact with the interior of the human body. Bacterial colonization of the medical device does not only precede infection, but it can also adversely affect the function of an indwelling device. [1-3] Therefore, different ways are investigated in order to reduce this risk. Among them, suppression of bacteria adherence and growth on the surface of the device is considered as a viable strategy in MDI's management.[4] As polymers are the most used materials in medical devices, antimicrobial polymer additives (APA) can play an important role. [5]

While many antimicrobial additives are referred to as biocides, there are actually two different effects: biocidal (killing the organism) and biostatic (preventing the reproduction). Inorganic additives combine biocidal and biostatic properties, therefore, the use of inorganic APAs compounded into the polymer matrix, the so-called antimicrobial polymer systems (APS), can produce a good antibacterial effect for medical application. [6, 7] Recently, attention has been focused on various metals, metal oxides and metal salts which have proven their antibacterial performance, especially if used in the form of nanoparticles. [8-11] Combinations of different metals, metal oxides and particle coatings were investigated and found as even more promising. [12-14] Among these advanced systems, hybrid metal-semiconductor materials have

For Peer Review

attracted great attention because joined metal and semiconductor nanoparticles have not only a large specific surface area and a high fraction of surface atoms but also have a unique electronic band structure resulting in a specific chemical activity. [15] Different methods are used for the preparation of such hybrid system with specific functional properties tailored towards the desired application, e.g. sol-gel, photoreduction method, laser heating techniques, photolysis method, ultrasonic spray pyrolysis, microwave techniques, and so on. [16-20]

Several attempts to design various Ag/ZnO nanocomposites with an antibacterial activity against gram-positive and gram-negative bacteria have been introduced in the literature. [21, 22] Metallic Ag and $Ag^+$ ions have a strong antibacterial effect which has been known and used for a long time [11, 23-25]. Zinc oxide (ZnO) in the form of nanoparticles has proven as a strong antibacterial agent against a broad spectrum of bacteria. However, the principle of its activity is not fully understood yet. [10] In general, silver has a stronger antibacterial performance against gram-negative than against gram-positive bacteria, while ZnO proves a better antibacterial activity against gram-positive than against gram-negative bacteria. [9, 11, 26, 27] Synergetic effects of both components used in hybrid metal-semiconductor nanoparticles result in an enhanced antibacterial performance against both kinds of bacteria. [22]

Another advantage of these materials could be their relatively mild effect in contrast to the application of soluble mineral salts as additives, although these simple compounds are very efficient against bacteria. Composite materials based on $AgNO_3$ and $ZnNO_3$ additives were successfully prepared and their efficiency was proven by standard zone inhibition - “Halo” - tests on agar plates [28, 29]. Large diameters of the observed inhibition zones testify for a diffusion of the active agent over a relatively long



For Peer Review

distance; however, this could cause inevitable damage to the patient's tissue in proximity to the inserted device made from such material as silver cations at a high concentration are toxic for mammalian cells [30, 31]. Therefore, we consider the zone inhibition test being not predicative enough for the APS application, because the best observable effect could be achieved by using strong chemical agents in a high concentration having the ability to kill all living cells around. Moreover, the halo test cannot distinguish between the true biocidal action and biostatic action which prevents the bacteria only from reproducing and forming visible colonies. Indeed, an APS of a rational design should assure the protection of the device against bacterial adherence and colonization as much as it is possible, but the activity should rapidly decrease with a growing distance from the surface, and the tissue of the patient's body in contact with the device mustn't be harmed by any species released from the material to body liquids. Therefore, the test of antibacterial activity on plastic surfaces according to ISO 22196:2007(E) is considered by the authors as the most indicative among viable count test methods.

Following from above, this work is focused on the Ag/ZnO system used as filler with the aim to suppress association and survival of bacteria on the surface of the composite material. In this paper, we offer an original method for the preparation of Ag/ZnO hybrid nanostructured microfiller by microwave (MW) assisted synthesis. The preparation of hybrid Ag/ZnO nanostructures by MW was already reported by Bhattacharyya et al. 2008 [20] and Karunakaran et al. [17] where they either used microwave polyol synthesis conducted under argon atmosphere yielding silver nanoparticles inserted into the mesoporous ZnO structure within a 15-minute reaction, or worked with Ag/ZnO-citric acid gels in a domestic microwave oven in the on/off

For Peer Review

cycle mode yielding silver doped ZnO powders within 15 minutes, respectively. However, our method of hybrid Ag/ZnO nanostructured particles' preparation using a microwave domestic oven with an external reflux cooling system is faster, simple, water based, reproducible and does not require any template, catalyst, or surfactant in contrast to the above mentioned references and even to our preliminary short study [32]. Next, the product is easy to collect and wash by microfiltration; hence, it was chosen for the preparation of filler for APS.

Medical grade Poly (vinyl chloride) (PVC) was selected as the representative polymer for the APS's matrix. Although a lot of effort has been made to replace PVC in biomedical applications, it still remains the most used polymer in medical device fabrication. Applications of PVC include blood bags and tubing, intravenous containers and components, catheters, dialysis equipment, examination gloves inhalation masks and other generally known uses. [33] Material systems based on PVC are continually subjected to searching for new and improved modifications, especially for those minimizing the leaching of plasticizers, confirming thus the reliability of PVC utilization in future [34, 35].

## 2. Experiment

### *2.1. Materials*

Silver nitrate $AgNO_3$ (≥99.5 % purity) and zinc acetate dihydrate $Zn(CH_3COO)_2{\cdot}2H_2O$ (> 99 % purity) were delivered by Penta (Prague, Czech Republic) and hexamethylenetetramine (HMTA) $C_6H_{12}N_4$ (>99 % purity) was supplied by Sigma-Aldrich (Prague, Czech Republic). Demineralized water was used throughout these experiments. Medical grade plasticized PVC RB3 was used as the polymer matrix for



For Peer Review

the composite preparation. The RB3 resin is biocompatible according to ISO 10993 USP, Class VI and it was delivered by Modenplast Medical (Italy).

*2.2. Synthesis of Ag/ZnO*

A domestic oven (CWR-TECH, 1150W/230V-50Hz) was modified for the open vessel solvothermal synthesis with an external condenser. All chemical reagents were dissolved in demineralized water. Firstly, the solution of 10.8 g $Zn(CH_3COO)_2 \cdot 2H_2O$ in approx. 60 mL was mixed together with the solution of 0.699 g $AgNO_3$ in approx. 40 mL so that the total volume of water used for the dissolution of both salts was 100 mL. The obtained solution was placed in the microwave oven and heated for 2 minutes, and then a solution of 6.998 g $C_6H_{12}N_4$ in 50 mL water was added quickly through a dropping funnel, and microwave heating continued for another 3 minutes. In this way, HMTA was used both as a precipitation agent and as a growth modifier. The product was collected and washed by filtration and the obtained powder was dried in the laboratory oven, with the typical yield of 1.2 g of dry powder. Therefore, the synthesis was repeated several times in order to produce enough filler for the preparation of composite samples.

*2.3. Preparation of composites*

The filler concentrations chosen were 1, 3, 5 wt% . PVC pellets were mechanically premixed with the filler and fed into the mixing chamber of Brabender (measuring mixer W 50 Brabender® GmbH & Co. KG) compounder. The mixing was performed at 170 °C and 20 rpm during the first two minutes and then 50 rpm during the next five minutes. The homogenization process was controlled in all cases; the

For Peer Review

measured torque of the drive motor was constant after five minutes, suggesting a high degree of homogeneity. The obtained PVC compounds were compression moulded for 2 minutes at 170 °C into sheets 1 mm thick. These sheets were further used for the preparation of testing specimens for measuring of mechanical, electrical and antibacterial properties. The specimens were cut according to the requirements of the used measurement techniques. Neat PVC without filler was processed in the same way to obtain reference specimens.

*2.4. Structural characterization*

The crystalline structure of the obtained powder was characterized by X-ray diffraction (XRD) utilizing multi-purpose X-ray diffractometer PANalytical X´Pert PRO MPD (The Netherlands) with a Cu-Kα X-ray source (λ = 1.5418 Å) operating at 40 kV and 30 mA. The phase composition was evaluated by the use of PANalytical X'Pert HighScore software employing the ratio between the integrated normalized intensities of the peak of interest and that of a known standard. The micrographs of the prepared particles and composite were taken by the scanning electron microscope Vega II LMU (Tescan, Czech Republic), after coating with a thin layer of gold/palladium by the sputter coater SC 7640 (Quorum Technologies Ltd, UK). TEM images of the prepared particles were taken on a transmission electron microscope (TEM, JEOL 1200, JEOL Ltd., Japan). The composite structure was observed on freeze fracture surfaces obtained in liquid nitrogen. Elemental microanalysis was done using the energy dispersive X-ray analyzer (Oxford Instruments INCA) connected to the SEM.

*2.5. Testing of mechanical properties*

For Peer Review

The tensile tests were carried out by means of a Testometric universal-testing machine M 350-5CT (supplied by LABOR machine, Ltd. Opava, Czech Republic) equipped with a cell-load of 1 kN. All measurements were conducted using a crosshead speed of 500 mm/min and a gauge length of 50 mm on Dumb-bell shaped specimens of the Type 2 as indicated in ISO 37:2005. Six specimens of each material were tested.

*2.6. Measurement of electrical properties*

The conductivity of the materials was measured using the four-point van der Pauw method at room temperature with the use of the Electrometer/High Resistance Meter KEITHLEY 6517B. The specimens were prepared by cutting discs with a diameter of 25 mm from compression molded sheets. In order to determine the conductivity of the filler, disc pellets with a diameter of 13 mm and a thickness of 0.8-1.2 mm were compressed at 7 MPa with a manual hydraulic press.

*2.7. Antibacterial activity evaluation*

The antibacterial activity of the composite surface was assessed in vitro against *Escherichia coli* ATCC 8739 and *Staphylococcus aureus* ATCC 6538P as representatives of Gram-negative and Gram-positive bacteria respectively, according to the ISO 22196: 2007 (E) Plastics – Measurement of antibacterial activity on plastics surfaces. The dimension of the test pieces was 50 x 50 $mm^2$ and 1 mm in thickness, and the duration of the test after inoculation was 48 h at 35 °C. All tests were done in triplicate.

The antibacterial activity R was calculated using the Equation (1)

$$R = (U_t - U_0) - (A_t - U_0) = U_t - A_t \quad (1)$$



For Peer Review

Where $R$ is the antibacterial activity; $U_0$ is the average of the logarithm of the number of viable bacteria, in cells/cm$^2$, recovered from the untreated test specimens immediately after inoculation; $U_t$ is the average of the logarithm of the number of viable bacteria, in cells/cm$^2$, recovered from the untreated test specimens immediately after 48 h; $A_t$ is the average of the logarithm of the number of viable bacteria, in cells/cm$^2$, recovered from the treated test specimens immediately after 48 h.

It should be noted that a slight modification of the original procedure according to ISO 22196:2007(E) was made to reduce the risk of false results. The number of colonies grown from the recovered cells was estimated not only after 24 hours as required by the original standard protocol but checked after 48 hours of cultivation, to be assured once again whether all colonies had developed into countable size. In several cases, some colonies were found by this procedure on plates which prevented incorrect too-good results caused just by a slower growth of colonies than needed for all of them to be fully developed within 24 hours.

## 3. Results and discussion

### *3.1. Crystal structure of the filler*

Fig. 1 presents the X-ray diffractogram of the nano Ag/ZnO filler obtained by microwave synthesis. The powder exhibited typical patterns consistent with the known positions of diffraction lines for two materials: the hexagonal structure of ZnO (JCPDS-ICDD PDF-2 entry 01-079-0207) and of face-centered-cubic Ag metal (JCPDS-ICDD PDF-2 entry 01-087-0720). All diffraction peaks were unambiguously assigned by the appropriate structure and reflection plane indices, and no other

For Peer Review

crystalline phases were found. The crystalline phase composition of the hybrid filler was estimated as 34 wt% of Ag and 66 wt% of ZnO.

*3.2. Morphology of filler particles*

A SEM micrograph of the prepared filler is shown in Fig. 2a. BSE detector enables to distinguish the composition of particles by material contrast showing phases containing elements with a higher atomic number brighter. It is clearly seen that the Ag/ZnO powder is comprised of two different structures: Larger light grey hexagonal frustums with six trapezoidal facets are ZnO particles sized up to 2 μm and white smaller silver spherical particles are sized up to 200 nm. More details can be seen in the TEM image in Fig. 2b. It is apparent that the zinc oxide particles possess an inhomogeneous internal structure and the silver particles are spherical with the diameter up to 200 nm. However, there are two forms of silver manifested. First, single smaller nanoparticles concomitant with ZnO prisms are visible in the TEM image. Next, grape-like agglomerates can be seen in the SEM image at lower magnification (Fig. 2a).

*3.3. Structure of PVC compounds*

The microstructure of the prepared PVC composites was observed by SEM. The results are demonstrated in Fig. 3 by the images of neat PVC fracture surface and those obtained by fraction of the composites with 1, 3, and 5 wt% of the hybrid filler. A good dispersion and distribution of the filler in the PVC polymer matrix can be seen in Fig. 3. Single hexagonal microparticles of ZnO and smaller nanoparticles of silver are visible. In addition, it is evident that the morphology of the filler was not changed by the process of compounding.

For Peer Review

To determine the composition of the final products, the samples were characterized by the Energy dispersive X-ray analysis (EDX). A typical EDX spectrum recorded on the composite material shows the presence of Ag, Zn, Cl, C and O elements as exemplified in Fig. 4 for the sample with 5 wt% of Ag/ZnO powder mixed in the polymer matrix. The analysis reveals the composition as 1.8 wt% of silver and 2.1 wt% of Zn. This corresponds well with the content and composition of the filler. The EDX analysis was used for elemental mapping in combination with the BSE image capturing as well. It can be seen in Fig. 5 that on a large scale the filler distribution is still good; however, the dispersion of silver nanoparticles is worse as agglomerates are visible. The material contrast in BSE image in the upper part of the Fig. 5 highlights silver particles over zinc oxide particles and polymer matrix background due to the difference in atomic number of their constituting elements. The selected area of the observed material fracture surface indicated in the figure by a rectangle in the middle of the SEM image was simultaneously analyzed by EDX and the results are shown for each main X-ray fluorescence line of the following elements: carbon, chlorine, zinc, silver, oxygen. As can be expected for C, Cl, and O as the constituting elements of the polymer matrix, they are distributed homogeneously over the whole inspected area. Silver shows a good distribution, however, a worse dispersion as large variations are seen in signal density for Ag Lα1 line, i.e. white and grey spots on a very dark background. A perfect correlation between the silver distribution map and the upper image confirms the preferential assignment of the material contrast manifestation to the presence of silver. On the other hand, zinc is distributed homogeneously in the polymer matrix at the given resolution. This seemingly contradictory result can be explained by the tendency of silver particles to agglomerate, hence the clusters of white spots results from the above

For Peer Review

described grape-like structures while the small silver nanoparticles concomitant the zinc microparticles were not manifested in this analysis as their concentration in interaction volume of the electron beam is small. On the other hand, it might be expected that they are distributed and dispersed together with zinc particles.

*3.4. Mechanical properties*

The mechanical properties of particulate–polymer composites depend strongly on the particle size and aspect ratio, particle–matrix interface adhesion, elastic module of matrix and particles and particle loading. However, in our case, composites with low volume filler concentrations were prepared as indicated in Table 1, and no significant changes of mechanical properties were either expected or required. The chosen PVC matrix has optimum mechanical properties for the intended application range, and the main intention in this study was to avoid their worsening. No discoloration, no burning, char or fume formation or other manifestations of accelerated degradation of the PVC were observed during the compounding, which, indeed, proceeded so smoothly as for the neat reference PVC sample mixing, regardless of the amount of added filler. The evaluation of mechanical tensile test can be seen in Table 1. All composite materials show similar mechanical properties such as the Young's modulus, strain at break and stress at break. The value of the Young's modulus varies slightly between 7.3 MPa for neat PVC and 4.9 MPa for 3 wt% composite. The maximum value was observed for 5 wt% composite again. The initial decrease of the elastic modulus is in contradiction with the common mixing rules [36]; however, it can be explained by the overbalance of the inevitable introduction of defects with a small concentration of the filler in comparison with its stiffening effect, most likely due to the imperfection of the material

For Peer Review

compounding. An uprise of the modulus appeared with 5 wt% again. Strain at break and stress at break showed opposite trends as can be expected.

*3.5. Electrical properties*

Zinc oxide is a well-known semiconductor with a broad range of resistivity depending on the materials' morphology and, especially, on the type and concentration of dopant within the range $10^{-4}$-$10^{9}$ Ω cm, which means that ZnO can be successfully prepared even in a conductive state although it requires a heavily doped material and special conditions. [37] In contrast to that, silver is an excellent metallic conductor with a resistivity of 1.59 x $10^{-6}$ Ω cm [38]. A combination of these materials could produce a hybrid with a reasonably high electrical conductivity approaching the limits of defining materials as conductors, and powder Ag/ZnO could cause conductivity even at low content of filler in the polymer matrix if the critical threshold value is exceeded. However, according to our best knowledge, no systematic studies have been done with similar materials. On the other hand, PVC is typical insulating polymer material and its room temperature volume conductivity in a dry state is as low as $10^{-15}$-$10^{-13}$ S $cm^{-1}$ [39] The percolation threshold for most metal-filled polymer systems is nearly ten volume percent, where the plateau region on percolation curves usually began. The critical volume content of the filler is even lower for randomly cut and anisotropic particles. [40] Therefore, the use of hybrid particles which can have a high number of contacts between superiorly conductive particles must be examined carefully. The electrical insulating property is required for plastic medical devices used by patients in hospitals for safety reasons in case of an emergency procedure with the aid of a defibrillator for resuscitation. Another reason for good insulating properties is the aim to avoid

For Peer Review

interference with connections to the electronic instruments monitoring the patient's body functions. The electrical resistivity of prepared materials is summarised in Table 2.

The resistivity of neat PVC was found higher than the measurement range limit $10^9$ Ω cm of the used method. The hybrid material compressed into a pellet exhibited a very good conductivity with the resistivity value in the $10^{-3}$ Ω cm order of magnitude which is similar as those in common metal conductors. Hence, the issue of the composite conductivity must be treated seriously. All three composite materials have a resistivity in the $10^7$ Ω cm order of magnitude, being thus on the safe side of the percolation curve. The observed values of the prepared composite resistivity are significantly, i.e. several orders, higher than the magnitudes reported for the human body. Approximate values of the tissue volume resistivity were found to be about 160 Ω cm for blood, 2000 Ω cm for lungs, 2500 Ω cm for fat, 700 Ω cm for liver, 250 and 550 Ω cm (anisotropic) for the heart muscle and 150 and 2500 Ω cm (anisotropic) for skeletal muscles.[41]

*3.6. Antibacterial activity of the composite*

For APS, not only the antibacterial properties of the selected combination of fillers are important but the whole system including the polymer matrix must assure a reasonable release rate of the active species to the surface of the plastic article. A quantitative assessment of the antibacterial activity of the tested samples was performed, and the *R*-values are shown in Table 3. The value of the antibacterial activity *R* of the composite against *E. coli* is very high, of about 6.6 for all (1, 3, 5 wt% ) concentrations of filler in the PVC matrix. The antibacterial activity of the composite against *S. aureus* is lower, but it is still high enough for 3 and 5 wt% of the filler in


John Wiley & Sons
For Peer Review

PVC, as the critical *R-value* should not be less than 2.0 for materials that can be categorized as having an effective antibacterial surface. [7]

The difference in activity against the two tested types of bacteria can be attributed to structural and chemical compositional differences of the cell walls. Gram-positive bacteria typically have one cytoplasmic membrane and a thick wall composed of multilayer of peptidoglycan. In contrast, gram-negative bacteria possess a more complex cell wall structure, with a layer of peptidoglycan between the outer membrane and the cytoplasmic membrane. The difference in the antibacterial action towards *E. coli* and *S. aureus* is assumed to be caused by different sensitivities towards $H_2O_2$ generated by Ag/ZnO, although the exact mechanisms responsible for the antibacterial activity of silver and ZnO nanostructures are still not fully clear, and the exact cause of the membrane damage requires further study. [42-44] It must be noted that the cultivations of bacteria were done in the dark condition - in a closed incubator, so that the antibacterial effectiveness based on the peroxide action was not expected to be manifested. Another explanation can be based on a different availability of metallic cations related to the different size of particles. Lower *R*-values achieved against *S. aureus,* which is theoretically more sensitive to zinc than to silver, correlate with a bigger size of the ZnO particles than the Ag particles that are more efficient against *E.coli* according to the literature.

**4. Conclusions**

A simple efficient microwave assisted synthetic route for the preparation of hybrid Ag/ZnO filler was developed. The obtained powder material consists of metallic nanosilver and semiconducting ZnO microparticles with multiscale morphology. The



For Peer Review

composite material based on the medical grade flexible PVC compounded with the prepared filler was shown as an effective Antibacterial Polymer System with a surface activity excellent against *Escherichia coli* and sufficient against *Staphylococcus aureus.* Besides, the composite demonstrated suitable electrical and mechanical properties with respect to its utilization in medicine in contact with a patient's body. These facts suggest that the PVC composite has potential in medical plastics industries as a material for medical devices.

For Peer Review

## References


1 S. Noimark, C. W. Dunnill, M. Wilson and I. P. Parkin, *Chem Soc Rev,* **38**, 3435 (2009).

2 S. Monroe and R. Polk, *Current Opinion in Microbiology,* **3**, 496 (2000).

3 C. von Eiff, B. Jansen, W. Kohnen and K. Becker, *Drugs,* **65**, 179 (2005).

4 R. O. Darouiche, *Clinical Infectious Diseases,* **33**, 1567 (2001).

5 G. J. Gabriel, A. Som, A. E. Madkour, T. Eren and G. N. Tew, *Materials Science & Engineering R-Reports,* **57**, 28 (2007).

6 J. Simmons, *Plastics, Additives and Compounding,* **2**, 20 (2000).

7 A. Jones, *Plastics Engineering,* **64**, 34 (2008).

8 K. Chaloupka, Y. Malam and A. M. Seifalian, *Trends Biotechnol,* **28**, 580 (2010).

9 O. Yamamoto, K. Nakakoshi, T. Sasamoto, H. Nakagawa and K. Miura, *Carbon,* **39**, 1643 (2001).

10 Q. L. Li, S. Mahendra, D. Y. Lyon, L. Brunet, M. V. Liga, D. Li and P. J. J. Alvarez, *Water Res,* **42**, 4591 (2008).

11 C. Marambio-Jones and E. M. V. Hoek, *Journal of Nanoparticle Research,* **12**, 1531 (2010).

12 C. M. N. Chan, H. S. Cheng, A. B. Djurisic, A. M. C. Ng, F. C. C. Leung and W. K. Chan, *J Appl Polym Sci,* **122**, 1572 (2011).

13 R. Gokulakrishnan, S. Ravikumar and J. A. Raj, *Asian Pacific Journal of Tropical Disease,* **2**, 411 (2012).

14 Q. L. Cheng, C. Z. Li, V. Pavlinek, P. Saha and H. B. Wang, *Appl Surf Sci,* **252**, 4154 (2006).

15 Y. H. Zheng, L. R. Zheng, Y. Y. Zhan, X. Y. Lin, Q. Zheng and K. M. Wei, *Inorg Chem,* **46**, 6980 (2007).

16 M. Catauro, M. G. Raucci, F. De Gaetano and A. Marotta, *J Mater Sci: Mater Med,* **15**, 831 (2004).

17 C. Karunakaran, V. Rajeswari and P. Gomathisankar, *Solid State Sci,* **13**, 923 (2011).

18 X. Y. Ye, Y. M. Zhou, Y. Q. Sun, J. Chen and Z. Q. Wang, *Journal of Nanoparticle Research,* **11**, 1159 (2009).


For Peer Review

19 G. Zhou and H. C. Deng, *Mater Sci Semicond Process,* **10**, 90 (2007).

20 S. Bhattacharyya and A. Gedanken, *J Phys Chem C,* **112**, 659 (2008).

21 L. H. Li, J. C. Deng, H. R. Deng, Z. L. Liu and X. L. Li, *Chemical Engineering Journal,* **160**, 378 (2010).

22 W. W. Lu, G. S. Liu, S. Y. Gao, S. T. Xing and J. J. Wang, *Nanotechnology,* **19**, (2008).

23 G. Zhao and S. E. Stevens Jr, *BioMetals,* **11**, 27 (1998).

24 S. K. Gogoi, P. Gopinath, A. Paul, A. Ramesh, S. S. Ghosh and A. Chattopadhyay, *Langmuir,* **22**, 9322 (2006).

25 C. Aymonier, U. Schlotterbeck, L. Antonietti, P. Zacharias, R. Thomann, J. C. Tiller and S. Mecking, *Chemical Communications,* 3018 (2002).

26 S. Shrivastava, T. Bera, A. Roy, G. Singh, P. Ramachandrarao and D. Dash, *Nanotechnology,* **18**, (2007).

27 F. Zeng, C. Hou, S. Z. Wu, X. X. Liu, Z. Tong and S. N. Yu, *Nanotechnology,* **18**, (2007).

28 M. Merchan, J. Sedlarikova, A. Vesel, V. Sedlarik, M. Pastorek and P. Saha, *Int J Polym Anal Charact,* **15**, 360 (2010).

29 T. Galya, V. Sedlarik, I. Kuritka, J. Sedlarikova and P. Saha, *Int J Polym Anal Charact,* **13**, 241 (2008).

30 N. R. Panyala, E. M. Pena-Mendez and J. Havel, *Journal of Applied Biomedicine,* **6**, 117 (2008).

31 S. Silver, *Gene,* **179**, 9 (1996).

32 P. Bazant, Z. Kozakova, O. Hudecek, M. Machovsky, M. Pastorek and I. Kuritka, in *Nanocon 2011*, 459 (2011).

33 C. E. Wilkes, J. W. Summers, C. A. Daniels and M. T. Berard, *PVC handbook*, Hanser, Munich ; Cincinnati (2005).

34 N. M. K. Lamba, J. M. Courtney, J. D. S. Gaylor and G. D. O. Lowe, *Biomaterials,* **21**, 89 (2000).

35 M. Messori, A. Toselli, F. Pilati, E. Fabbri, P. Fabbri, L. Pasquali and S. Nannarone, *Polymer,* **45**, 805 (2004).

36 R. W. Siegel, S. K. Chang, B. J. Ash, J. Stone, P. M. Ajayan, R. W. Doremus and L. S. Schadler, *Scr Mater,* **44**, 2061 (2001).

For Peer Review

37 S. J. Pearton, D. P. Norton, K. Ip, Y. W. Heo and T. Steiner, *Progress in Materials Science,* **50**, 293 (2005).

38 J. G. Speight, N. A. Lange and J. A. Dean, *Lange's handbook of chemistry*, McGraw-Hill, New York ; London (2005).

39 J. Stepek and H. Daoust, *Additives for plastics*, Springer-Verlag, New York (1983).

40 L. Rupprecht, Conductive thermoplastic compounds for EMI/RFI application, in *Conductive polymers and plastics in industrial applications*, ed by L. Rupprecht. Plastics Design Library; Society of Plastics Engineers, Norwich, NY; Brookfield, CT, pp. 143 (1999).

41 S. Rush, R. Mcfee and J. A. Abildskov, *Circ Res,* **12**, 40 (1963).

42 G. F. Fu, P. S. Vary and C. T. Lin, *J Phys Chem B,* **109**, 8889 (2005).

43 M. Heinlaan, A. Ivask, I. Blinova, H. C. Dubourguier and A. Kahru, *Chemosphere,* **71**, 1308 (2008).

44 X. Y. Ma and W. D. Zhang, *Polym Degrad Stab,* **94**, 1103 (2009).

For Peer Review

**Table 1** Mechanical properties of Ag/ZnO/PVC composites and neat PVC obtained by tensile tests

| Concentration of Ag/ZnO (wt% ) | Young's modulus (MPa) | Strain at break (%) | Stress at break (MPa) |
|---|---|---|---|
| 0[a] | 7.3 ± 0.9 | 640 ± 30 | 17.8 ± 0.2 |
| 1 | 5.17 ± 0.14 | 660 ± 70 | 18.3 ± 1.3 |
| 3 | 4.87 ± 0.12 | 660 ± 40 | 17.7 ± 0.6 |
| 5 | 7.8 ± 0.8 | 460 ± 50 | 15.6 ± 1.2 |

[a] zero concentration represents the neat PVC sample

For Peer Review

**Table 2** Electrical properties of Ag/ZnO/PVC composites, neat PVC and compressed Ag/ZnO samples as measured by van der Pauw method

| Concentration of Ag/ZnO (wt% ) | Resistivity *R* (Ω cm) |
|---|---|
| 0[a] | out of range (>$10^9$) |
| 1 | (9 ± 5) x $10^7$ |
| 3 | (13 ± 6) x $10^7$ |
| 5 | (11 ± 6) x $10^7$ |
| 100[b] | (6.6 ± 1.1) x $10^{-3}$ |

[a] zero concentration represents the neat PVC sample
[b] 100 wt% represents compressed filler material

For Peer Review

**Table 3** Antibacterial activity of Ag/ZnO/PVC composites tested according to the modified ISO 22196:2007 (E)

| Concentration Ag/ZnO filler in polymer (wt% ) | The treated specimens after 48h *E. coli* $N$ (cfu/cm$^2$) | The treated specimens after 48h *S. aureus* $N$ (cfu/cm$^2$) | Antibacterial activity (Log CFU) *E. coli* $R = U_t - A_t$ | Antibacterial activity (Log CFU) *S. aureus* $R = U_t - A_t$ |
|---|---|---|---|---|
| 0[a] | $4.4.10^6$ | $2.1 \times 10^5$ | $U_t = 6.6$ | $U_t = 5.3$ |
| 1 | 1 | $3.1 \times 10^3$ | 6.6 | 1.8 |
| 3 | < 1 | $1.9 \times 10^1$ | > 6.6 | 4.0 |
| 5 | 1 | $5.9 \times 10^1$ | 6.6 | 3.5 |

[a] zero concentration represents the reference neat PVC sample

For Peer Review

**Figure captions**

**Fig. 1** XRD patterns of the Ag/ZnO particles.

**Fig. 2** SEM a) and TEM b) pictures of Ag/ZnO powder.

**Fig. 3** BSE microphotographs of freeze fracture surfaces of prepared materials for: a) neat PVC and for composites with Ag/ZnO filler concentrations: b) 1 wt% , c) 3 wt% , and d) 5 wt% .

**Fig. 4** EDX spectrum of the material containing 5 wt% of Ag/ZnO filler.

**Fig. 5** BSE image with EDX maps of material containing 5 wt% of Ag/ZnO filler for selected elements.

For Peer Review

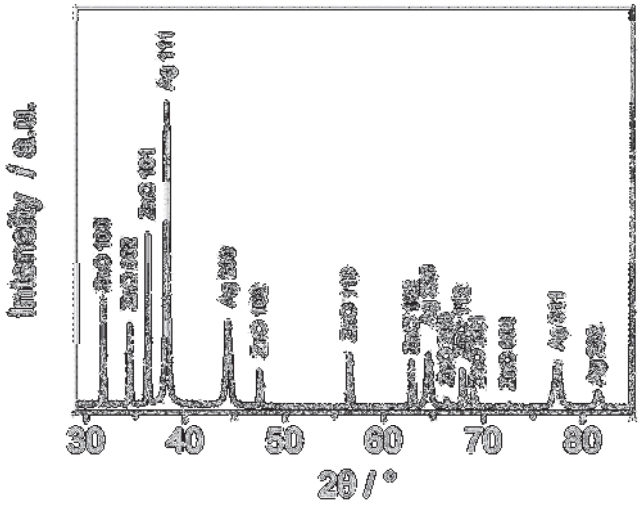


Bazant, Fig1
62x43mm (600 x 600 DPI)

Review

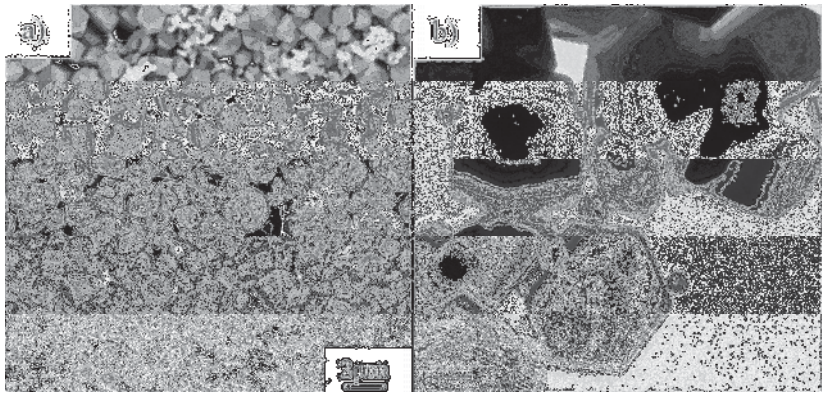

Bazant, Fig2
42x20mm (600 x 600 DPI)

Peer Review

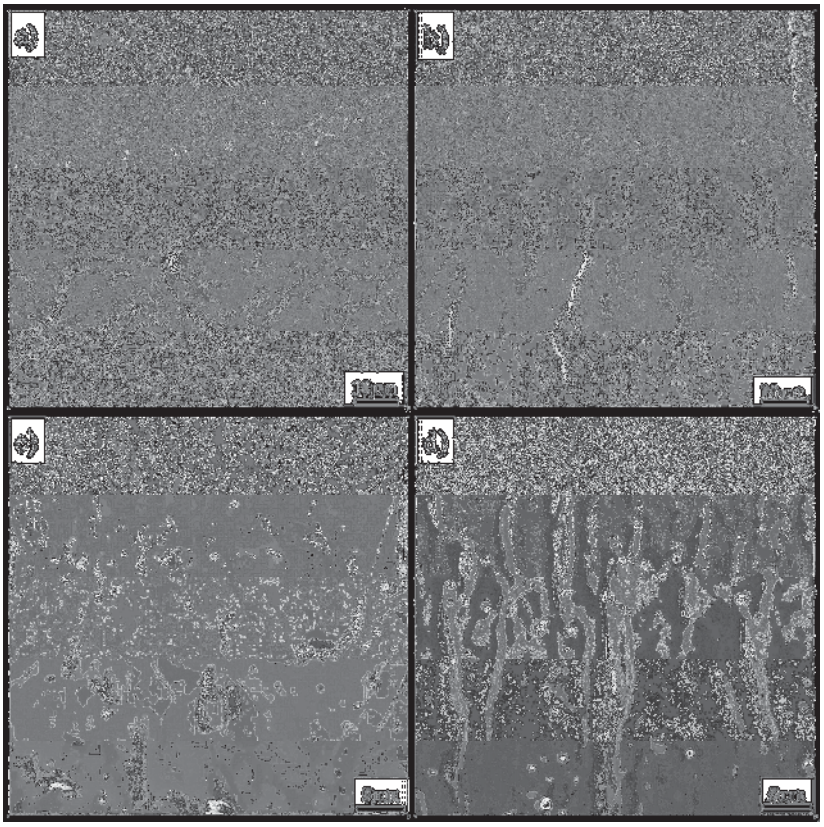

Bazant, Fig3
90x90mm (600 x 600 DPI)

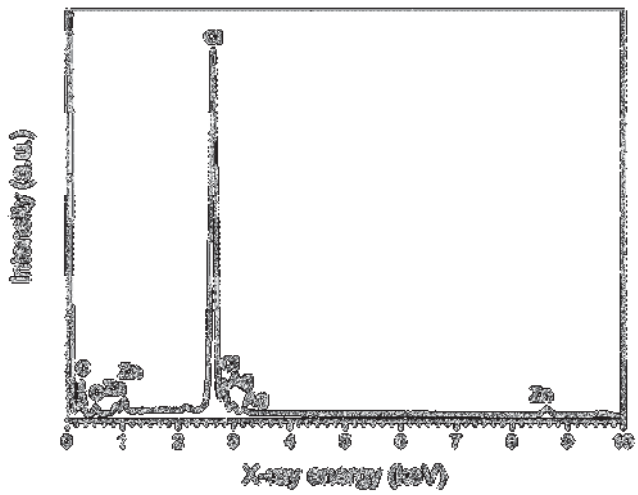


Bazant, Fig4
63x44mm (600 x 600 DPI)

Review

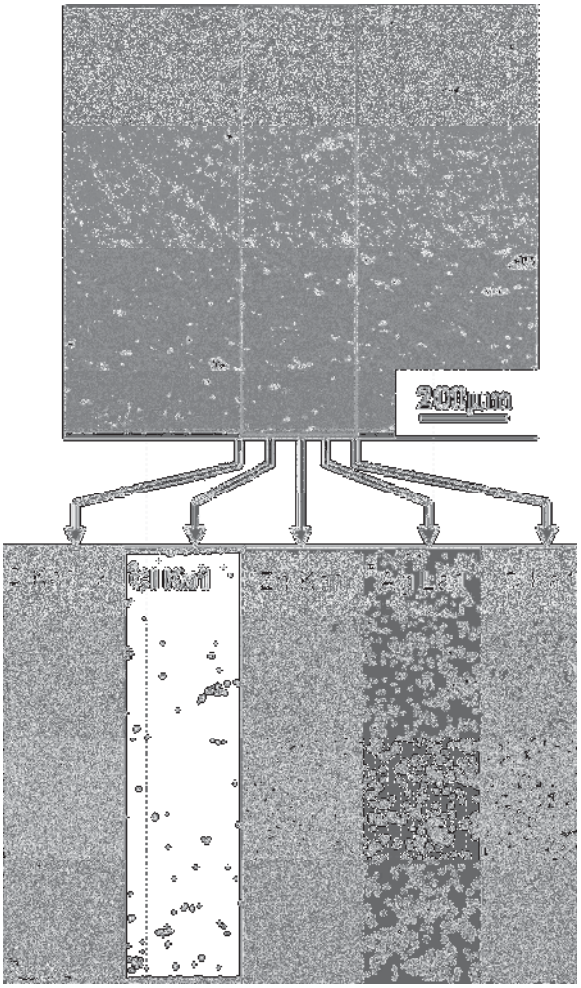

Bazant, Fig5
153x262mm (600 x 600 DPI)